Metabolic network analysis of the marine bacterium *Dinoroseobacter shibae*

Dissertation zur Erlangung des Grades
des Doktors der Ingenieurwissenschaften
der Naturwissenschaftlich-Technoschen Fakulät III
Chemie, Pharmazie, Bio- und Werkstoffwissenschaften
der Universität des Saarlandes

von
Dipl. Biotechnol. Annekathrin Franziska Bartsch

Saarbrücken
April 2015

Tag des Kolloquiums:	18.03.2016
Dekan:	Univ.-Professor Dr.-Ing. Dirk Bähre
Berichterstatter:	Prof. Dr. Christoph Wittmann
	Prof. Dr. Elmar Heinzle
	.....
	.....
Vorsitz:	Prof. Dr. Gert-Wieland Kohring
Akad. Mitarbeiter:	Dr. Björn Becker

Publications

Partial results of this work have been published in advance. This was authorized by the Institute of Systems Biotechnology (Saarland University) represented by Prof. Dr. Christoph Wittmann:

Peer-reviewed articles

Klingner A, **Bartsch A**, Dogs M, Wagner-Döbler I, Jahn D, Simon M, Brinkhoff T, Becker J, Wittmann C (2015) "Large-scale ^{13}C-flux profiling reveals conservation of the Entner-Doudoroff pathway as glycolytic strategy among glucose-using marine bacteria". Applied Environmental Microbiology 81.7, pp 2408-2422.

Laaß S, Kleist S, Bill N, Drüppel K, Koßmehl S, Wöhlbrand L, Rabus R, Klein J, Rohde M, **Bartsch A**, Wittmann C, Schmidt-Hohagen K, Tielen P, Jahn D, Schomburg D (2014) "Gene Regulatory and Metabolic Adaptation Processes of *Dinoroseobacter shibae* DFL12^{T} during Oxygen Depletion". The Journal of Biological Chemistry 289.19, pp 13219-13231.

Conference contributions

Klingner A, **Bartsch A**, Becker J, Wittmann C (2011) Metabolic network analysis of the Roseobacter clade: Pathways and pathway fluxes in *Dinoroseobacter shibae*, *Phaeobacter gallaeciensis* and other members. 3rd Status seminar of the Transregio 51, Delmenhorst, Germany

Klingner A, **Bartsch A**, Becker J, Wittmann C (2012) Fluxomics of selected marine bacteria and first results of a mesocosm experiment on metafluxomics. 5th Status seminar of the Transregio 51, Braunschweig, Germanys

Bartsch A, Klingner A, Becker J, Wittmann C (2012) Metabolic pathway fluxes of the marine model bacterium *Dinoroseobacter shibae* under changing environmental conditions. VAAM Annual Conference, Tübingen, Germany

Klingner A, **Bartsch A**, Becker J, Wittmann C (2012) Systems biology of the marine antibiotic producer *Phaeobacter gallaeciensis*. VAAM Annual Conference, Tübingen, Germany

Bartsch A, Klingner A, Becker J, Wittmann C (2012) Systems-wide metabolic flux analysis of *Dinoroseobacter shibae*. PhD-Seminar of the Transregio 51, Braunschweig, Germany

Bartsch A, Klingner A, Becker J, Wittmann C (2012) Functional contribution of central metabolic pathways to carbon dioxide assimilation in the marine bacterium *Dinoroseobacter shibae*. 7th Status seminar of the Transregio 51, Delmenhorst, Germany

Klingner A, **Bartsch A**, Becker J, Wittmann C (2012) Large-scale ^{13}C flux profiling of the *Roseobacter* clade. 7th Status seminar of the Transregio 51, Delmenhorst, Germany

Klingner A, **Bartsch A**, Becker J, Wittmann C (2012) ^{13}C metabolic flux profiling of *P. gallaeciensis* and novel isolates of the *Roseobacter* clade. PhD-Seminar of the Transregio 51, Braunschweig, Germany

Bartsch A, Klingner A, Becker J, Wittmann C (2012) Metabolic flux response of *Dinoroseobacter shibae* to genetic and environmental burdens. PhD-Seminar of the Transregio 51, Braunschweig, Germany

Bartsch A, Klingner A, Becker J, Wittmann C (2013) Functional contribution of central metabolic pathway to carbon dioxide assimilation in the marine bacterium *Dinoroseobacter shibae*. PhD-Seminar of the Transregio 51, Braunschweig, Germany

Bartsch A, Klingner A, Becker J, Wittmann C (2013) Functional contribution of central metabolic pathways to carbon dioxide assimilation in the marine bacterium *Dinoroseobacter shibae*. 8th Status seminar of the Transregio 51, Delmenhorst, Germany

Participants - Colleagues

Partial results were determined in collaboration with colleagues as referred to in this thesis.

Dr. Patrick Kiefer, Institute for Microbiology, ETH Zürich

M.Sc. Biotechnol. Georg Richter, Institute of Biochemical Engineering, TU Braunschweig
M.Sc. Biotechnol. Arne Klingner, Institute of Biochemical Engineering, TU Braunschweig

Participants - Bachelor students

Partial results were determined in collaboration with students during their bachelor thesis as referred to in this thesis.

Sebastian Tesche, 2011, TU Braunschweig

Samuel Hauf, 2012, TU Braunschweig

Abbreviations and Symbols

μ	Growth rate	$[h^{-1}]$
$Y_{X/S}$	Biomass yield	$[g\ mol^{-1}]$
q_S	Substrate consumption rate	$[mmol\ g^{-1}\ h^{-1}]$
OD	Optical density	[-]
EA	Enzymatic activity	$[U\ g^{-1}_{BDW}]$
MF	Metabolic fluxes	$[U\ g^{-1}_{BDW}]$

6PG	6-Phosphogluconate
6PG – D	6-Phosphogluconate dehydratase
6PG – DH	6-Phosphogluconate dehydrogenase
AAnP	Aerobic anoxygenic phototrophs
AcCoA	Acetyl-CoA
ADP	Adenosine diphosphate
AHL	Acetylated homoserine lactones
AKG	α-Ketoglutarate
ATCC	American Type Culture Collection
ATP	Adenosine triphosphate
CDW	Cell dry weight
CoA	Coenzyme A
DHAP	Dihydroxyacetone phosphate
DMSP	Dimethylsulfoniopropionate
DNA	Deoxyribonucleic acid
DOC	Dissolved organic carbon
DTNB	2,2'-Dinitro-5,5'-dithiodibenzoeic acid
DTT	Dithiothreitol
E4P	Erytrose 4-phosphate
ED	Entner-Doudoroff
EDTA	Ethylenediaminetetraacetic acid
EMP	Embden-Meyerhof-Parnas
EMU	Elementary metabolite units

F6P	Fructose 6-phosphate
FBPase	Fructose bisphosphatase
G6P	Glucose 6-phosphate
G6P – DH	Glucose 6-phosphate dehydrogenase
GAP	Glyceraldehyde 3-phosphate
GC	Gas chromatography
HPLC	High performance liquid chromatography
ICI – DH	Isicitrate dehydrogenase
KDPG	2-keto-3-deoxyphosphogluconate
KEGG	Kyoto Encyclopedia of Genes and Genomes
LDH	Lactate dehydrogenase
MAL – E	Malic enzyme
MBDSTFA	N-methyl-N-tert-butyldimethylsilyl-trifluoroacetamide
MFA	Metabolic flux analysis
MS	Mass spectrometry
MBDSTFA	N-methyl-N-tert-butyldimethylsilyl-trifluoroacetamid
MTBE	Methyl tert-butyl ether
NAD/NADH	Nicotinamide adenine dinucleotide
NADP/NADPH	Nicotinamide adenine dinucleotide phosphate
OAA	Oxaloacetate
PEP	Phosphoenolpyruvate
PFK	Phosphofructokinase
PGA	3-phosphoglycerate
PHB	Polyhydroxybutyrate
PP	Pentose phosphate pathway
PTS	Phosphotransferase system
PYR	Pyruvate
R5P	Ribose 5-phosphate
RNA	Ribonucleic acid
ROS	Reactive oxygen species
rTCA	Reverse tricarboxylic acid cycle
SFL	Summed fractional labelling
SWM	Sea water medium
TBDMS	tert-butyldimethylsilyl
TCA	Tricarboxylic acid
TRAP	Tripartite ATP-independent periplasmatic transporters

List of Tables

List of Figures

Contents

Summary

Dinoroseobacter shibae is a member of the *Roseobacter* clade, a dominant group of marine bacteria. This study investigated the intracellular differences in its metabolism, while reacting on environmental changes, often hampering its living conditions.
Metabolic flux analysis with *D. shibae* revealed a highly conserved and effective glucose metabolism, with degradation solely via the Entner-Doudoroff pathway, while anaplerotic reactions and TCA cycle were more flexible. Using succinic acid it is totally different, and only small fluxes over the ED pathway remained, to adapt fast on environmental changes. In experiments using diamide, a substrate-independent and positive effect of the ED pathway in handling oxidative stress was confirmed for *D. shibae*.
Labeling studies showed no influence of changing light regimes on the metabolism. Using different substrates revealed, that *D. shibae* used substrate-specific heterotrophic carbon incorporation via anaplerotic reactions, most effective with propionate. Further analysis of the acetate metabolism discovered the use of the ethylmalonyl-CoA pathway for its assimilation.
For analysis of quorum sensing mutants, which do not communicate at all, the established metabolic flux anaysis was adapted and revealed only small changes in central carbon metabolism. Consequently, *D. shibae* seemed to be highly adapted to the marine environment and able to react flexible on changing environmental conditions.

Zusammenfassung

Dinoroseobacter shibae gehört zu den *Roseobacteria*, einer weit verbreiteten Gruppe mariner Bakterien. In dieser Arbeit wurden die metabolischen Unterschiede untersucht, die durch wechselnde Umwelteinflüsse entstehen.
Mittels metabolischer Flussanalyse konnte ein hoch konservierter und effektiver Glucosemetabolismus gezeigt werden, der ausschließlich den Entner-Doudoroff Weg nutzt, während anaplerotische Reaktionen und der Citrat Zyklus flexibler sind. Der Stoffwechsel auf Succinat zeigt große Unterschiede, sodass nur noch kleine Flüsse über den ED Weg führen. Dies bietet die Möglichkeit einer schnellen Anpassung an wechselnde Bedingungen. Experimente mit Diamid zeigten einen Substrat unabhängigen und positiven Effekt des ED Weges beim Umgang mit oxidativem Stress.
Markierungsstudien zeigten keinen Einfluss wechselnder Lichtbedingungen auf den Metabolismus. Werden dagegen unterschiedliche Substrate verwendet, zeigt *D. shibae* einen Substrat spezifischen heterotrophen Kohlenstoffeinbau über anaplerotische Reaktionen, am effektivsten für Propionat. Analysen des Acetatmetabolismus enthüllen die Nutzung des Ethylmalonyl-CoA Weges.
Analyse mittels metabolischer Flussanalyse von Quorum Sensing Mutanten, die kein AHL mehr produzieren, zeigt nur geringe Unterschiede im zentralen Kohlenstoffmetabolismus.
Zusammenfassend scheint *D. shibae* sehr gut an den marinen Lebensraum angepasst zu sein und dabei fähig, sehr flexibel auf sich verändernde Umweltbedingungen reagieren zu können.

1. Introduction and Objectives

1.1. General Introduction

Oceans are covering a large part of the earth's surface and offer a wide range of habitats for different organisms with a great diversity of environmental conditions (Pepper et al. 2014). But, astonishingly, there exists only little knowledge about this huge habitat. One conspicuous fact is, that the marine environment is not affected by good conditions for growth or survival and long periods of low nutrient concentrations are often found in the open sea (Hahnke et al. 2013). In addition, changes in salt levels (Kirst 1990), different light regimes and oxidative stress are also influencing marine habitats and their residents (Tomasch et al. 2011). Although these conditions seem unsuitable, diverse bacteria are abundant all over the oceans and contribute to the different nutrient cycles (Zinger et al. 2011). One of these interesting and dominant groups of bacteria are the *Roseobacteria* (Brinkhoff et al. 2008, Buchan et al. 2005). Members of this versatile bacterial group are wide spread over the oceans and live in different habitats, like coastal water, open sea or deep sea sediments (Buchan et al. 2005, Giebel et al. 2009, Tada et al. 2011, Lenk et al. 2012 or B. Wang et al. 2009). They appear in different shapes and colors and most of them are heterotrophic and mesophilic (Brinkhoff et al. 2008). Furthermore, they show various habits linked to the carbon core metabolism and have interesting survival strategies for such nutrient-poor environments.
Dinoroseobacter shibae, as one of the most studied representative of the *Roseobacter* group, seems to be a good candidate for investigations of this bacterial group. It is known for planktonic and biofilm forming growth, attached to algae (Biebl et al. 2005) and belongs to the group of aerobic anoxygenic phototrophic bacteria (AAnP bacteria). Due to their high abundance, especially AAnP bacteria are ecologically important microorganisms and great interest exists in understanding their metabolism. Changes in light regimes leads for AAnP bacteria to the building of a photosystem in the dark and to generation of additional energy during phases of light exposure (Tomasch et al. 2011). These photoheterotrophic bacteria play therefore, a complex role in the marine carbon cycle (Koblížek 2011). Other interesting metabolic traits of *D. shibae* are the exclusively

use of the Entner-Doudoroff pathway for glucose degradation (Tomasch et al. 2011), the possibility of DMSP degradation or the cell communication over quorum sensing (Wagner-Döbler et al. 2010).
For the detailed analysis of metabolic functions in bacteria, the systems biology provide a powerful tool to show directly the intracellular fluxes of the involved metabolites. Metabolic flux analysis (MFA) can be used to calculate the intracellular flux distribution with stable isotopes and for bacteria often ^{13}C labeled carbon sources were used. These labelings were distributed through the different metabolic pathways into the amino acids of the cell protein and their analysis can identify used pathways. For *Roseobacter litoralis* first qualitative labeling studies on carbon fixation and on identification of pathways were done, using GC-MS analysis of amino acids (Tang et al. 2009). In a different approach the identification of DMSP and acetate assimilation pathways used by *Ruegeria pomeroyi* were analyzed by NMR analysis of labeled nucleosides and amino acids and a metabolic model calculated (Reisch et al. 2013). First qualitative studies with GC-MS analysis of labeled amino acids in *D. shibae* revealed the use of the ED pathway for glucose degradation, but quantitative studies are still missing (Fürch et al. 2009).
To address the identification of metabolic networks used under different environmental conditions, the metabolic flux analysis combined with other omics data seems to be a suitable technique to analyze this in *Roseobacteria*. This can provide novel insights into used metabolic traits and mechanisms to survive in the different habitats of the nutrient poor marine environment.

1.2. Objectives of this work

The aim of this thesis was the investigation of the metabolism of *D. shibae* under environmental changes. The first part focused on glucose as substrate, known as most common carbon source for marine environments. After the establishment of suitable cultivation settings and medium optimization, the metabolism was studied in detail. Therefore metabolic flux analysis was used as state of the art technique, to determine the *in vivo* reaction rates of the central carbon metabolism for *D. shibae*. In further analyses of the central carbon metabolism succinic acid was used, to unravel the differences occuring in the central carbon core metabolism, when a different carbon source is used. Detailed flux maps elucidated the fluxes through the main pathways for both substrates. These results were combined with analyses on the reaction on oxidative stress, to provide information about the advantages of *D. shibae* preferring the Entner-Doudoroff pathway (EDP) in its environment. Additionally, differences of the robustness against oxidative

stress for both substrates completed these analyses.
It is a fact, that the marine environment is not affected by good conditions for growth or survival and the availability of nutrients are often changing during the year. Especially, for AAnPs the changes in light regimes are relevant growth parameters. To investigate these topics it was interesting to study, how bacteria react on environmental changes in their marine habitats. Therefore the main change during algal bloom, the availability of different carbon sources, were studied. Additionally to glucose and succinic acid, the more reduced substrates acetate and propionate seemed to be promising candidates for pathway analyses. Especially for acetate metabolism, it was interesting to show, that the ethylmalonyl-CoA pathway is the used pathway in *D. shibae* as also known for *R. pomeroyi*. To address this question, stationary labeling experiments with ^{13}C carbonate were conducted. Then a set of static and dynamic ^{13}C isotope labeling experiments were designed with *D. shibae* as model organism, to provide information about the contribution of the clade and *D. shibae* to CO_2 fixation and to investigate whether *Roseobacter* members act as a sink or source of CO_2. In a next step, to account for the light-induced transcriptional changes of the proposed 3-HP cycle (Tomasch et al. 2011), the influence of different illumination conditions on growth and metabolism were analyzed.
Another wide spread property under *Roseobacters* is quorum sensing, a technique, that controls divers physiologies in cell populations. This interesting behavior might have also influences on metabolic traits and the analysis of the *in vivo* fluxes is a prospective way to investigate the communication of the cell population on a metabolic level. Therefore the established analysis on metabolic fluxes for the wildtype strain were adapted for two mutant strains, lacking AHL production, the necessary molecule for cell communication. The resulted flux maps gave more information on metabolic changes linked with quorum sensing.

2. Theoretical Background

Over 70 % of the earth's surface is covered with oceans and the enormous volume underlines its importance for life in general and as an important habitat for different organisms. However, there is still limited knowledge about this ecosystem with its great diversity of environmental conditions (Pepper et al. 2014). The variety of habitats, such as coastal water, pelagic zones and deep sea sediments is being subject to continuous fluctuations in temperature, pressure, light and nutrient supply (Pepper et al. 2014). Especially, the open sea is an area with long periods of low nutrient concentrations (Hahnke et al. 2013). Although these starving conditions seem unsuitable, diverse bacteria are abundant all over the oceans and contribute to the different nutrient cycles (Zinger et al. 2011).

2.1. The *Roseobacter* clade - a most prevalent and versatile bacterial group in the oceans

Most bacteria, living in the marine ecosystem, belong to the group of *Alpha-* or *Gammaproteobacteria* (Zinger et al. 2011). The *Roseobacter* clade, affiliated to the *Alphaproteobacteria*, represents one of the dominating and prevalent groups and can constitute up to 25 % of the bacterioplankton community (Brinkhoff et al. 2008, Buchan et al. 2005). Bacteria, belonging to this clade, are wide spread and live in different habitats like coastal water, open oceans, coastal sediments or deep sea sediments, but exclusively in marine or hypersaline environments (Buchan et al. 2005, Giebel et al. 2009, Tada et al. 2011, Lenk et al. 2012 or B. Wang et al. 2009). Thereby, they appear free-living and surface-associated on algae, sponges or corals (Wagner-Döbler et al. 2010, Buchan et al. 2005).
They occur as small rods (Biebl et al. 2005), spirilla e. g. *Roseobacter denitrificans* (Shiba 1991) and as rosette forming colonies, e. g. *Phaeobacter* species (Bruhn et al. 2007). Many species are pigmented and belong to the aerobic anoxygenic phototrophs (AAnP) showing a red color from bacteriochlorophyll *a*, when cultivated in the dark, e. g. *D. shibae* or *Roseobacter litoralis* (Tomasch et al. 2011, Allgaier et al. 2003). Other

members show dark brownish pigments, e. g. *Phaeobacter inhibens* (Dogs et al. 2013). The prosperous group of *Alphaproteobacteria* seems to be highly adapted to their nutrient-poor environment. While autotrophic growth could not be observed (Shiba 1991), most *Roseobacter* are heterotrophic and mesophilic (Brinkhoff et al. 2008). The diversity of metabolic traits includes aerobic anoxygenic phototrophy (Shiba 1991), carbon monoxide degradation (Cunliffe 2011), aromatic compound degradation (Buchan et al. 2010), DMSP degradation (Reisch et al. 2013) or denitrification (Moran et al. 2007a). Other organisms of this group are able to produce storage compounds such as polyhydroxyalkanoates (Xiao et al. 2011), antibiotics (Brinkhoff et al. 2004, Dogs et al. 2013) or acetylated homoserine lactones (AHL) (Patzelt et al. 2013, Gram et al. 2002, Cude et al. 2013, Wagner-Döbler et al. 2005, Zan et al. 2012). Many of these diverse habits of the *Roseobacter* clade are linked to the carbon core metabolism. To obtain a deeper insight in the dominance of this clade in bacterioplankton communities, it appears promising to investigate suitable model organisms, e. g. *D. shibae*, *R. denitrificans* or *P. inhibens* as prominent and interesting members of this group.

2.2. *Dinoroseobacter shibae* - a prominent member of the *Roseobacter* clade

D. shibae DFL-12 is one of the most prominent and most studied members of the *Roseobacter* clade, a subgroup of the *Alphaproteobacteria*. The Gram-negative small oval rod bacterium has first been isolated from the toxic marine algae *Prorocentrum lima* occurring in sand and sediment (Pradella et al. 2004, Wagner-Döbler et al. 2010, Biebl et al. 2005). It is known for both planktonic and biofilm forming growth (Biebl et al. 2005). It belongs to the group of AAnP and has a dark red pigmentation, when grown in darkness (Biebl et al. 2006, Allgaier et al. 2003). Its adaptation to dark-light cycles results in additional energy generation from light under heterotrophic, especially under starving conditions (Soora et al. 2013). Transcriptional dynamics follow the day and night cycle, revealing the adaptation (Tomasch et al. 2011). Furthermore, *D. shibae* produces polyhydroxybutyrate (PHB) as storage compound in high concentrations of cell dry mass as many AAnP (Xiao et al. 2011).

D. shibae shows interesting metabolic traits, such as the ability to grow anaerobically, via arginine fermentation or nitrate respiration (Laass et al. 2014). In symbiosis with algae, *D. shibae* is able to synthesize vitamin B_1 and B_{12}, to support the algal growth (Wagner-Döbler et al. 2010). Furthermore, traits known for the *Roseobacter* clade are present in the genome of *D. shibae*, e. g. carbon monoxide oxidation, aromatic compound degrada-

tion or dimethylsulfoniopropionate degradation (Wagner-Döbler et al. 2010). *D. shibae* is able to degrade various organic acids, especially intermediates from the TCA cycle (fumarate, succinate, or citrate), possibly released from the algal host (Biebl et al. 2005). Additionally, acetate, pyruvate and glucose can be metabolized as prevalent compounds of marine dissolved organic carbon (Amon et al. 2003, Aluwihare et al. 2002, Biersmith et al. 1998).
For the uptake of nutrients from the environment, *D. shibae* does not utilize a PTS or ABC transport system, but seems to prefer tripartite ATP-independent periplasmic transporters (TRAP) (Wagner-Döbler et al. 2010). Genomic studies of *D. shibae* revealed the EMP pathway and the ED pathway as pathways for glucose degradation, while the 6-phosphogluconate dehydrogenase for the oxidative PP pathway is not annotated (Wagner-Döbler et al. 2010). In recent studies, labeling analysis with [1-^{13}C] glucose revealed the exclusive degradation of glucose via the ED pathway (Fürch et al. 2009). PEP synthesis via pyruvate orthophosphate dikinase or PEP carboxykinase was not identified (Fürch et al. 2009), but heterotrophic CO_2 fixation seems only be possible via pyruvate carboxylase, because PEP carboxylase is not annotated (Fürch et al. 2009). Additional transcriptomic studies to identify the role of *D. shibae* in marine carbon fixation path-ways, revealed a possible activity of the 3-hydroxypropionate cycle for carbon fixation during day and night cycles (Tomasch et al. 2011).
Quorum sensing is a mechanism to control physiology among cell populations and is wide spread within *Roseobacters* (Cude et al. 2013). It is also responsible for changes in morphology of *D. shibae* (Patzelt et al. 2013, Wagner-Döbler et al. 2010, Wagner-Döbler et al. 2005). Genome analysis revealed the rule of *luxI* genes as autoinducer and that of *luxR* genes as regulator of AHL production. A *luxI* deficiency mutant showed complete lack of AHL production and a change in morphology to only small cells (Patzelt et al. 2013).

2.3. The carbon core metabolism

Central metabolic pathways are used by bacteria to convert carbohydrates or carboxylic acids to precursors for cell components and energy generation (ATP and NAD(P)H) (Romano et al. 1996). Depending on the substrate, different pathways are active. While glucose can be metabolized via three amphibolic glycolytic routes, followed by the TCA cycle, many organic acids enter the central carbon metabolism directly via the TCA cycle. Carbon-two compounds like acetate also feed into the TCA cycle i.e. via the glyoxylate shunt or ethylmalonyl-CoA pathway (EMC pathway) (Tang et al. 2011). Pathways have

been studied by genomics, transcriptomics, metabolomics, proteomics and fluxomics i.e. to identify unknown reactions (Peyraud et al. 2009), flux distributions (Sauer et al. 2005), adaptation processes (Kohlstedt et al. 2014) or even genetic optimization potential of production strains (Becker et al. 2011).
The central metabolic carbon metabolism of *D. shibae* is shown in Figure: 2.1 and will be shortly described below.

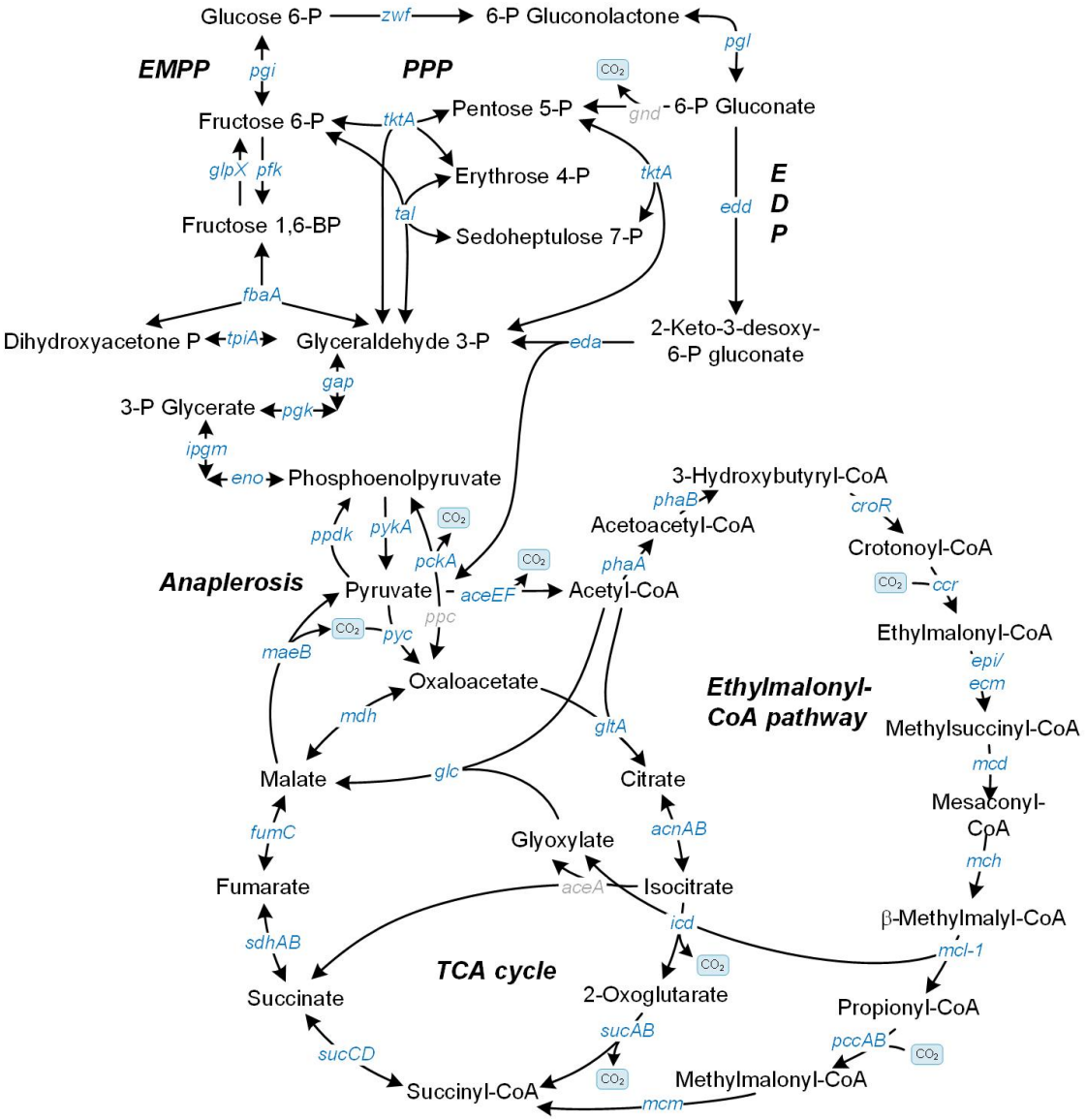

Figure 2.1.: The central carbon metabolism including the EMP pathway, the ED pathway, the oxidative and non-oxidative PP pathway, the glyoxylate-shunt, the TCA cycle, the anaplerosis and the EMC pathway. Additionally, the gene names are given. Blue colored gene names are annotated genes for *D. shibae*, based on information from KEGG database, gray colored genes are not registered so far.

2.3.1. Glucose metabolism

Glucose can be metabolized via three different glycolytic pathways, the Emden-Meyerhoff-Parnas pathway (EMP pathway), the pentose phosphate pathway (PP pathway) and the Entner-Doudoroff pathway (ED pathway), respectively, to generate pyruvate and different cell component precursors (Moat et al. 2002). The pathways differ in stoichiometry and generation of energy and reduction equivalents. Further degradation of pyruvate via the tricarboxylicacid cycle (TCA cycle) leads to additional energy and precursors. To replenish the TCA cycle with oxaloacetate, anaplerotic reactions are used (Sauer et al. 2005).

EMP pathway

In the well studied organisms *Escherichia coli* and *Bacillus subtilis*, glucose is mainly metabolized via the EMP pathway (Fuhrer et al. 2005) and is known as one of the main pathways for glucose assimilation in various other bacteria. Glucose is degraded in the EMP pathway via glyceraldehyde 3-phosphate and dihydroxyacetone phosphate to pyruvate. In these reactions energy and reduction equivalents are generated (Formula: 2.1). In the upper part of the EMP pathway two ATPs are invested for phosphorylating glucose and fructose 6-phosphate catalyzed by hexokinase (*glk*) and phosphofructokinase (*pfk*) (Moat et al. 2002). These catalyze irreversible steps of this pathway. Finally two molecules of pyruvate, two molecules of NADH and four molecules of ATP are generated (Moat et al. 2002). Obviously no NADPH is generated in this pathway.
Embden-Meyerhof-Parnas pathway:

$$\begin{aligned} \text{Glucose} + 2\ \text{NAD}^+ + 2\ \text{ADP} + 2\ \text{P}_\text{i} \rightarrow \\ 2\ \text{Pyruvate} + 2\ \text{NADH} + 2\ \text{H}^+ + 2\ \text{ATP} + 2\ \text{H}_2\text{O} \end{aligned} \tag{2.1}$$

While in AAnP bacteria, the EMP pathway was found active (Tang et al. 2011), investigations suggested its inactivity in *Roseobacteria* (Fürch et al. 2009, Tang et al. 2009), although in *D. shibae* all involved enzymes are annotated (Figure: 2.1). This conclusion has been been drawn because of the lacking enzymatic activity for phosphofructokinase, a key enzyme of this pathway (Fürch et al. 2009).

PP pathway

The main function of the PP pathway is the supply of NADPH, ribose 5-phosphate and erythrose 4-phosphate for the organism (Michal et al. 2012). Therefore the reactions are divided in an oxidative and non-oxidative branch. The oxidative part comprises

the conversion of glucose 6-phosphate over 6-phosphogluconate to ribulose 5 phosphate through the release of one carbon dioxide. Thereby, the key enzymes glucose 6-phosphate (*zwf*) and 6-phosphogluconate dehydrogenase (*gnd*) generate one molecule of NADPH each. Ribulose 5-phosphate itself is a precursor for nucleotides and intermediate of the non-oxidative part of the pathway. First, it is converted to ribose 5-phosphate and xylulose 5-phosphate via isomerase and epimerase. Followed by a rearrangement of the carbon atoms by transketolase (*tktA*) and transaldolase (*tal*) to produce erythrose 4-phosphate, fructose 6-phosphate and glyceraldehyde 3-phosphate. erythrose 4-phosphate is a precursor for aromatic amino acids and fructose 6-phosphate and glyceraldehyde 3-phosphate are intermediates of the EMP pathway, which connects both pathways. The further degradation to pyruvate is part of to the EMP pathway. In total three glucose react to five pyruvate and three carbon dioxide, while generating eight ATP, six NADPH and five NADH (Formula: 2.2).

This pathway is often used additionally to the EMP pathway, due to the lack of NADPH production along this pathway as shown for the well studied organisms *E. coli* (Wittmann et al. 2007), *B. subtilis* (Dauner et al. 2001) and *Corynebacterium glutamicum* (Marx et al. 1996). In some organisms, fructose 6-phosphate and glyceraldehyde 3-phosphate can be reconverted to glucose 6-phosphate, resulting in a gluconeogenetic backflux (Fuhrer et al. 2005, Conway 1992). While in organisms, lacking the key enzyme of the oxidative part of the PP pathway (6-phosphogluconate dehydrogenase), the non-oxidative PP pathway is operating in the reverse direction for precursor generation, as proposed for *R. denitrificans* (Tang et al. 2009). This is also common for many phototrophic bacteria, including the AAnP (Tang et al. 2011). Some phototrophic bacteria, able to fix inorganic carbon autotrophically, have an active RuBisCO part of the reductive PP pathway. This variation of the PP pathway is also known as Calvin-Benson cycle (Tang et al. 2011). However, for photoheterotrophic bacteria belonging to the group of *Roseobacteria*, this pathway is missing, because the RuBisCO is not annotated (Swingley et al. 2007). For *D. shibae* and many other *Roseobacteria*, the 6-phosphogluconate dehydrogenase is also missing (Figure: 2.1) resulting in zero flux through the oxidative part of the PP pathway, while the non-oxidative part is used for precursor generation (Fürch et al. 2009).

Pentose-Phosphate pathway:

$$\begin{aligned} 3\ \text{Glucose} + 6\ \text{NADP}^+ + 5\ \text{NAD}^+ + 8\ \text{ADP} + 5\ \text{P}_\text{i} \rightarrow\ & 5\ \text{Pyruvate} \\ & + 3\ \text{CO}_2 + 6\ \text{NADPH} + 5\ \text{NADH} + 8\ \text{H}^+ + 8\ \text{ATP} + 2\ \text{H}_2\text{O} \end{aligned} \tag{2.2}$$

ED pathway

As alternative pathway for glucose assimilation the ED pathway has been first reported in 1952 for *Pseudomonas saccharophila* (Peekhaus et al. 1998). Over the years it has been shown that many Gram-negative bacteria mainly use this pathway for glucose assimilation including *Pseudomonas* species e. g. *Pseudomonas fluorescens* (Fuhrer et al. 2005), *Pseudomonas putida* (Chavarría et al. 2013) and *Pseudomonas aeruginosa* (Berger et al. 2014), but also *Rhodobacter sphaeroides* (Imam et al. 2013), Zymomonas mobilis (Rutkis et al. 2013) and *Roseobacteria* like *D. shibae*, *Phaeobacter gallaeciensis* (Fürch et al. 2009) or *R. denitrificans* (Tang et al. 2009). In *E. coli*, the ED pathway is mainly used for gluconate, glucuronate or galacturonate degradation, which might give advantages in colonization of mammalian intestinal parts (Peekhaus et al. 1998). As one of a few *Actinobacteria* as well as Gram-positive bacteria, *Streptomyces tenebrarius* shows an active ED pathway, when grown on glycerol (Borodina et al. 2005).
Glucose is degraded via 6-phosphogluconate and KDPG to pyruvate and glyceraldehyde 3-phosphate. Hereby, one molecule of NADPH is generated by glucose 6-phosphate dehydrogenase (*zwf*), also part of the pentose phosphate pathway. The key enzymes are 6-phosphogluconate dehydratase (*edd*), converting 6-phosphogluconate to KDPG, and the KDPG aldolase, further degrading KDPG to pyruvate and glyceraldehyde 3-phosphate, which is then further metabolized to pyruvate as part of the EMP pathway. Additionally, one molecule of NADH and ATP are produced during these reactions, respectively (Formula: 2.3).
Entner-Doudoroff pathway:

$$\begin{aligned} \text{Glucose} + \text{NADP}^+ + \text{NAD}^+ + \text{ADP} + \text{P}_\text{i} + 2\,\text{H}_2\text{O} \rightarrow \\ 2\,\text{Pyruvate} + \text{NADPH} + \text{NADH} + \text{ATP} \end{aligned} \tag{2.3}$$

TCA cycle

The TCA cycle is almost ubiquitously distributed in the bacterial kingdom for energy generation from various substrates. Sugars, organic acids, amino acids or fatty acids, entering the TCA cycle via different intermediates, are oxidized, which results in the generation of reduction equivalents (NADH/NADPH) and carbon dioxide. Furthermore, the TCA cycle provides precursors for amino acid synthesis and biomass generation. The pathway is directly coupled with the glycolysis, via pyruvate dehydrogenase (*aceEF*), generating acetyl-CoA. To replenish metabolites, used for anabolic purposes, anaplerotic reactions are utilized (Michal et al. 2012).

TCA cycle:

$$\begin{aligned} \text{Acetyl}-\text{CoA} + 2\,\text{NAD}^+ + \text{NADP}^+ + \text{FAD} + \text{GDP} + \text{P}_\text{i} \rightarrow \\ \text{CoA} + 2\,\text{NADH} + \text{NADPH} + \text{FADH}_2 + \text{H}^+ + \text{GTP} \end{aligned} \tag{2.4}$$

As starting reaction acetyl-CoA and oxaloacetate are condensed to citrate (*gltA*). After rearrangement to isocitrate, two decarboxylation steps follow, which are catalyzed by isocitrate dehydrogenase (*icd*) and by α-ketoglutarate dehydrogenase (*sucAB*). In the next step, succinate is synthesized (*sucCD*) and then further oxidized to fumarate (*sdhAB*). Fumarate is hydrated to malate (*fumC*), which is finally oxidized to oxaloacetate again (*mdh*). In total two molecules of NADH, one molecule of NADPH, $FADH_2$ and GTP are generated per cycle and acetyl-CoA (Formula: 2.4).
For *R. denitrificans* and *D. shibae*, belonging to the *Roseobacteria*, a fully active TCA has been shown (Tang et al. 2009, Fürch et al. 2009). In addition, the TCA is a key pathway in the central carbon metabolism for energy generation for many other AAnP bacteria (Tang et al. 2011, Yurkov et al. 1998).

Anaplerosis

Under the designation of anaplerosis a couple of enzymatic reactions are summarized, linking the glycolysis, the gluconeogenesis and the TCA cycle at the phosphoenolpyruvate-pyruvate-oxaloacetate node. These carboxylating and decarboxylating enzymes are used to distribute the carbon fluxes within the major pathways of carbon metabolism (Sauer et al. 2005). For growth on carbohydrates the main pathways used are the EMP and the ED pathway. These are followed by carboxylation of phosphoenolpyruvate and pyruvate to replenish compounds deprived from the TCA cycle for anabolic purposes. As these carboxylating enzymes pyruvate and phosphoenolpyruvate carboxylase are described (Formula: 2.5 and 2.6). Additionally, acetyl-CoA, as starting component of the TCA cycle, is produced by decarboxylation of pyruvate (Michal et al. 2012, Petersen et al. 2000). For break down of TCA cycle intermediates or substrates entering the central carbon metabolism via acetyl-CoA the gluconeogenesis is active (Sauer et al. 2005). To connect both pathways malate or oxaloacetate are decarboxylated by phosphoenolpyruvate carboxykinase (Formula: 2.7) or malic enzyme (Formula: 2.8) to provide pyruvate and phosphoenolpyruvate (Michal et al. 2012, Petersen et al. 2000).
All together, these enzymes are able to catalyze the incorporation of inorganic carbon. Thereby, only the two carboxylases are generally responsible for the carboxylation during glycolytic growth (Sauer et al. 2005), while malic enzyme and phosphoenolpyruvate carboxykinase strongly prefer the direction of decarboxylation (Bar-Even et al. 2010).

Pyruvate carboxylase:

$$\text{Pyruvate} + \text{ATP} + \text{CO}_2 \rightarrow \text{Oxaloacetate} + \text{ADP} + \text{P}_\text{i} \tag{2.5}$$

Phosphoenolpyruvate carboxylase:

$$\text{Phosphoenolpyruvate} + \text{CO}_2 + \text{H}_2\text{O} \rightarrow \text{Oxaloacetate} + \text{P}_\text{i} \tag{2.6}$$

Phosphoenolpyruvate carboxykinase:

$$\text{Oxaloacetate} + \text{GTP} \leftrightarrows \text{Phosphoenolpyruvate} + \text{GDP} + \text{CO}_2 \tag{2.7}$$

Malic enzyme:

$$\text{Malate} + \text{NADP}^+ \leftrightarrows \text{Pyruvate} + \text{NADPH} + \text{CO}_2 \tag{2.8}$$

Heterotrophic bacteria require organic carbon sources for growth. Understanding of the utilization and especially the assimilation of CO_2 might result in a deeper insight into the bio-energy metabolism and the role of the marine wide-spread *Roseobacteria* in the global carbon cycle (Tang et al. 2009). For photoheterotrophic bacteria like AAnPs, the four anaplerotic enzymes are reported (Tang et al. 2011). The reactions catalyzed by these enzymes are also known to be a possible alternative mechanism for heterotrophic CO_2 fixation in the *Roseobacter* clade (Swingley et al. 2007, Tang et al. 2009), but the actual impact has not been verified experimentally. First studies of *R. denitrificans* revealed, that it fixes approximately 10–15 % of protein carbon from CO_2 over anaplerotic pathways, mainly through malic enzyme from pyruvate to malate (Tang et al. 2009), although this is not the preferred direction for this enzyme. These first evidences support the assumption of heterotrophic CO_2 fixation via anaplerotic reactions in *R. denitrificans*, member of the *Roseobacter* clade (Swingley et al. 2007).

2.3.2. Growth on organic acids

Many bacteria are able to use organic acids, amino acids or alcohols for growth, which are entering the main metabolic carbon metabolism at the TCA cycle. This comprises many organic acids like succinate, malate and citrate, direct intermediates of the TCA cycle. Other substances (propionate, glutamate or acetate) are first converted to these intermediates or enter via pyruvate and acetyl-CoA the TCA (acetate, lactate, alanine or ethanol). The further metabolization progresses via gluconeogenesis, which is coupled through anaplerosis with the TCA cycle (Michal et al. 2012).

Gluconeogenesis

Bacteria, growing on substrates, that enter the metabolism via the TCA cycle have to be able to derive sugars for storage purposes and precursors e. g. for purines via gluconeogenesis. Mainly, gluconeogenesis recruits reversible enzymes from glycolysis, while irreversible steps are by-passed through specific enzymes. These key enzymes are glucose 6-phosphatase, generating glucose from glucose 6-phosphate, and fructose bisphosphatase replacing phosphofructokinase (Michal et al. 2012). To concatenate the TCA cycle with gluconeogenesis, anaplerotic reactions are involved. Starting from pyruvate, two different ways are possible to generate phosphoenolpyruvate. The pyruvate phosphate dikinase is able to produce phosphoenolpyruvate directly. Another possibility is the conversion to oxaloacetate by pyruvate carboxylase, followed by phosphoenolpyruvate carboxykinase, producing phosphoenolpyruvate, the starting point of further gluconengenesis (Sauer et al. 2005). If the initial metabolite is an intermediate from the TCA cycle, the connection to gluconeogenesis can function via phosphoenolpyruvate carboxykinase or a combination of malic enzyme and pyruvate phosphate dikinase, as known for *E. coli* (Netzer et al. 2004, Kao 2005).

Gluconeogenesis:

$$\begin{aligned} 2\ \text{Pyruvate} + 4\ \text{ATP} + 2\ \text{GTP} + 2\ \text{NADH} + 6\ \text{H}_2\text{O} \rightarrow \\ \text{Glucose} + 4\ \text{ADP} + 2\ \text{GDP} + 6\ \text{P}_\text{i} + 2\ \text{NAD}^+ + 2\text{H}^+ \end{aligned} \tag{2.9}$$

Gluconeogenesis is a highly energy consuming process (Equation: 2.9) using four ATP, two GTP and two NADH to generate one glucose, but it is necessary for growth.

The different pathways known for acetate assimilation

Various organisms are able to metabolize carbon-two compounds e. g. acetate. Two different ways of acetate degradation are so far known. Substances entering the metabolism via acetyl-CoA (e. g. alcohols, PHA and DMSP) also uses the assimilation pathway of acetate, as connection to the TCA cycle (Schneider et al. 2012). Under these substances, especially DMSP is known as an osmolyte of algae and is therefore a prevalent carbon source for *Roseobacter* (Reisch et al. 2013). From this point of view, it seems important to study the metabolism of acetate.

Glyoxylate shunt:

$$\begin{aligned} 4\ \text{Acetyl}-\text{CoA} + 2\ \text{NAD}^+ + 6\ \text{H}_2\text{O} \rightarrow \\ 2\ \text{Malate} + 4\ \text{HS}-\text{CoA} + 6\ \text{H}^+ + 2\ \text{NADH} \end{aligned} \tag{2.10}$$

The problem arising during aerobic acetate assimilation is a lack of oxaloacetate, which is necessary for the TCA cycle. One pathway to assimilate acetate is the glyoxylate shunt (Alber et al. 2006). This pathway comprises first the cleavage of isocitrate to glyoxylate and succinate catalyzed by isocitrate lyase. This is followed by synthesis of malate from glyoxylate and acetyl-CoA catalyzed by malate synthase (Figure: 2.1). The assimilation of four molecules of acetyl-CoA produces two molecules of malate and two molecules of NADH (Formula: 2.10) (Hädicke et al. 2011). This common pathway for acetate assimilation is active in many bacteria containing the isocitrate lyase (Alber et al. 2006). The strategy of anaerobic bacteria is the utilization of the pyruvate:ferredoxin oxidoreductase to generate pyruvate directly. Furthermore, the reductive acetyl-CoA pathway was described as a possible route. However, under aerobic conditions, the involved enzymes of these pathways are inhibited by oxygen (Erb 2011). For organisms without isocitrate lyase, alternative routes for acetate assimilation e. g. EMC pathway and methylaspartate cycle, were detected (Erb 2011). While the methylaspartate cycle is only known for haloarchaea, the EMC pathway seems to be wide spread and it is the only acetate assimilation pathway reported for AAnPs Tang et al. 2011.

Ethylmalonyl-CoA pathway:

$$3\ \text{Acetyl}-\text{CoA} + 2\ CO_2 + 2\ \text{NADPH} + H_2O \rightarrow 2\ \text{Malate} + 3\ \text{HS}-\text{CoA} + 6\ H^+ + 2\ \text{NADP}^+ \quad (2.11)$$

For many bacteria, belonging to the group of *Rhizobiales*, *Actinomycetales* and *Rhodobacterales*, the potential of the EMC pathway was shown (Erb et al. 2009) and some of the first studies of this pathway were done for *R. sphaeroides* by Alber et al. (2006) and Erb et al. (2007). Via this pathway, three molecules of acetyl-CoA are assimilated into two molecules of malate, one acetyl-CoA less than required for the glyoxylate shunt. The EMC pathway is known to involve the incorporation of inorganic carbon, catalyzed by crotonyl-CoA carboxylase/reductase (*ccr*) and propionyl-CoA carboxylase (*pccAB*) (Formula: 2.11) (Hädicke et al. 2011). For this, two molecules of NADPH are necessary. The first step of this pathway is the condensation of two acetyl-CoA molecules into acetoacetyl-CoA, which is further modified into crotonoyl-CoA, the substrate for the first carboxylation reaction. Further modifications result in methylmalyl-CoA, which is cleaved by β-methylmalyl-CoA/(3S)-malyl-CoA (*mcl-1*) lyase into glyoxylate and propionyl-CoA. While glyoxylate is metabolized to malate by malate synthase (*glc*) propionyl-CoA is decarboxylated into methylmalonyl-CoA and enters the TCA cycle via succinyl-CoA (Alber 2011). For this pathway, unique reactions catalieze the conversion of crotonoyl-CoA and mesaconyl-CoA. This involves a coenzyme B_{12}-dependent mutase, recently discovered

as new subclade of mutases (Erb et al. 2008).

The activity of this pathway was demonstrated for *Methylobacterium extorquens* using dynamic labeling experiments (Peyraud et al. 2009, Schneider et al. 2012). The first *Roseobacter*, supposed to use the EMC pathway, is *Ruegeria pomeroyi* (Reisch et al. 2013). It was shown, that during DMSP degradation, this route is used to catabolize acetyl-CoA. For AAnP bacteria, the EMC pathway is the only acetate assimilation pathway, so far reported (Tang et al. 2011). First studies, concerning the genomic potential of *D. shibae*, revealed all enzymes of this pathway as illustrated in Table: 2.1 (Erb et al. 2009). So it seems possible that *D. shibae* is using this pathway for acetate assimilation.

2.3.3. Carbon fixation in the marine environment and the potential connection to aerobic anoxygenic phototrophy

Global warming due to greenhouse gases is an important issue, affecting today's industrialized society, which relies on fossil resources to supply energy, materials and chemicals (Buschke et al. 2013b). In particular, anthropogenic carbon dioxide production significantly contributes to the increasing temperature worldwide and influences the global carbon cycle (Liu et al. 2008). Approximately half of the released CO_2 is re-absorbed by the marine and terrestrial biosphere (Liu et al. 2008). These major CO_2 sinks significantly lower greenhouse gas emissions. In addition, they are key factors in balancing autotrophic and heterotrophic life on Earth (Hügler et al. 2011). It is estimated that

Table 2.1.: Annotated genes of *D. shibae* for the potential EMC pathway extracted from KEGG and Erb et al. (2009).

Gene	Gene ID
phaA	Dshi_3066
phaB	Dshi_3067
croR	Dshi_2926
ccr	Dshi_2853
epi	Dshi_2630
ecm	Dshi_2855
mcd	Dshi_0204
mch	Dshi_2871
mcl-1	Dshi_3050
pccAB	Dshi_0723/0718
mcm	Dshi_0726

the marine biota is responsible for approximately half of the annual primary production of CO_2 (Hügler et al. 2011), highlighting their global importance for ecosystems and nutrient cycles. Overall, this results in a net carbon uptake flux by the oceans of 2 Pg of carbon per year (Takahashi et al. 2002).

Among the bacteria of the *Roseobacter* clade, aerobic anoxygenic photoheterotrophic bacteria (AAnP) appear particularly relevant, as they contribute a large portion of carbon to the upper trophic levels related to their fast growth and cell size (Xiao et al. 2011). They are lysed by numerous AAnP-specific viruses (Bergh et al. 1989) thereby releasing dissolved organic carbon (DOC) into the environment (Xiao et al. 2011). Due to their high abundance, AAnP are ecologically important microorganisms and great interest exists in understanding their metabolism.

For phototrophic bacteria, different pathways are known for carbon dioxide assimilation, and the most effective incorporation of CO_2 occurs during autotrophic growth. One of the most studied pathways is the Calvin-Benson cycle (reductive PP pathway), with RuBisCO as key enzyme (Hügler et al. 2011). This cycle is active in many photoheterotrophic bacteria, e. g. *Rhodopseudomonas palustris*, and is most effective on substrates with a low oxidation state (McKinlay et al. 2011). For autotrophic carbon fixation in bacteria, five additional pathways have been discovered (reductive TCA cycle, reductive acetyl-CoA pathway, 3-hydroxypropionate cycle, the 3-hydroxypropionate/4-hydroxybutyrate cycle, the dicarboxylate/4-hydroxybutyrate cycle) (Tang et al. 2011). So far no AAnP bacteria, which possesses a known with a completely annotated autotrophic carbon fixation pathway (Tang et al. 2011).

Recently, transcriptional profiling in different light regimes revealed expression changes of potential genes of the 3-hydroxypropionate (3-HP) cycle in *D. shibae* DFL-12, a member of the AAnP of the *Roseobacter* clade (Tomasch et al. 2011). The 3-HP cycle is one of three CO_2 fixation pathways discovered in photosynthetic bacteria to date (Hügler et al. 2011). In light of the high abundance of *Roseobacter* in the marine environment, there is high interest in quantifying their ability to fix CO_2. In addition to *D. shibae*, other *Roseobacter* members possess genes of this pathway and a mixotrophic co-metabolization of CO_2 and organic carbon emerges from their genomic repertoire (Swingley et al. 2007). It is tempting to conclude, but not scientifically proven, that there is a significant contribution of the clade to CO_2 fixation, which would have a strong impact on our understanding of marine carbon cycling.

2.4. Strategies against oxidative stress in the marine environment

In the marine environment, oxidative stress is prevalent. Especially the exposure to visible and ultraviolet radiation (Lesser 2012) or to phototrophic organisms (Berghoff et al. 2011), results in the generation of reactive oxygen species (ROS). Predominantly, free radicals of oxygen, known to be toxic, belong to ROS (Lesser 2006) and are produced during the reduction of molecular oxygen to water via superoxide radicals, singlet oxygen, hydrogen peroxide and hydroxyl radicals (Halliwell et al. 1984). Organisms try to keep these intermediates on a low level, to avoid damages of DNA, proteins and lipids, especially caused by hydroxyl radicals (Lesser 2006). For organisms, living in the marine realm, it is important to be adapted to such oxidative conditions. Thus they have developed antioxidant defence mechanisms. One mechanism is the reduction of ROS by different enzymes, the superoxide dismutase, peroxidases or catalases (Lesser 2006, Morano et al. 2012). High amounts of reduction potential in form of NADPH is used by many of these mechanisms (Pollak et al. 2007, Krömer et al. 2008) and supports the defense of oxidative stress (Storz et al. 1999, Singh et al. 2007, Storz et al. 1990). The production of this cofactor correlates the metabolic pathway directly to oxidative stress tolerance. The PP pathway and the ED pathway are known to provide enhanced redox power in form of NADPH and *P. putida* is known to have a robust resistance to oxidative stress mainly because it uses these pathways to metabolize glucose (Chavarría et al. 2013). During the same study, forcing *P. putida* to use the EMP pathway instead, decreased the resistance to oxidative stress significantly. Also *P. aeruginosa*, another exceedingly ED pathway pathway using organism, provides more NADPH than needed for anabolism and shows a better tolerance to oxidative stress (Berger et al. 2014). Among marine bacteria, resistance against UV radiation is common for *Gammaproteobacteria* and *Bacteroidetes*, while *Alphaproteobacteria* show a higher sensitivity. The *Roseobacter* clade especially seems to be better equipped with defense mechanisms against photo-oxidative stress (Alonso-Sáez et al. 2006) and also well prepared to live in strong association to marine algae, another stress causing situation (Wagner-Döbler et al. 2010, Seyedsayamdost et al. 2011).

To study resistance against oxidative stress, it is possible to quantify the supply of reducing power (NADPH) from the intensively studied stoichiometry of the central metabolic pathways combined with metabolic flux data (Berger et al. 2014). Another way is to investigate the tolerance to diamide or hydrogenperoxide (Chavarría et al. 2013), known as oxidative stress causing reagents (Pócsi et al. 2005). Diamide is known to be membrane-

permeable, it oxidizes sulfhydryl bonds in the cytoplasm of the cell and is in the following reduced by NADPH (Cumming et al. 2004, Storz et al. 1999, Morano et al. 2012). This can be measured in a plate-based assay including a filter disc supplemented with diamide causing an area of growth inhibition corresponding to the sensitivity to oxidative stress (Chavarría et al. 2013). In microtiter plate assays with diamide, added in the middle of the exponential growth phase, the inhibition/degradation time is used as direct correlation to oxidative stress sensitivity (Chavarría et al. 2013).

2.5. ^{13}C metabolic flux analysis

The field of systems biology, to understand microorganisms in total, increased enormously during the last years. Beyond focusing on only genomic, transcriptomic, proteomic, metabolomic or fluxomic data, the interpretation of these data reveals another level of information hiding in these multi-omics data (Kohlstedt et al. 2010, Zhang et al. 2010). Especially in the field of systems metabolic engineering, these technologies get a high level of attention (Kohlstedt et al. 2014, Stephanopoulos 1999) and the importance of fluxome analysis increased (S. Kind et al. 2013, Becker et al. 2013).
Metabolic flux analysis is about the investigation of *in vivo* flux distributions using substrates labeled with stable isotopes. For bacterial research, organic substrates are frequently used with ^{13}C labeled carbon atoms. Feeding the studied cells with these labeled substrates leads to incorporation into metabolites and furthermore into cell components, which can then be analyzed and used to deduce flux distributions within the cell. So, these informations can elucidate the flux through metabolic pathways (Wittmann 2007, Sauer 2006, Tang et al. 2012) or even identify new pathways (Reisch et al. 2013, Peyraud et al. 2009, Christensen et al. 2000).

2.5.1. ^{13}C MFA under steady state conditions

The aim of metabolic flux analysis (MFA) is the quantification of *in vivo* carbon fluxes. The ^{13}C labeling measurements are mostly performed by GC-MS analysis of all constituents derived from tracer studies and were originally used for biomedical purposes (Wittmann 2007, Antoniewicz 2013). Thereby ^{13}C metabolic flux analysis generally consists of two different parts, one experimental and one computational part (Figure: 2.2). In the experimental part, labeling studies are carried out, using stable isotopes. During the experimental part, the organism is cultivated on a defined medium, supplemented with the labeled carbon source (Wittmann 2007, Tang et al. 2012, Sauer 2006).

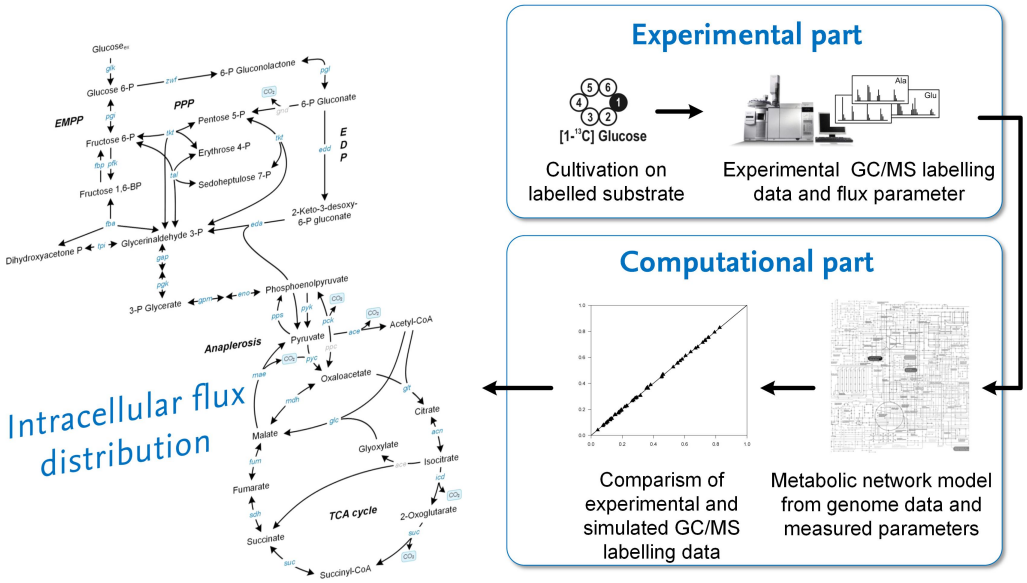

Figure 2.2.: Scheme of metabolic flux analysis, comprising an experimental part with labeling studies and a computational part simulating the metabolic network to determine the intracellular flux distribution (Wittmann 2007).

A common substrate is glucose used with labeling in different carbon atoms: [1-^{13}C], [6-^{13}C], [1,2-$^{13}C_2$], [1,6-$^{13}C_2$], [U-$^{13}C_6$] or mixtures of different labellings (Yang et al. 2005, Antoniewicz 2013). The substrate is metabolized during growth and the labeled carbon atoms are transferred into metabolites and finally into cell components, such as proteins. During metabolic steady state, generally occurring during exponential growth or in a chemostat, all internal fluxes remain stable, ending in a stable isotopic labeling pattern of all substances, involved in the metabolic network (isotopic steady state) (Wittmann 2007, Wiechert 2001, Schmidt et al. 1999). This timely stable state of the cell can be used not only to use the labeling information of small pool size metabolites, but also that from amino acids incorporated into cell protein, representing mostly 30-50 % of cell dry weight. Labeling of these protein bound amino acids refers to precursors of the central carbon metabolism and gives indirect information about the labeling in these intermediates (Szyperski 1995, Sauer 2006). Figure: 2.3 shows, which precursors leads to which amino acid during growth. The most important amino acids correspond directly to the carbon backbone of the precursor (alanine → pyruvate, serine → 3-phosphoglycerate, aspartate → oxaloacetate, glutamate → α-ketoglutarate and histidine → ribulose 5-phosphate). The complete relation of carbon skeleton between amino acid and precursor can be found at Wittmann (2007).

An easy way to determine the labeling in the protein bound amino acids is GC-MS

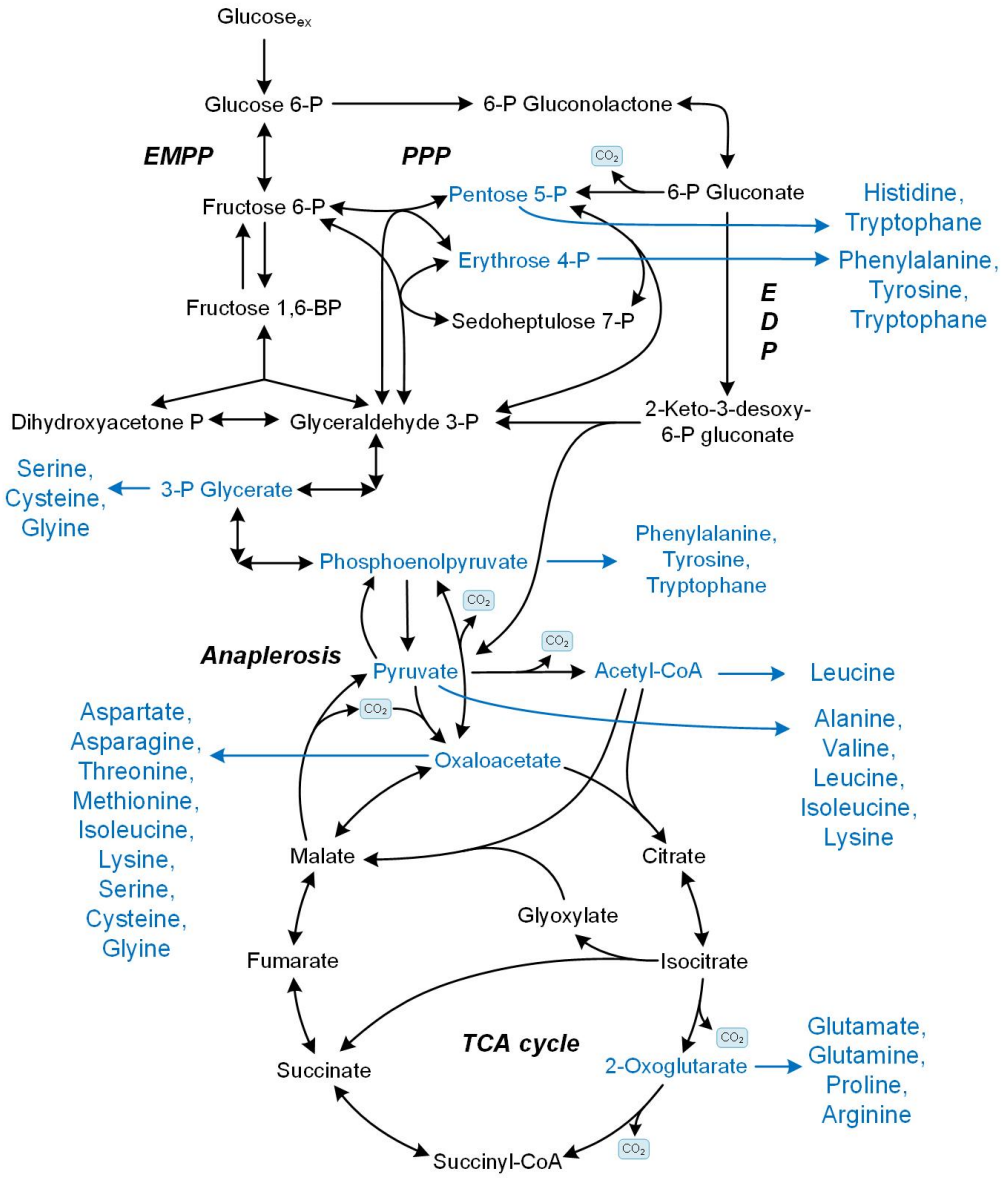

Figure 2.3.: Amino acid precursors of the central metabolic pathways (Wittmann 2007).

(Wittmann et al. 2002, Dauner et al. 2000). After hydrolysis of all protein into amino acids these are derivatized with MBDSTFA (N-methyl-N-tert-butyldimethylsilyl-trifluoro-acet-amide) to get TBDMS (tert-butyldimethylsilyl) derivates through silylation of -NH, -OH and -SH groups of the amino acid (Figure: 2.4). The derivates are more volatile for GC analysis (Dauner et al. 2000, Leighty et al. 2012, Wittmann 2007). During analysis substances are fragmented in the MS, with the post prominent fragments shown in Figure: 2.4. Fragment a $(M\text{-}15)^+$ and b $(M\text{-}57)^+$ contain the entire carbon backbone of the amino acid, while in fragment, c $(M\text{-}85)^+$ and d $(M\text{-}159)^+$ the carbon atom 1 is missing. The two last fragments, generated by cracking at e, contain C_1 and C_2 for

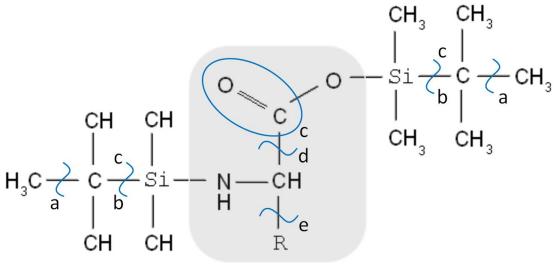

Figure 2.4.: TBDMS derivate of an amino acid (in gray) with fragments detected in GC-MS comprising the following fragments: a = $(M\text{-}15)^+$, b = $(M\text{-}57)^+$, c = $(M\text{-}85)^+$, d = $(M\text{-}159)^+$, e = $(f302)^+$ consisting of the upper part and $(sc)^+$ containing only the -R group (Dauner et al. 2000).

$(f302)^+$ and the side chain R of the amino acid in $(sc)^+$. From such fragments, the abundance of the different masses containing ^{12}C and ^{13}C in different counts are measured to get the ratio of M_0 (completely unlabeled), to M_{n+1} (fully labeled) (Dauner et al. 2000). These data provides enough information for network modeling. They can also be used for qualitative analysis on pathway usage as shown by Fürch et al. (2009) and Berger et al. (2014).

The first step of the computational part is the creation of a metabolic model describing all reactions of the central metabolic pathway, extracted from genomic data and validated by specific tests on activity of key enzymes. The model contains the determinable fluxes into biomass, products and from substrates. Information of theses reactions is extracted from biomass composition, product formation rates and substrate uptake rate, respectively, generated during labeling experiments. All other fluxes are calculated by a balancing analysis based on the measurements of selected mass isotopomer distributions by varying the free fluxes of the stoichiometric matrix until the deviation of the measured and simulated labeling data reaches a specific cut off value (Kohlstedt et al. 2010, Wittmann 2007). One favorite and current tool for calculation of these fluxes is the MATLAB based open source modeling software OpenFLUX (Quek et al. 2009, Berger et al. 2014, Becker et al. 2013, Nocon et al. 2014). This software uses one of the most efficient modeling strategies of elementary metabolite units (EMU) (Antoniewicz et al. 2007a, Young et al. 2008), a correction for naturally occurring labellings and a tool for statistical evaluation of the results (Quek et al. 2009). In the end, the fluxes and deviation can be assembled to a metabolic flux map.

2.5.2. Dynamic labeling incorporation for pathway identification

Another possibility for analysis of metabolic pathways is a dynamical, non-stationary approach (Hörl et al. 2013, Nöh et al. 2007, Peyraud et al. 2009, Wiechert et al. 2013). As described in Figure: 2.5, cells are first cultivated in unlabeled defined medium. At the time point of metabolic steady state, labeled substrate is added or the cells are transferred into labeled medium. To determine the successive labeling enrichment in the metabolome, a short time sampling is necessary (Peyraud et al. 2009, Nöh et al. 2007). Therefore different quenching methods are established to stop the metabolism instantaneously after sampling (Schneider et al. 2012, Bolten et al. 2008). The labeling of metabolites of the central carbon metabolism, free amino acids (Nöh et al. 2007, Okahashi et al. 2014, Krömer et al. 2004) or CoA-esters (Peyraud et al. 2009) are determined. Depending on the information needed, another possibility is to additionally specify the slower incorporation for example in the cell protein (Antoniewicz et al. 2007b). Measuring the labeling of metabolites can either be done by LC-MS or GC-MS analysis as described above (Chapter: 2.5.1). The time dependent incorporation of the labeling provides different information. Fluxes and pool sizes can be calculated as well as networks

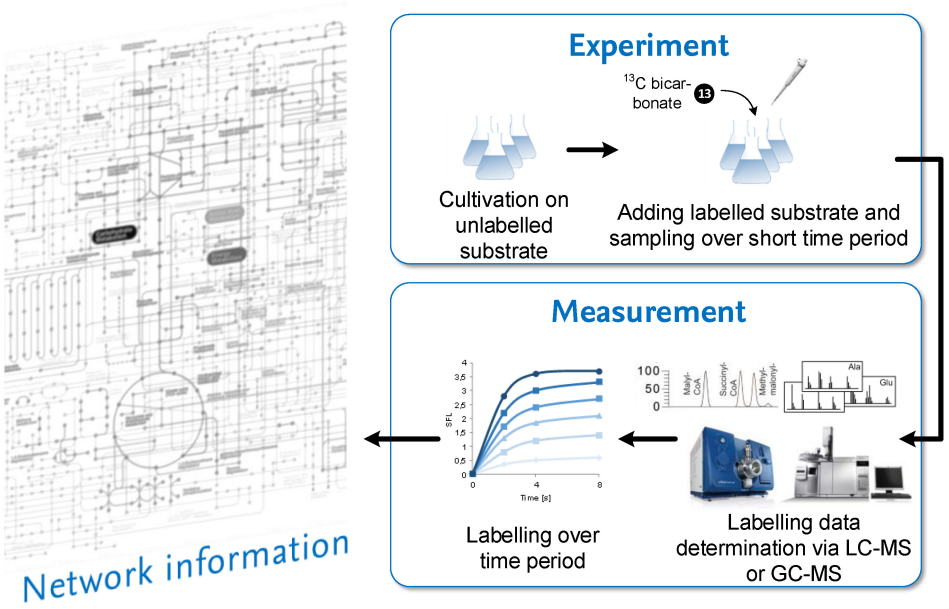

Figure 2.5.: Scheme of dynamic labeling experiment for pathway identification, comprising an experimental part with fast labeling studies and an analytical part determining the intracellular labeling incorporation over the time period to get information about the sequence of reactions of incorporation as pathway (Peyraud et al. 2009).

can be identified (Wiechert et al. 2013, Nicolae et al. 2014, Nöh et al. 2007). The data can also be used for MFA (Okahashi et al. 2014, Jordà et al. 2013, Young et al. 2008). Especially for network identification, the calculation of the complete labeling enrichment and the sum fractional labeling is necessary, to increase the information gain from labeling data. For example, the time dependent increase of the sum fractional labeling in metabolites within the sequence of a certain pathway is used for pathway identification, as described by Peyraud et al. (2009).
Both methods were successfully used in the past for analyzing bacterial metabolisms and will be applied in the following work to elucidate the central carbon core metabolism of the marine bacterium *D. shibae*.

3. Material and Methods

3.1. Bacterial strains

In Table 3.1 all used strains from the present work were listed. The genome-sequenced wild type strain *D. shibae* DFL-12 (DSM 16493) was obtained from the German Collection of Microorganisms and Cell Cultures (DSMZ, Braunschweig, Germany). The quorum sensing mutants *D. shibae* $\Delta luxI_1$ and $\Delta luxR_1$ were provided by the Helmholtz Centre for Infection Research from their previous work (Patzelt et al. 2013). *C. glutamicum* (ATCC 13032) was obtained from the American Type Culture Collection (Manassas, Virginia, USA) and *P. putida* (DSM 6125) from the German Collection of Microorganisms and Cell Cultures (DSMZ, Braunschweig, Germany).

Table 3.1.: Bacterial strains used in this study

Strain	Modification	Reference
Dinoroseobacter shibae DFL-12 (DSM 16493)	Wild-type	DSMZ Braunschweig
Dinoroseobacter shibae DFL-12 $\Delta luxI_1$	-$luxI_1$	(Patzelt et al. 2013)
Dinoroseobacter shibae DFL-12 $\Delta luxR_1$	-$luxR_1$	(Patzelt et al. 2013)
Corynebacterium glutamicum (ATCC 13032)	Wild-type	ATCC Manassas, USA
Pseudomonas putida KT 2440 (DSM 6125)	Wild-type	DSMZ Braunschweig

3.2. Medium composition

All chemicals were purchased from Sigma Aldrich (Steinheim, Germany), Merck (Darmstadt, Germany) and Fluka (Buchs, Switzerland), respectively, and were of analytical grade. In pre-cultures of *D. shibae* and *P. putida* the complex medium Marine broth (MB 2216, Becton Dickinson Franklin Lakes, USA) was applied and for agar plates, the medium was supplemented with 1.5 % agar (Table: 3.2). The second pre-cultivation and main cultivations were conducted in an optimized synthetic mineral salt seawater medium (SWM, Table: 3.3). Therefore all solutions were mixed at room temperature prior to inoculation (Table: 3.4). This medium was developed in this work based on

original artificial seawater medium (oSWM, Table: 3.6) mixed prior to inoculation (Table: 3.5). The medium is supplemented with the suitable substrate listed in Table 3.7. For labeling experiments, 99 % [^{13}C] sodium bicarbonate, 98-99 % [1-^{13}C] D-Glucose and 99 % [1,4$^{13}C_2$] succinic acid (Cambridge Isotope Laboratories Inc., Andover, USA) were used.

Cultivations of *C. glutamicum* were conducted in complex brain heart infusion medium (BHI, Becton Dickinson Franklin Lakes, USA) and was applied and for agar plates, the medium was supplemented with 1.5 % agar (Table: 3.8). For the detection of substrate specific enzyme activities a minimal medium supplemented with the suitable substrate was used (Table: 3.9).

Table 3.2.: Composition of complex medium Marine Broth

Component	**Concentration**
Difco Marine Broth (MB 2216)	37.4 g l^{-1}
Agar (Agar plates)	15 g l^{-1}
In aqua dest., autoclaved (121°C, 20 min)	

Table 3.3.: Solutions for modified artificial seawater medium (SWM) developed in this work

Solution 2	**Component**	**Concentration**
	KH_2PO_4	0.5 g l^{-1}
	In aqua dest., pH 8, autoclaved (121°C, 20 min)	

Solution 3	**Component**	**Concentration**
	NH_4Cl	2.5 g l^{-1}
	$NaSO_4$	40.0 g l^{-1}
	In aqua dest., pH 8, autoclaved (121°C, 20 min)	

Solution 4	**Component**	**Concentration**
	$MgCl_2 \times 6\ H_2O$	300.0 g l^{-1}
	In aqua dest., pH 8, autoclaved (121°C, 20 min)	

Solution 5	**Component**	**Concentration**
	$CaCl_2 \times 2\ H_2O$	15.0 g l^{-1}
	In aqua dest., pH 8, autoclaved (121°C, 20 min)	

Solution 6	**Component**	**Concentration**
	$NaHCO_3$	19.0 g l^{-1}
	In aqua dest., pH 8, autoclaved (121°C, 20 min)	

Solution 7	Component	Concentration
	NaCl	200.0 g l^{-1}
	KCl	5.0 g l^{-1}
	In aqua dest., pH 8, autoclaved (121°C, 20 min)	

Solution 8	Component	Concentration
	Triplex III (Na_2EDTA)	5.2 g l^{-1}
	In aqua dest., pH 12, sterile filtered	

Solution 9	Component	Concentration
	$Fe(SO_4) \times 7\ H_2O$	2.1 g l^{-1}
	H_3BO_3	0.03 g l^{-1}
	$MnCl_2 \times 4\ H_2O$	0.1 g l^{-1}
	$CoCl_2 \times 6\ H_2O$	0.19 g l^{-1}
	$NiCl_2 \times 6\ H_2O$	0.024 g l^{-1}
	$CuCl_2 \times 2\ H_2O$	0.002 g l^{-1}
	$ZnSO_4 \times 7\ H_2O$	0.144 g l^{-1}
	$Na_2MoO_4 \times 2\ H_2O$	0.036 g l^{-1}
	In aqua dest., pH 8, autoclaved (121°C, 20 min)	

Solution 10	Component	Concentration
	Biotin	0.2 g l^{-1}
	Niacin	2.0 g l^{-1}
	4-Aminobenzoic acid	0.8 g l^{-1}
	In aqua dest., pH 8, sterile filtered	

Table 3.4.: Final composition of SWM

Solution	Volume
1	25 ml
2	400 mL
3 + 7	100 ml
4	30 ml
5 + 6	10 ml
8 + 9	2 ml
10	20 ml
Aqua dest.	301 ml
	1000 ml

Table 3.5.: Final composition of original SWM

Solution	Volume
1	10 ml
2	100 mL
3	10 ml
4	1 ml
5	10 ml
Aqua dest.	869 ml
	1000 ml

Table 3.6.: Solutions for original artificial seawater medium (oSWM)

Solution 2: SWM-Basis	**Component**	**Concentration**
	KH_2PO_4	2.0 g l^{-1}
	NH_4Cl	2.5 g l^{-1}
	$NaSO_4$	40.0 g l^{-1}
	$MgCl_2 \times 6\ H_2O$	30.0 g l^{-1}
	$CaCl_2 \times 2\ H_2O$	1.5 g l^{-1}
	NaCl	200.0 g l^{-1}
	KCl	5.0 g l^{-1}
	In aqua dest., pH 8, autoclaved (121°C, 20 min)	

Solution 3: Carbonate	**Component**	**Concentration**
	$NaHCO_3$	19.0 g l^{-1}
	In aqua dest., pH 8, autoclaved (121°C, 20 min)	

Solution 4: Trace elements	**Component**	**Concentration**
	Triplex III (Na_2EDTA)	5.2 g l^{-1}
	$Fe(SO_4) \times 7\ H_2O$	2.1 g l^{-1}
	H_3BO_3	0.03 g l^{-1}
	$MnCl_2 \times 4\ H_2O$	0.1 g l^{-1}
	$CoCl_2 \times 6\ H_2O$	0.19 g l^{-1}
	$NiCl_2 \times 6\ H_2O$	0.024 g l^{-1}
	$CuCl_2 \times 2\ H_2O$	0.002 g l^{-1}
	$ZnSO_4 \times 7\ H_2O$	0.144 g l^{-1}
	$Na_2MoO_4 \times 2\ H_2O$	0.036 g l^{-1}
	In aqua dest., pH 8, autoclaved (121°C, 20 min)	

Solution 5: Vitamins	**Component**	**Concentration**
	Biotin	0.2 g l^{-1}
	Niacin	2.0 g l^{-1}
	4-Aminobenzoic acid	0.8 g l^{-1}
	In aqua dest., pH 8, sterile filtered	

Table 3.7.: Substrate solutions for minimal medium

Solution 1a	**Component**	**Concentration**
	Succinic acid	47.2 g l^{-1}
	In aqua dest., pH 8, autoclaved (121°C, 20 min)	

Solution 1b	**Component**	**Concentration**
	Glucosemonohydrate	79.2 g l^{-1}

	In aqua dest., pH 8, autoclaved (121°C, 20 min)

Solution 1c	Component	Concentration
	Acetic acid Na-salt	32.75 g l^{-1}
	In aqua dest., pH 8, autoclaved (121°C, 20 min)	

Solution 1d	Component	Concentration
	Propionate Na-salt	38.4 g l^{-1}
	In aqua dest., pH 8, autoclaved (121°C, 20 min)	

Table 3.8.: Composition of complex medium BHI

Component	Concentration
BHI	37 g l^{-1}
Agar (Agar plates)	15 g l^{-1}
In aqua dest., autoclaved (121°C, 20 min)	

Table 3.9.: Solutions for minimal medium used for the cultivation of *C. glutamicum*

Solution A	Component	Concentration
	NaCl	2.00 g l^{-1}
	$CaCl_2$	0.11 g l^{-1}
	$MgSO_4 \times 7\ H_2O$	0.40 g l^{-1}
	In aqua dest., autoclaved (121°C, 20 min)	

Solution B	Component	Concentration
	$(NH_4)_2SO_4$	150.0 g l^{-1}
	In aqua dest., pH 7, autoclaved (121°C, 20 min)	

Buffer solution	Component	Concentration
	K_2HPO_4	316.0 g l^{-1}
	KH_2PO_4	77.0 g l^{-1}
	In aqua dest., pH 7.8, autoclaved (121°C, 20 min)	

Fe Solution	Component	Concentration
	$Fe(SO_4) \times 7\ H_2O$	2.0 g l^{-1}
	In aqua dest., pH 1, sterile filtered	

Trace element solution	Component	Concentration
	$FeCl_3 \times 6\ H_2O$	0.20 g l^{-1}
	$MnSO_4 \times H_2O$	0.20 g l^{-1}
	$ZnSO_4 \times H_2O$	0.05 g l^{-1}
	$CuCl_2 \times 2\ H_2O$	0.02 g l^{-1}
	$Na_2B_4O_7 \times 10\ H_2O$	0.02 g l^{-1}
	$Na_2MoO_4 \times 4\ H_2O$	0.01 g l^{-1}
		In aqua dest., sterile filtered

Vitamin solution	Component	Concentration
	Biotin	0.025 g l^{-1}
	Thiamin × HCl	0.05 g l^{-1}
	Pantothenic acid Ca-salt	0.05 g l^{-1}
		In aqua dest., pH 1, sterile filtered

DHB solution	Component	Concentration
	3,4-dihydroxybenzoic acid	30.0 g l^{-1}
	NaOH (6M)	50 mL
		In aqua dest., sterile filtered

Glucose solution	Component	Concentration
	Glucose	0.10 g l^{-1}
		In aqua dest., autoclaved (121°C, 20 min)

Acetate solution	Component	Concentration
	Acetate Na-salt	32.75 g l^{-1}
		In aqua dest., autoclaved (121°C, 20 min)

Table 3.10.: Composition of minimal medium used for the cultivation of *C. glutamicum*

Solution	Volume
A	500 mL
B + Buffer	100 ml
Glucose or Acetate	100 ml
Vitamin	20 ml
Fe + Trace element	10 ml
DHB	1 ml
Aqua dest.	301 ml
	1000 ml

3.3. Cultivation

3.3.1. Cryoconservation

For long-time cryoconservation, *D. shibae* was grown in complex medium (MB medium) under permanent light. In the exponential growth phase, 0.5 ml of broth were harvested at an OD_{650} of 0.8 and mixed with 0.5 ml of 60 % glycerol stock solution. After shaking of the tubes, the cells were frozen directly at -80°C. All strains of *D. shibae* were stored at -80°C.

3.3.2. Cultivation in shake flasks

For standard cultivations in shake flasks, cells from glycerol stocks were first streaked out on MB agar plates, incubated for 2 days at 30°C, and were then used as the inoculum for pre-cultivation in liquid culture. Illumination settings (dark or light) were adjusted to the subsequent settings of the cultivation. To this end, the shaker was equipped with an illumination unit (3 × 18 W Biolux, Osram, Munich, Germany). For main cultivations in permanent light, the illumination condition of the pre-culture was accordingly adjusted. All other pre-cultures were grown in the dark.
Pre-cultivation was inoculated with a colony of *D. shibae*, and conducted for 12 h in 25 ml of MB medium in 250-ml baffled shake flasks. The cells were then harvested by centrifugation (5,000 × *g*, 5 min, 4°C), washed with sterile 0.9 % NaCl and used as inoculum for the second pre-cultivation in SWM. The second pre-culture was inoculated to an OD_{650} of 0.05. After 24 h, cells were harvested as described above. The main cultivation (25 ml of SWM medium in 250-ml baffled shake flasks) was then inoculated to an initial OD_{650} of 0.001. All main cultivations were conducted in triplicate at 30°C on an orbital shaker (180 rpm, Certomat BS-1, shaking diameter 50 mm, Sartorius AG, Göttingen, Germany).

3.3.3. Cultivation of *C. glutamicum* as control for enzymatic assays

For standard cultivations in shake flasks cells from glycerol stocks were first streaked on BHI agar plates, incubated for 1 day at 30°C and then used as the inoculum for pre-cultivation in liquid culture. Pre-cultivation was conducted with one colony of *C. glutamicum* for 12 h in 25 ml of BHI medium in 250-ml baffled shake flasks. The cells were then harvested by centrifugation (5,000 × *g*, 5 min, 4°C), washed with sterile 0.9 % NaCl and used as inoculum for the second pre-cultivation in minimal medium. The second

pre-culture was inoculated to an initial optical density of 0.05 and after 12 h, the cells were harvested for the main cultivation. The main cultivation (25 ml of minimal medium in 250-ml baffled shake flasks) was then inoculated with an initial OD_{660} of 0.05. All main cultivations were conducted at 30°C on an orbital shaker (180 rpm, Certomat BS-1, shaking diameter 50 mm, Sartorius AG, Göttingen, Germany). During main cultivations the growth is monitored by measuring the optical density.

3.4. Analytical methods

3.4.1. Quantification of cell concentration

Measurement of optical density

Cell concentration was measured as optical density at 650 nm (OD_{650}) using a photometer (Libra S11, Biochrom Ltd, Cambridge, England). To avoid osmotic effects during measurement, samples were diluted with 24 g l^{-1} of NaCl solution, corresponding to the salinity of the medium.

Determination of bio dry weight

The bio dry weight (BDW) for *D. shibae* grown on SWM with succinic acid and glucose as carbon source, respectively, was determined gravimetrically. To this end, cells from 15 ml of cultivation broth were harvested by centrifugation (10 min, 5,000 × *g*, room temperature) in pre-dried and weighted falcon tubes (80°C, 2 days) and washed once with water. Then, the washed cells were dried at 80°C until constant weight (Driouch et al. 2010).

Correlation of optical density and bio dry weight

The correlation factor between BDW and OD_{650} was determined to 0.383 g_{BDW} per OD_{650} for glucose and 0.323 g_{BDW} per OD_{650} for succinic acid (Figure: 3.1). The difference between the correlations for two carbon sources based on differences in the shape of the cells (Patzelt et al. 2013) and their PHB content (see below).

3.4.2. Quantification of organic acids

Organic acids in the cultivation broth were quantified by HPLC (La Chrome Elite® HPLC, HWR-Hitachi International HPLC, Darmstadt, Germany). Therefore 500 µl cultivation broth was harvested (10 min, 5,000 × *g*, 4°C) and the supernatant was frozen at

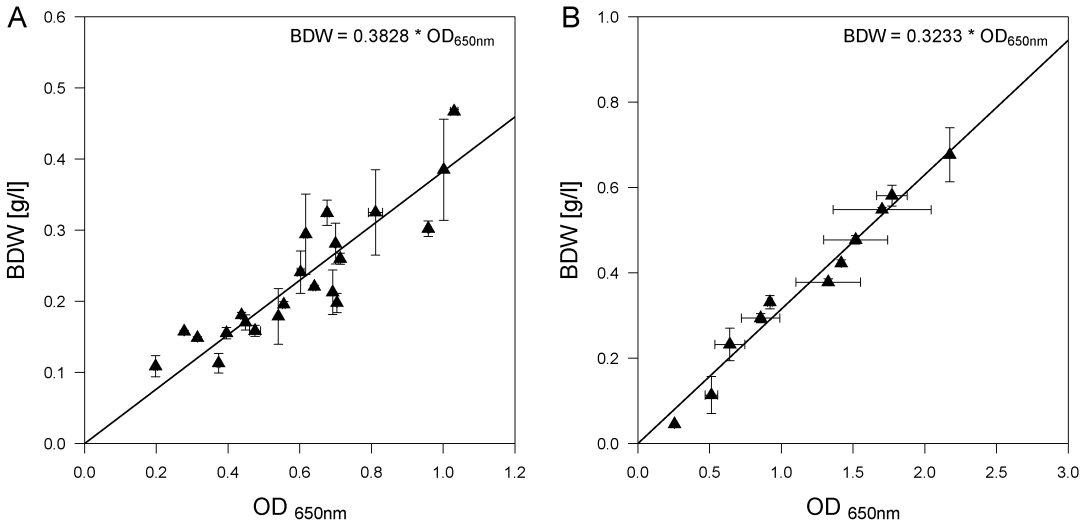

Figure 3.1.: Correlation of bio dry weight and optical density for *D. shibae* SWM with glucose (A) and succinic acid (B) as sole carbon source

-18°C. After thawing of the sample, 10 µl 1 M H_2SO_4 were added and precipitated proteins were removed by centrifugation (10 min, 5,000 × *g*, 4°C). For the quantification, the samples and standards with defined concentrations were separated on an Aminex HPX-87H column (300 mm × 7.8 mm; Bio-Rad, Hercules, USA) at 45°C with 12 mM H_2SO_4 as mobile phase with a flow rate of 0.5 ml min^{-1}. For detection, the refraction index or UV absorption at a wavelength of 220 nm was used.

3.4.3. Quantification of glucose

The concentration of glucose in the cultivation broth was measured by a glucose analyser (YSI 2700 select, YSI Incorporated, Yellow Spring, USA). Before measurement, 500 µl cultivation broth was centrifuged (10 min, 5,000 × *g*, 4°C) and then the glucose concentration of the supernatant was measured.

3.4.4. Quantification of amino acids

To determine the concentration of amino acids in the cultivation broth, 500 µl were harvested (10 min, 5,000 × *g*, 4°C). Therefrom, a 100 µl aliquot was dried under constant airflow and resuspended in 1 ml 200 mM ABU (α-aminobutyric acid) as internal standard. Quantification was then conducted via HPLC (Agilent 1200 Series, Agilent Technologies GmbH, Santa Clara Californien, USA) as described before (Krömer et al. 2005). To avoid the interfering of disulfide bridges with the derivatisation reagent, the samples were

pretreated with 2-mercaptopropionate (0.5 % in 0.4 M borat buffer) and then capped with iodacetic acid (50 mg ml^{-1} in 0.4 M borat buffer) as described earlier (Carducci et al. 1999). Afterwards, the analytes were derivatised using O-phtaldialdehyde (OPA) before seperating them via a reversed phase column (Gemini 5µ C18 110A, 150 x 4.6 mm, Phenomenex, Aschaffenburg, Germany) equipped with a pre-column (Gemini C18, MAX-RP, 4 x 3 mm; Phenomenex, Aschaffenburg, Germany) with a gradient of eluent A (40 mM NaH_2PO_4, pH 7.8) and eluent B (45 % methanol, 45 % acetonitrile, 10 % water) with a flow rate of 1 ml min^{-1} at 40 °C (Table: 3.11). For the detection of the OPA-derivated amino acids, a fluorescence detector (340 nm excitation, 540 nm emission; Agilent, Waldbronn, Germany) was used.

Table 3.11.: Gradient of eluent A and B for the determination of amino acids with HPLC

Time [min]	Eluent A [%]	Eluent B [%]
0.0	100.0	0.0
40.5	59.5	40.5
41.0	39.0	61.0
43.0	39.0	61.0
57.5	0.0	100.0
59.5	0.0	100.0
60.5	25.0	75.0
61.5	50.0	50.0
62.5	75.0	25.0
63.5	100.0	0.0
65.5	100.0	0.0

3.4.5. Enzymatic assays

The cultivation of *D. shibae* and *C. glutamicum* for enzymatic assays was carried out the same way as described in chapters: 3.3.2 and 3.3.3 with slight differences: The main cultivation was carried out in 500 ml baffled shake flasks filled with 50 ml broth and started with an initial optical density of 0.02 for succinic acid and acetate medium and 0.1 for minimal medium supplemented with glucose. In the middle of the exponential growth phase at OD_{650} of 1.0 the cells were harvested (5,000 × *g*, 5 min, 4°C) and washed twice with 0.9 % NaCl solution cooled to 4°C. Afterwards the cells were resuspended in 2 ml cell disruption buffer per g cell wet weight and then disrupted using a FastPrep (FastPrep®-24 Instrument, MP Biomedicals, Santa Ana, California, USA) for 20 s with glass beads (∅ 0.15 - 0.25 mm). In the following, the cell debris was centrifuged (5,000 × *g*, 5 min, 4°C) and the supernatant was used for enzyme activity tests. To assure a sufficient protein concentration for further analysis, the protein content of the cell extract was

determined with bicinchoninic acid by using a commercial kit (Thermo Fisher Scientific, Rockford, USA). To minimize enzyme degradation, all steps were carried out on ice.

Quantification of enzyme activity

Enzyme activities were determined in micro plate based assays. Usually, a master mix was prepared from stock solutions of cell disruption buffer, cofactors and coupling enzymes and incubated for 10 min at reaction temperature of 30 °C to avoid influences of changing temperatures. For the enzymatic reaction, 5 µL of substrate solution and 5 µL cell extract were provided in a 96 well microtest plate (Kisker Biotech GmbH & Co. KG, Steinfurth, Germany) and the measurement was started by addition of 190 µl master mix to a total volume of 200 µL. The time rate of change in absorbance was monitored in a Tecan Microplate Reader (Sunrise^{TM}, Tecan Trading AG, Männedorf, Switzerland). Negative controls were carried out without substrate and without cell extract, respectively, and all measurements were performed in triplicate.
Enzyme activity was generally calculated as specific enzyme activity [U mg^{-1}] with 1 U = 1 µmol min^{-1} at 30 °C from the change in absorbance [A min^{-1}] and the specific extinction coefficient (ε_{340} = 6.22 L $mmol^{-1}$ cm^{-1} for NAD(P)H and ε_{412} = 13.6 L $mmol^{-1}$ cm^{-1} for DTNB).

Table 3.12.: Composition of the standard cell disruption buffer

Component	Concentration
Tris	100 mM
$MgCl_2$	10 mM
DTT	0.75 mM
EDTA	1 mM
	pH 7.8

Glucose 6-phosphate dehydrogenase

The harvesting of the cells was carried out in standard cell disruption buffer. NADP or NAD were added as cofactor to determine the cofactor dependency. The reaction mix for measuring the glucose 6-phosphate dehydrogenase activity contained 100 mM Tris/HCl (pH 7.8), 10 mM $MgCl_2$, 0.75 mM DTT, 1 mM EDTA, 5 mM NADP/NAD, 1 mM glucose 6-phosphate and 5 µl crude cell extract.

6-Phosphogluconate dehydrogenase

The harvesting of the cells was carried out in standard cell disruption buffer. NADP or NAD were added as cofactor to determine the cofactor dependency. The reaction mix for measuring the 6-phosphogluconate dehydrogenase activity contained 100 mM Tris/HCl (pH 7.8), 10 mM $MgCl_2$, 0.75 mM DTT, 1 mM EDTA, 5 mM NADP/NAD, 1 mM 6-phosphogluconate and 5 µl crude cell extract.

Isocitrate dehydrogenase

The harvesting of the cells was carried out in standard cell disruption buffer. NADP or NAD were added as cofactor to determine the cofactor dependency. The reaction mix for measuring the isocitrate dehydrogenase activity contained 100 mM Tris/HCl (pH 7.8), 10 mM $MgCl_2$, 0.75 mM DTT, 1 mM EDTA, 5 mM NADP/NAD, 10 mM isocitrate and 5 µl crude cell extract.

6-Phosphogluconate dehydratase and KDPG aldolase

The harvesting of the cells was carried out in standard cell disruption buffer. NADH was added as cofactor, LDH was used as coupling enzyme and the reaction mix for measuring the activity of the 6-Phosphogluconate dehydratase and KDPG aldolase contained 100 mM Tris/HCl (pH 7.8), 10 mM $MgCl_2$, 0.75 mM DTT, 1 mM EDTA, 0.25 mM NADH, 20 U LDH, 2.5 mM glucose 6-phosphate and 5 µl crude cell extract. Due to conversion of NADH to NAD without cell extract added a high protein concentration of 6 mg ml_{-1} is essential for the measurement to overlay the high background activity.

Phosphofructokinase

The harvesting of the cells was carried out in a cell disruption buffer containing 150 mM Tris/HCl (pH 8.0), 0.2 M KCl, 1 mM ATP, 0.75 mM DTT, 5 % (v/v) glycerin, 5 mM $MgCL_2$, 50 mM K_3PO_4. NADH was added as cofactor and the reaction mix contained 100 mM Tris/HCl (pH 8.0), 5 mM $MgCl_2$, 195 mM KCl, 10 mM K_3PO_4, 0.25 mM NADH, 0.2 mM ATP, 0.5 U aldolase, 0.5 U glycerol 3-phosphate dehydrogenase, 1 U triosephosphate isomerase, 4 mM fructose 6-phosphate and 10 µl crude cell extract.

Fructose bisphophatase

The harvesting of the cells was carried out in standard cell disruption buffer. NADP was added as cofactor and the reaction mix for measuring the fructose bisphosphatase activity contained 100 mM Tris/HCl (pH 7.8), 10 mM $MgCl_2$, 0.75 mM DTT, 1 mM EDTA,

5 mM NADP, 2 U Phosphoglucose isomerase, 1 U glucose 6-phosphate dehydrogenase, 50 mM fructose-1,6-bisphosphate and 5 µl crude cell extract.

Malic enzyme

The harvesting of the cells was carried out in standard cell disruption buffer. NADP was added as cofactor and the reaction mix for measuring the malic enzyme activity contained 100 mM Tris/HCl (pH 7.8), 10 mM $MgCl_2$, 200 mM KCl, 0.75 mM DTT, 1 mM EDTA, 5 mM NADP, 40 mM malate and 5 µl crude cell extract.

Malate synthase

The harvesting of the cells was carried out in standard cell disruption buffer. DTNB was added as cofactor and the reaction mix for measuring the malate synthase activity contained 100 mM Tris/HCl (pH 7.8), 10 mM $MgCl_2$, 0.75 mM DTT, 1 mM EDTA, 0.2 mM DTNB, 0.25 mM acetyl-CoA, 1 mM glyoxylate and 5 µl crude cell extract.

Isocitrate lyase

The harvesting of the cells was carried out in standard cell disruption buffer. NADH was added as cofactor, LDH was used as coupling enzyme and the reaction mix for measuring the isocitrate lyase activity contained 100 mM Tris/HCl (pH 7.8), 10 mM $MgCl_2$, 0.75 mM DTT, 1 mM EDTA, 0.25 mM NADH, 20 U LDH, 10 mM Isocitrate and 5 µl crude cell extract. Due to conversion of NADH to NAD without cell extract added a high protein concentration of 6 mg ml_{-1} is essential for the measurement.

3.5. Determination of biomass composition

To determine fluxes in the carbon metabolism to biomass precursor, the main composition of biomass had to be determined. For this purpose, cells were grown as described above in a mineral salt medium with succinate or glucose as a carbon source. In the mid-exponential growth phase, the biomass was harvested by centrifugation (5,000 $\times$ *g*, 5 min, 4°C) and used for the quantification of protein, DNA, RNA, PHB and lipids. All analytics were conducted for three biological replicates with three technical replicates, each.

3.5.1. DNA content

To determine the DNA content, cells corresponding to 1.2 mg BDW, were first incubated for 30 min in 560 µl of lysis buffer (25 mM tris, 25 mM EDTA, 300 mM saccharose, 50 mg l^{-1} lysozyme) at 30°C. This was followed by mechanical disruption (2 × 4 min, 30 Hz, Ribolyzer MM301, Retsch, Haan, Germany) using glass beads with a diameter of 0.15 – 0.25 mm, and RNase treatment (140 µl of RES Buffer, 60 µg ml^{-1} of RNase A, Macherey-Nagel, Düren, Germany) for 30 min at 30°C. DNA was then extracted with 700 µl of phenol-chloroform-isoamyl alcohol (25:24:1, Carl-Roth GmbH, Karlsruhe, Germany), and phase separation was conducted by centrifugation (5,000 × *g*, 10 min, 4°C). The DNA-containing aqueous phase was transferred in a novel reaction tube. The DNA was then precipitated by adding 65 µl of sodium acetate (3 mol l^{-1}) and 1.3 ml of 100 % ethanol (5,000 × *g*, 20 min, 4°C). After a washing step with 70 % (v/v) ethanol, the dried DNA pellet was resuspended in 300 µl of ultra-pure water. Quantification was conducted with the Nanodrop photospectrometer at 260 nm (ND-1000, Peqlab Biotechnology GmbH, Erlangen, Germany). OD_{260} of 1 was equivalent to 50 ng $µl^{-1}$ DNA.

3.5.2. RNA content

RNA extraction from 0.4 mg BDW and subsequent quantification was conducted as described previously (Dauner et al. 2001). The cell pellet was initially washed twice with 1 ml 0.7 M $HClO_4$. After resuspending the pellet in 1 ml 0.3 M KOH, it was incubated for 60 minutes at 37°C for hydrolysis. Then 100 µl 3 M $HClO_4$ was added, the solution was centrifuged (5,000 × *g*, 2 min, room temperature) and the supernatant was collected. The pellet was washed twice with 450 µl $HClO_4$ and the supernatant was pooled. The RNA content was determined at wavelength of 260 nm with Nanodrop 1000 photospectrometer (ND-1000, Peqlab Biotechnology GmbH, Erlangen, Germany). OD_{260} of 1 was equivalent to 40 ng $µl^{-1}$ RNA.

3.5.3. PHB content

For quantification of the PHB content, cells corresponding to 0.4 mg BDW were hydrolyzed as previously described (Don et al. 1994), resuspended in 1 mL 2 M NaOH and incubated for 30 minutes at 100°C. The hydrolysis was stopped on ice and the sample was neutralized with an equivalent amount of 2 M HCl. After centrifugation (5,000 × *g*, 5 min, room temperature), the PHB content in the supernatant was determined by HPLC. PHB was quantified by HPLC (La Chrome Elite® HPLC, HWR-Hitachi Inter-

national HPLC, Darmstadt, Germany) using an Aminex HPX-87H column (300 mm × 7.8 mm; Bio-Rad, Hercules, USA) at 45°C with 12 mM H_2SO_4 as mobile phase, with a flow rate of 0.5 ml min^{-1} and UV detection at 210 nm. In parallel, standards with pure PHB (Sigma Aldrich, Steinheim, Germany) were analyzed in the same way.

3.5.4. Protein content

The cell protein from 0.4 mg BDW was extracted using the BugBuster® Protein Extraction Reagent (Novagene®, Leuven, Belgium) as recommended by the supplier. The harvested cells were resuspended in 200 µL of BugBuster® with 2 µL ml^{-1} Lysonase solution (Lysonase™ Bioprocessing Reagent, Merck KGaA, Darstadt, Germany) and shaked 30 min at 27°C. Subsequently the dell debris were seperated by centrifugation (5,000 × *g*, 5 min, 4°C) and the protein quantification was performed according to the bicinchoninic acid method using a Pierce commercial kit (Thermo Fisher Scientific, Rockford, USA).

3.5.5. Lipid content

Biomass, corresponding to 8 mg BDW, was resuspended in 200 µl of ultra-pure water. Lipids were extracted with methyl tert-butyl ether as described before (Matyash et al. 2008). Then, 1.5 ml methanol was added to the resuspended cells and the mixture was transferred to glass tubes. After addition of 5 mL MTBE, the solution was shaken for one hour at 30°C. Then, 1.25 ml ultra-pure water was added for phase separation and the sample was centrifuged (1,000 × *g*, 4°C, 10 min). The upper organic phase was collected in a dried and weighed glass tube. In the following, the aqueous phase was extracted again with 1290 µl MTBE, 387 µl methanol and 323 µl ultra-pure water as described before. The upper organic phases was pooled and dried at 80°C until constant weight. The lipid content was then quantified gravimetrically (Analytical balance BP210D, Sartorius, Göttingen, Germany).

3.6. Determination of metabolic fluxes

For the determination of the *in vivo* fluxes of the central carbon metabolism of *D. shibae* stationary metabolic flux analysis was performed as described before (Wittmann 2007). This method comprised an experimental and a computational part. During the experimental part, labeling experiments with ^{13}C labeled substrates were performed and the *in vivo* incorporation into the proteinogenic amino acids were measured using GC-MS. In

the computational part a model of the metabolic network simulated the labeling of these amino acids. By variation of free fluxes of the model these simulated labeling data is optimized until a minimum of deviation to the experimental measurements was reached and the flux distribution was calculated (Wittmann 2007 and Kohlstedt et al. 2010).

3.6.1. Metabolic modeling

To create the metabolic network model for *D. shibae*, all relevant reactions of the central carbon metabolism were implemented adapted from genome annotations based on information from databases like KEGG (Kyoto Encyclopedia of Genes and Genomes) or IMG of the JGI (Intergated Microbial Genomes of DOE Joint Genome Institute) and validated by enzymatic activity assays (Fürch et al. 2009). The implemented reactions for the flux calculations were dependent on the used carbon source (glucose, succinic acid). Additionally, information of directly measured intracellular fluxes was incorporated. Under metabolic and isotopic constant growth conditions, the product building rates, substrate uptake rate, biomass yield and biomass composition were determined and the anabolic precursor demand was calculated. Furthermore, mass spectrometric data from amino acids of the cell protein, produced in ^{13}C labeling studies were included to calculate the unknown fluxes. For these calculations mass spectra from the following amino acids were used: alanine, valine, aspartate, threonine, glutamate, serine, glycine, lysine and tyrosine. Other signals were not used because of low abundance (cysteine, methionine, asparagine and glutamine), unambiguous fragment ions (leucine, isoleucine), isobaric interference (proline) or overlapping substances (phenylalanine). The mass isotopomer distributions were corrected for natural abundance of stable isotopes (Wittmann et al. 1999). The flux calculations was conducted with OpenFlux (Quek et al. 2009), implemented in Matlab 2010 (Mathworks Inc., Natick, USA) until a minimum deviation between simulated and experimental mass isotopomer distributions was reached. To validate the results statistically, a Monte-Carlo approach was used (Quek et al. 2009, Schmidt et al. 1999).

3.6.2. Isotope labeling studies

To investigate the central carbon metabolism of *D. shibae* DFL-12, the main cultivation was carried out with [1-^{13}C] glucose or [1,4$^{13}C_2$] succinic acid. The mass isotopomer fractions of amino acids from cell protein were determined by GC-MS and the metabolic fluxes of the central carbon metabolism were calculated via OpenFlux (Wittmann et al. 2002, Quek et al. 2009).

Quantification of ^{13}C labeling in amino acids

To determine the ^{13}C-labeling pattern of protein-bound amino acids 10 ml of culture was harvested and the obtained pellet was washed once with 0.9 % NaCl. The washed cells were hydrolyzed with 500 µl 6 M HCl at 105°C for 20 h. After clearing the hydrolyzate from insoluble matter (0.2-µm centrifugal filter device, Ultrafree MC, Millipore, Bedford, MA, USA), 20 µl of the sample was lyophilized and used for GC-MS analysis (Fürch et al. 2009).
The ^{13}C-labeling enrichment in amino acids was determined by GC-MS analysis of their tert-butyl-dimethylsilyl-derivatives (Becker et al. 2011). For this purpose, the lyophilized samples were derivatised with 50 µl 0.1 % pyridine in dimethylformamide and 50 µl N-methyl-N-tert-butyldimethylsilyl-trifluoroacetamide (MBDSTFA) for 30 min at 80°C. After centrifugation (1 min, 5,000 $\times$ g) to remove insoluble salts, the samples were analyzed by GC-MS.
The measurement of the labeling in amino acids was conducted on a GC-MS with an HP5MS capillary column (5 % phenyl-methyl-siloxane diphenylpolysiloxane, 30 m $\times$ 250 µm), electron impact ionization at 70 eV, and a triple quadrupole detector (Agilent Technologies, Waldbronn, Germany). The optimized conditions for the measurement of amino acids in cell extracts were as follows. The injected volume was 1 µl with a split ratio of 30:1, and the carrier gas flow was helium at 1 ml min^{-1}. The temperature gradient for the separation was 120°C for 2 min, 8°C min^{-1} up to 200°C and 10°C min^{-1} to 325°C. Further operation temperatures were 250°C (inlet), 280°C (interface) and 230°C (quadrupole). As standard, a mixture of amino acids was measured (Figure: 3.2) and the labeling pattern was compared to abundances of natural isotopes (Wittmann et al. 2002). The deviation should be under 1 %.

3.6.3. Dynamic isotope labeling studies

To investigate the carbon dioxide fixation capacity of *D. shibae* DFL-12, the culture broth for the main cultivation was supplemented with 3.5 g l^{-1} of ^{13}C-labeled and with naturally labeled sodium bicarbonate, respectively. Cells were harvested after five days of incubation. For dynamic labeling experiments, main cultures were grown until an OD_{650} of 0.5. Subsequently, ^{13}C sodium bicarbonate was added from a sterile stock solution to a final concentration of 3.5 g l^{-1}. The cells were harvested by rapid sampling to investigate the dynamic labeling incorporation over a time course of 8 h.

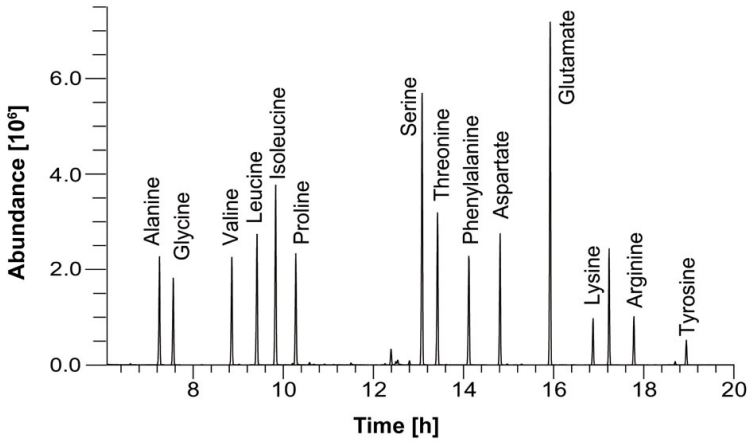

Figure 3.2.: Total ion chromatogram of a standard measurement of amino acid mixture with GC-MS

^{13}C labeling analysis in CoA thioesters

The ^{13}C labeling patterns of intracellular CoA thioesters were determined as recently described (Buschke et al. 2013a, Peyraud et al. 2009). For sampling via fast filtration, a culture volume that contained approximately 0.6 mg bio dry weight was harvested by vacuum filtration (cellulose acetate filter, 0.2-µm pore size, Sartorius AG, Göttingen, Germany). The filters were then immediately transferred into 8 ml of precooled quenching solution (-20°C) containing 0.1 M formic acid in 80 % (v/v) acetonitrile/water. The cells were disrupted by sonication (2 × 30 seconds, Snorex Super RK 31 with 35 kHz, Bandelin electronic GmbH & Co. KG, Berlin, Germany). After incubation for 15 min on ice the obtained extract was chilled with liquid nitrogen, cooled down to -80°C and then freeze dried. Subsequently, samples were dissolved in 100 µl of ammonium formate buffer (50 mM, pH 3.5, 2 % MeOH). After mixing, the samples were centrifuged (20,000 × *g*, 5 min, 4°C). The collected supernatant was used for LC-MS analysis.

Quantification of ^{13}C labeling in CoA esters

The ^{13}C-labeling incorporation into CoA thioesters was determined by LC-MS on a Rheos 2200 HPLC system (Flux Instruments, Basel, Switzerland), equipped with an electrospray ionization probe, that was coupled to an LTQ Orbitrap mass spectrometer (Thermo Fisher Scientific, Waltham, MA, USA). The measurement was conducted by Dr. Patrick Kiefer (Institute of Microbiology, ETH Zürich). The quantification of CoA thioesters was determined as described previously (Buschke et al. 2013a) with slight modifications (Kuntze et al. 2011). To desalt the samples prior to LC separation two C18 analytical columns (Gemini 50 × 2.0 mm and 100 × 2.0 mm, particle size 3 mm;

Phenomenex, Torrance, CA, USA) were used (flow rate 220 l/min, solvent A: 50 mM formic acid adjusted to pH 8.1 with NH_4OH, solvent B: methanol, Injection volume: 10 µL). The samples were then loaded on 50 × 2.0 mm C18 column and washed for 5 min with 100 % solvent A. The short column was connected to waste and in the meantime the 100 × 2.0 mm column was equilibrated with solvent A by an additional pump. In a next step, after complete desalting, both columns were connected in series. To separate CoA thioesters a gradient of solvent B was applied (Table: 3.13). The equilibration time between two measurement was 6 min at initial elution conditions. For detection, the LC was coupled to the mass spectrometer with sheath gas flow rate of 40, auxiliary gas flow rate of 30, tube lens of 80 V, capillary voltage of 35 V, and ion spray voltage of 4.3 kV. For the MS analysis the positive FTMS mode at a resolution of 60000 (m/z 400) was used.

Table 3.13.: Gradient for solvent B used for quantification of CoA esters by LC-MS

Time	Solvent B
5 min	5 %
15 min	23 %
25 min	80 %
27 min	80 %

Identification of intermediates of 3-hydroxypropionate cycle and ethylmalonyl-CoA pathway

Potential CoA thioesters and metabolites were analyzed using two different approaches to search for intermediates of the 3-hydroxypropionate cycle and ethylmalonyl-CoA pathway in LC-MS data as described before (Kuntze et al. 2011). These analysis was conducted by Dr. Patrick Kiefer (Institute of Microbiology, ETH Zürich). In the first approach a mass lists of potential CoA thioesters was calculated and compared to exact measurements of $[M+H]^+$ ions. Only comparisons with a deviation below 5 ppm were selected as positive match. In a second approach a targeted LC-MS/MS analysis was conducted. Therefore only selected mass ions were fragmented and searched for specific CoA thioester fragment ions. Lists of molecular formulas to detect these mass peaks were extracted from the PubChem compound database (http://pubchem.ncbi.nlm.nih.gov) from all compounds of category metabolic pathways composed of C and H, N, O, P, or S. In a further step, a 'CoA thioester solution space' was calculated (T. Kind et al. 2007). Only when two condition were fulfilled for triplicates of measurements, a molecular formula of the database was assigned to a mass peak. On the one hand, the differences between

theoretical and measured m/z values of the monoisotopic peak M0 were below 1.5 mmu, and on the other hand the requirements of an M0 peak in an isotopic pattern were fulfilled. Furthermore the LC-MS data were searched for the predicted CoA thioesters of the 3-hydroxypropionate cycle and ethylmalonyl-CoA pathway.

^{13}C labeling analysis in intracellular amino acids

The ^{13}C labeling pattern of intracellular amino acids was measured by GC-MS (Becker et al. 2011, Wittmann et al. 2002). For sampling via fast filtration, a culture volume that contained approximately 2.5 mg bio dry weight was harvested by vacuum filtration (cellulose acetate filter, 0.2-µm pore size, Sartorius, Göttingen, Germany) including a washing step with 1 ml of NaCl solution (24 g l^{-1}), which corresponded to the ionic strength of the medium (S. Kind et al. 2010, Wittmann et al. 2004). The filters were then directly transferred into 2 ml of deionized water and incubated for 15 min at 100°C for metabolite extraction. The obtained extracts were cooled on ice and centrifuged (5 min 13,000 × *g*, 4°C, centrifuge 4515R, Eppendorf AG, Hamburg, Germany) to remove cell debris. The supernatant was chilled with liquid nitrogen, frozen at -80°C and freeze dried before GC-MS analysis.

Quantification of ^{13}C labeling in amino acids

The ^{13}C-labeling enrichment in amino acids was determined by GC-MS analysis of their tert-butyl-dimethylsilyl-derivatives (Becker et al. 2011). Measurement was conducted on a GC with an HP5MS capillary column (5 % phenyl-methyl-siloxane diphenylpolysiloxane, 30 m × 250 µm), electron impact ionization at 70 eV, and a triple quadrupole detector (Agilent Technologies, Waldbronn, Germany). The optimized conditions for the measurement of amino acids in cell extracts were as follows. The injected volume was 0.5 µl with a split ratio of 30:1, and the carrier gas flow was helium at 1 ml min^{-1}. The temperature gradient for the separation was 120°C for 2 min, 8°C min^{-1} up to 200°C and 10°C min^{-1} to 325°C. Further operation temperatures were 250°C (inlet), 280°C (interface) and 230°C (quadrupole). The labeling enrichment determined for the protein-bound amino acids was identical with the maximum ^{13}C enrichment of the free amino acid pools. These results indicated sufficient supply of the ^{13}C bicarbonate throughout the entire tracer cultivation.

3.6.4. Quantification of intermediates of the central carbon metabolism

For analysis of intracellular intermediates, e. g. from EMP pathway (Glucose 6-phosphate, Fructose 6-phosphate, Fructose 1,6-bisphosphate, dihydroxyacetonephosphate, Glyceraldehyde 3-phosphate, 3-phosphoglycerate, 2-phosphoglycerate, Phosphoenolpyruvate, Pyruvate), PP pathway (Ribose 5-phosphate, Ribulose 5-phosphate, Xylose 5-phosphate, Seduheptulose 7-phosphate), ED pathway (6-phosphogluconate, KDPG) and TCA cycle (Acetyl-CoA, Citrate, Isocitrate, α-Ketoglutarate, Succinyl-CoA, Succinate, Fumarate, Malate). In addition the method allowed the analysis of energy metabolites (AMP, ADP, ATP) and of reducing equivalents (NAD, NADH, NADP, NADPH). For identification and quantification of intermediates of the central carbon metabolism in *D. shibae* DFL-12 on different substrates, the culture broth for the main cultivation was supplemented with 10 mM glucose and succinic acid, respectively. Cells were harvested by fast filtration and quenching. Then further identification and quantification was conducted by LC-MS/MS. Shortly, the LC-MS/MS measurements and data processing were conducted by Dipl. Biotechnol. Georg Richter (Institute of Biochemical Engineering, TU Braunschweig).

Analysis of intracellular intermediates of the central carbon metabolism

The amount of intracellular intermediates of the central carbon metabolism was measured by LC-MS/MS. For sampling via fast filtration, a 1 mL cultivation broth was harvested by vacuum filtration (cellulose acetate filter, 0.2-µm pore size, Sartorius, Göttingen, Germany). The filtrates were transferred into 5 ml of precooled quenching solution (-20°C) containing 60 % methanol in water, mixed and frozen in liquid nitrogen. During quenching 1 mL cultivation broth was directly transferred into 5 ml of precooled quenching solution (-20°C), mixed and chilled with liquid nitrogen. To extract the metabolites 2.5 mL extraction solution (75 % ethanol in water) and 100 µL intern standard were added to 500 µL sample or filtrate. After boiling for 3 minutes, the samples were cooled on ice for 5 minutes and centrifuged (5 min 13,000 × *g*, 4°C, centrifuge 4515R, Eppendorf AG, Hamburg, Germany) to remove cell debris. The supernatant was chilled with liquid nitrogen, frozen at -80°C and freeze dried. Before LC-MS/MS analysis the samples were solved in 500 µL eluent A. For metabolite analysis, a liquid chromatography (LC, Agilent 1290, Agilent Technologies, Waldbronn, Germany) was coupled to a triple quadrupole mass spectrometer (QTRAP 5500 , AB Sciex, Darmstadt, Germany), equipped with a TurbolonSpray source. The chromatic procedure (16 min) recruited a reversed phase

Table 3.14.: Gradient profile applied in the LC-MS/MS method for the identification of intermediates of the central carbon metabolism

Step	Total time [min]	Eluent A [vol. %]	Eluent B [vol. %]
1	0.0	95.0	5.0
2	2.0	95.0	5.0
3	22.0	10.0	90.0
4	23.0	95.0	5.0
5	28.0	95.0	5.0

Eluent A: 6 mM tributylamine aqueous solution adjusted to pH 6.2 with 6 mM acetic acid,
Eluent B: 6 mM tributylamine in a mixture of water/acetonitrile 50:50 (v/v) adjusted to pH 6.2 with 6 mM acetic acid.

column (VisionHT C18 HL, 100 mm × 2 mm I.D., 1.5 µm, Grace, Columbia, MD, United States). Separation was performed by ion exclusion chromatography usage at 50 °C was used with eluent A (6 mM aqueous tributylamine solution, adjusted to pH 6.2 with acetic acid) and eluent B (aqueous acetonitrile solution (50% v/v) with 6 mM tributylamine, adjusted to pH 6.2 with acetic acid). The gradient profile is shown in Table 3.14. The injection volume was 10 µL. The mobile phase was introduced into the mass spectrometer via the turbo ionspray source at a flow rate of 350 µL min^{-1}.
The MS was operated in the negative ionization mode, using multiple reaction monitoring (MRM) mode. The entrance potential (EP) was fixed at -10 V. The dwell time was 5 ms for all transitions. The source dependent parameters were set as follows: ionspray voltage -4500 V, nebulizer gas (GS1) auxiliary gas (GS2), curtain gas (CUR) and collision gas CAD were 60, 60, 35 medium, respectively. The auxiliary gas temperature was set to 550 °C. The mass spectrometer was run in unit resolution to obtain adequate selectivity and sensitivity.

3.7. Monitoring of oxidative stress response

Two different methods were used to investigate the influence of oxidative stress on growth of *D. shibae* (Chavarría et al. 2013, Sternberg et al. 1991). In a microtiter plate experiment, different diamide concentrations were used to determine the growth inhibition in SWM with glucose or succinic acid as sole carbon source. The soft-agar plates were also treated with diamide to measure the zone of inhibition as described in Klingner et al. 2015. These analysis were conducted and developed in cooperation with Dipl. Biotechnol. Arne Klingner (TU Braunschweig).

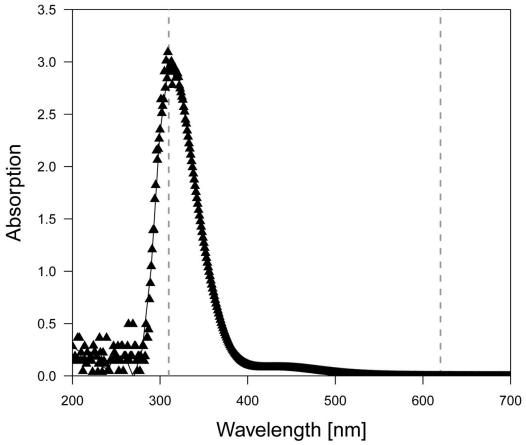

Figure 3.3.: Full spectrum of diamide in water with a maximum of absorption at 310 nm and obviously no influence on measurements of the optical density at 620 nm

3.7.1. Analysis in microtiter plates

The pre-cultivation was carried out as described for cultivations in shake flasks (Chapter: 3.3.2). The main cultivation (200 µl of SWM medium per well in an 96 well plate) was then inoculated with an initial OD_{650} of 0.005 for succinic acid and of 0.05 for glucose. After 20 hours, diamide was added to a concentration of 1, 2, 3, 3.5, 4, 5 and 8 mM. All cultivations were conducted in triplicate at 30°C in an microplate reader (Infinite® 200 PRO series, Tecan Trading AG, Switzerland). The OD_{620} was recorded and adjusted to the measurement at OD_{650} on the photometer (Figure: 3.4), while the diamide degradation could be observed at 310 nm, confirmed by the complete spectrum

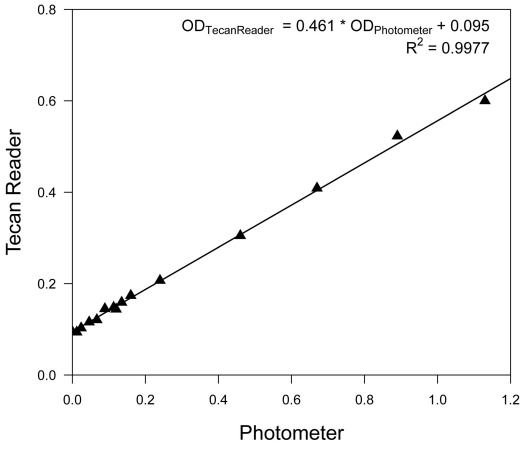

Figure 3.4.: Correlation of the optical density of the photometer used for growth analytic and of the Tecan Reader

of the diamide solution (Figure: 3.3). The time between diamide addition and restarting growth or complete degradation of diamide was used as indicator for inhibition.

3.7.2. Analysis on soft-agar plates

For soft agar plates, petri dishes (∅ 60 mm) were filled with 8 mL SWM agar with glucose or succinic acid as carbon source. The pre-cultivation in marine broth was carried out as described for cultivations in shake flasks (Chapter: 3.3.2). After harvesting, the cells were resuspended in SWM with an initial OD_{650} of 0.02 and then mixed with soft agar (24 g l^{-1} NaCl and 7.5 g l^{-1} agar in water). 3 mL of this solution was filled on the SWM plates. Small filters (∅ 6 mm) immersed with 110 g l^{-1} diamide in water were placed in the middle of the plate. After 2 days of incubation at 30°C the zone of inhibition was measured.

4. Results and Discussion

D. shibae was chosen as model to study metabolic pathways of a representative of the *Roseobacter* clade, wide spread in the marine realm. Previous analysis of its carbon metabolism on glucose elucidated the exclusive use of the Entner-Doudoroff pathway, but did not further resolve the fluxome (Fürch et al. 2009). However, such detailed knowledge appears crucial to understand which pathways are preferred under which growth condition and how the metabolism responds to changes during adaptation. Stationary and dynamic labeling studies, performed in this work, provide such insights into the metabolism of *D. shibae* on different substrates and clarify the contribution of different metabolic reactions to carbon dioxide fixation in this AAnP. Additionally, these results are interpreted with oxidative stress defense mechanisms and quorum sensing to provide a carefully created picture of the physiology of this marine model bacterium.

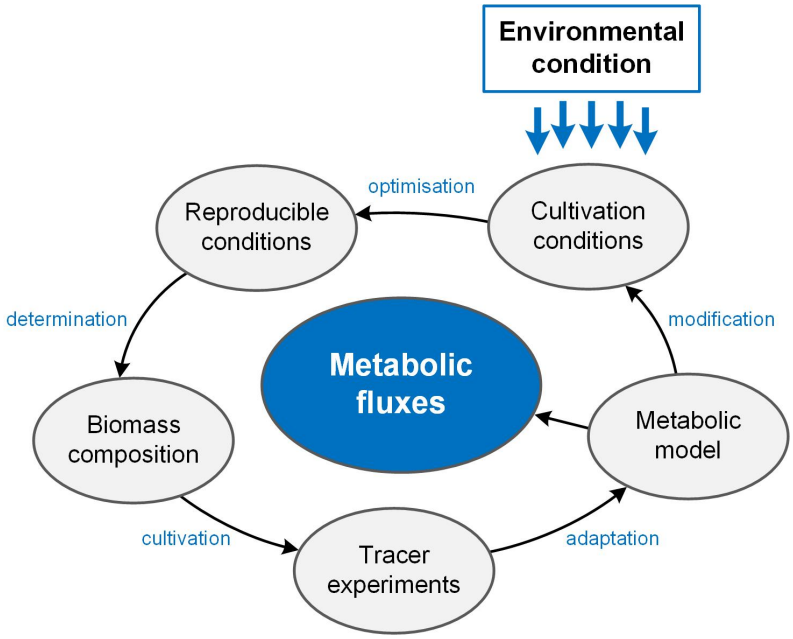

Figure 4.1.: Established work-flow for metabolic flux analysis of *D. shibae* under changing environmental conditions. For each condition, the cultivation set-up was optimized to reach reproducible growth profiles. After determination of biomass composition, tracer experiments were conducted and the metabolic model adapted for the calculation of the corresponding metabolic fluxes.

4.1. Analysis of the glucose metabolism of *D. shibae* in permanent darkness.

For ^{13}C metabolic flux analysis of *D. shibae*, a suitable work-flow was established (Figure: 4.1). First, it was necessary to optimize the cultivation parameters for reproducible growth at metabolic and isotopic steady state. In addition, the biomass composition had to be precisely determined to provide valid information on extracellular and anabolic fluxes. These data were then interpreted with ^{13}C labeling information from the cell protein to estimate the intracellular fluxes. Thereby the metabolic model was adapted to the conditions of the labeling experiment.

4.1.1. Growth physiology of *D. shibae*.

To investigate the carbohydrate metabolism of *D. shibae*, glucose was chosen as carbon source, because it is known as the most abundant free aldose in seawater (Alonso et al. 2006). Like in other AAnP bacteria, the metabolism of *D. shibae* is influenced by the illumination conditions. During the night, photosynthetic complexes and pigments are produced, which then enhance metabolism by additional energy generation during the day, changing bacterial growth from heterotrophic to photoheterotrophic (Tomasch et al. 2011). Especially under starving conditions, wide spread in the nutrient poor oceans, growth is thereby enhanced (Soora et al. 2013). Cells of *D. shibae* grown in permanent dark, however, show a dark red coloring (Figure: 4.2). This suppresses the influence of dark-light cycles on energy level as described previously by Tomasch et al. (2011). Here,

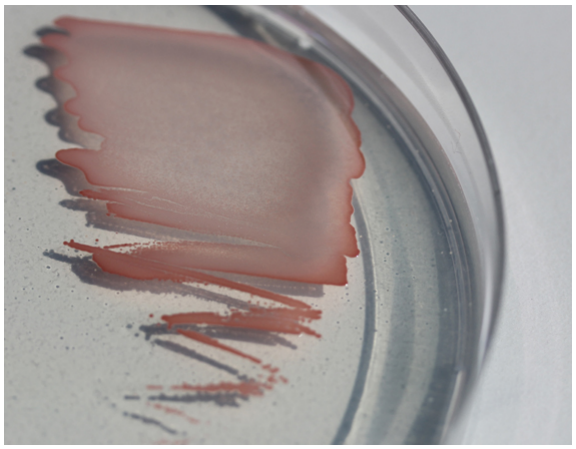

Figure 4.2.: Agar plate with *D. shibae* cells cultivated at permanent darkness, showing characteristic red pigmentation.

Table 4.1.: Growth rate on SWM with 10 mM succinate as carbon source with and without pH regulation

growth condition	growth rate [h^{-1}]
without pH regulation	0.14
with pH regulation	0.17

metabolic flux analysis was conducted in permanent dark to exclude influence with these dynamic changes.
The first focus in this work was now the establishment of suitable cultivation conditions for *D. shibae*. First cultivations of *D. shibae* in original SWM did not allow a reproducible growth profile, which, however, was necessary for metabolic flux analysis. At higher cell concentrations, growth was rather linear because of three key problems: changing pH values, evaporation and inefficient nutrient supply.

In a first step, to reduce the influence of changing pH values during growth, the pH was adjusted by adding 0.2 M NaOH or HCl manually over the time. The correct amount was determined by titration of the medium (Figure: 4.3). Control of the pH value resulted in a higher growth rate (Table: 4.1). The use of a carbonate or phosphate buffer appeared not feasible. Higher concentrations of carbonate or phosphate led to precipitation of magnesium and calcium carbonate, which was disturbing the photometric measurement of the optical density.

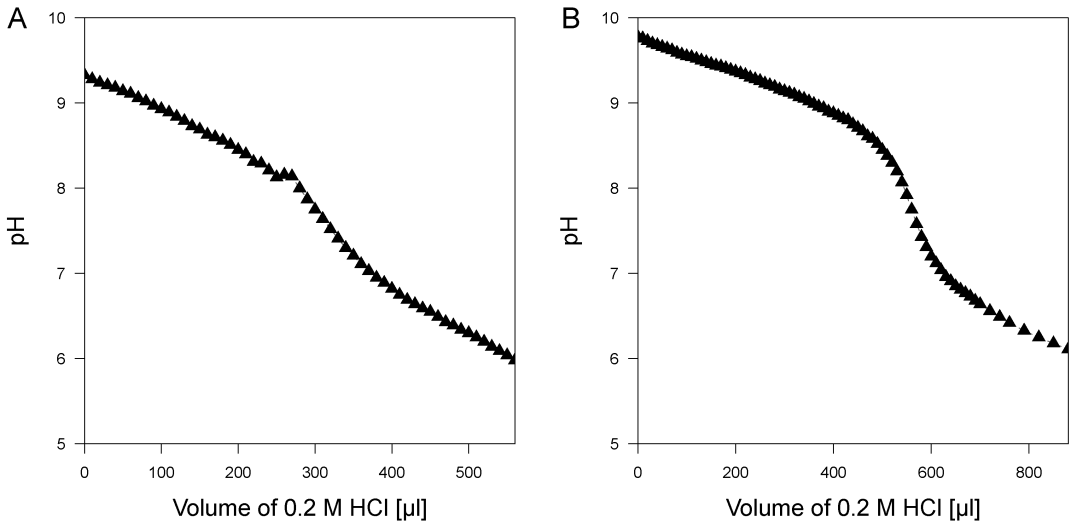

Figure 4.3.: Titration curve of 25 mL SWM with glucose (A) and succinic acid (B) as sole carbon source with 0.2 M HCl

Table 4.2.: Evaporation rates of cultivations with and without parafilm for *D. shibae* in SWM with glucose in light and dark. These analysis were conducted in cooperation with Sebastian Tesche during his bachelor thesis.

growth condition		evaporation rate [ml h^{-1}]	loss of liquid in 80 h [%]
without parafilm	light	0.20	63.7
	dark	0.14	45.4
with parafilm	light	0.01	2.2
	dark	0.01	4.5

In a second step, the evaporation rate for standard cultivations in light and in dark were considered (Table: 4.2). Especially for cultivations on glucose in the light with cultivation times up to 80 h a loss of 63.7 % of liquid was detected, which showed the necessity of minimisation.

As practical possibility to assure constant medium composition and avoid evaporation an additional sealing of the flasks with parafilm (Pechiney Plastic Packaging, Chicago, USA) was established. This still allowed sufficient oxygen supply as validated by online monitoring of the dissolved oxygen saturation (Figure: 4.4) (Schiefelbein et al. 2013). The examination of the evaporation rates showed also an effective decrease of the loss of liquid. For all cultivations the evaporation rate was reduced to 0.01 ml h^{-1} and the loss of liquid with parafilm was only 4.5 % at a standard cultivation time of 80 h.

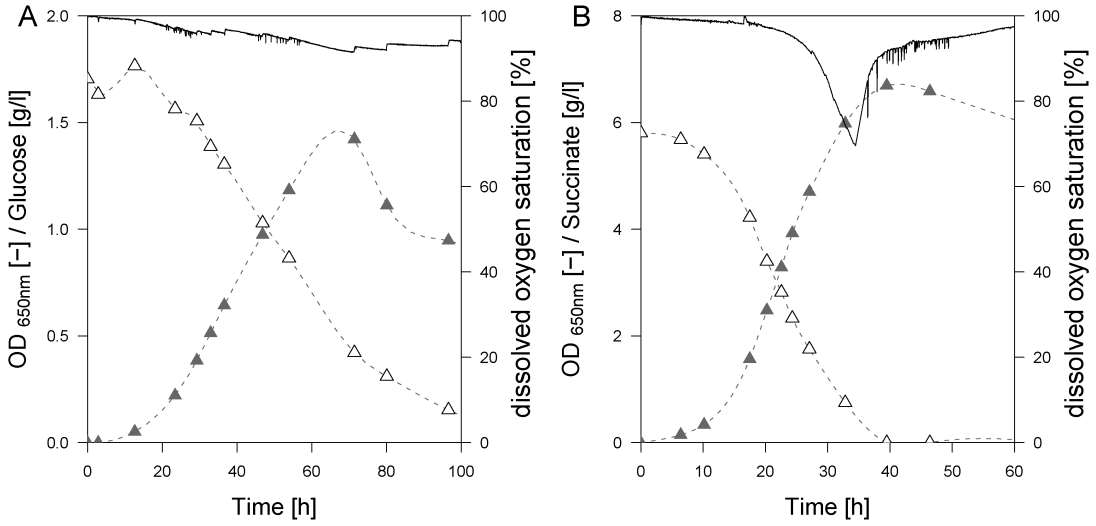

Figure 4.4.: Dissolved oxygen saturation in cultivations of *D. shibae* in SWM with 10 mM glucose (A) and 50 mM succinic acid (B) as sole carbon source in cultivations with parafilm. ▲ = optical density, △ = substrate concentration, solid line = oxygen saturation.

Table 4.3.: Composition of standard seawater, original SWM and modified SWM by comparison. The concentrations of substances were given in g l^{-1}

Media	Cl^-	Na^+	K^+	Mg^{2+}	Ca^{2+}	SO_4^{2-}	HCO_3^-
standard seawater[a]	19.35	10.75	0.39	1.30	0.42	2.70	0.15
original SWM	13.65	9.22	0.26	0.36	0.04	2.71	0.14
modified SWM	15.74	9.22	0.26	1.07	0.04	2.71	0.14

[a] Micale et al. (2009)

In a third step, to optimize the nutrient supply of *D. shibae*, the composition of the original SWM was compared to the growth conditions in the oceans (Table: 4.3). Remarkably, most concentrations were lower than in the oceans, especially for magnesium and calcium. To investigate the influence of these components on growth of *D. shibae*, the concentrations of all components were changed (Table: 4.4). Most substances showed no effect on growth of *D. shibae*. However, one key nutrient was identified that improved growth of *D. shibae*. An increased $MgCl_2$ concentration resulted in a longer exponential growth phase and higher growth rate for cultivations in SWM with glucose and succinate as sole carbon source (Figure: 4.5). The growth rate for cultivations on glucose increased from 0.09 h^{-1} to 0.11 h^{-1} and for succinic acid from 0.20 h^{-1} to 0.22 h^{-1} in SWM with an threefold increased magnesium concentration. Higher concentrations of vitamins and trace elements showed a positive effect on growth over long time periods. With an optimized glucose-based artificial seawater medium (SWM with

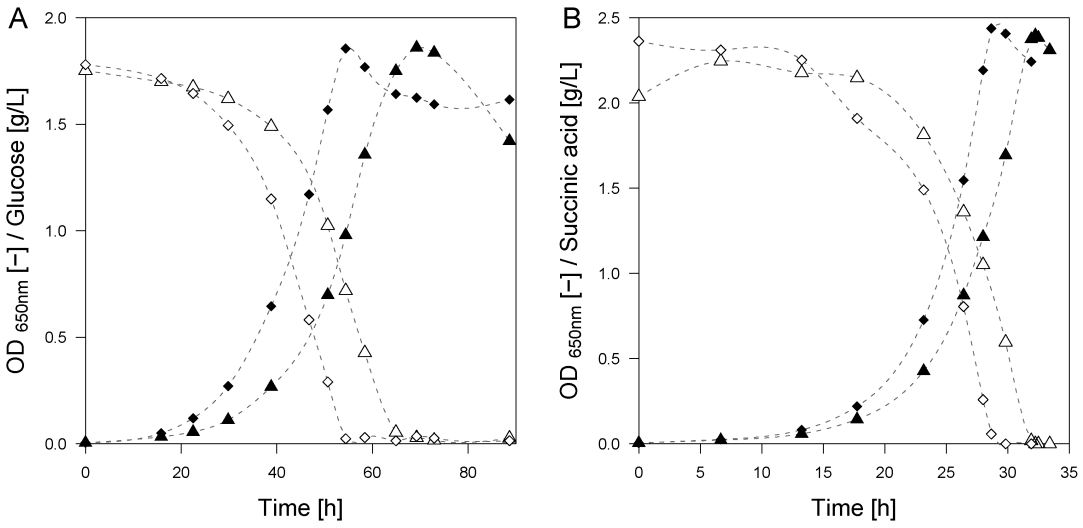

Figure 4.5.: Growth profiles of *D. shibae* in original (▲) and modified SWM (♦) with glucose (A) and succinic acid (B) as sole carbon source. △ represent the substrate concentration in original and ◇ in modified SWM.

Table 4.4.: Differences in growth behaviour for *D. shibae* with changing medium composition

Nutrient	Effect on growth
Carbonate	o
Phosphate	o
Sulfate	o
Sodium	o
Kalium	o
Calcium	o
Magnesium	+
Vitamins	(+)
Trace elements	(+)

10 mM glucose), representing the nutrient state of the marine environment, it was possible to get a satisfying reproducibility, as confirmed by small standard deviations between three biological replicates (Figure: 4.6 A). *D. shibae* grew exponentially with a specific growth rate of $\mu = 0.11\ h^{-1}$, until a maximum optical density of OD_{650} 1.8 was reached after 55 h (Figure: 4.6). This coincided with the depletion of the supplied glucose. A quantification of the biomass yield (70.3 g mol^{-1}) revealed efficient carbon utilization for anabolism (Table: 4.5), which was confirmed by the fact that biomass was the only product, formed during the cultivation. No extracellular products were detected by HPLC analysis, when screened for typical microbial excreted metabolites (e. g. acetate, pyruvate, ethanol, formate, lactate, acetoin).

During the exponential growth phase, metabolic and isotopic steady state was proven.

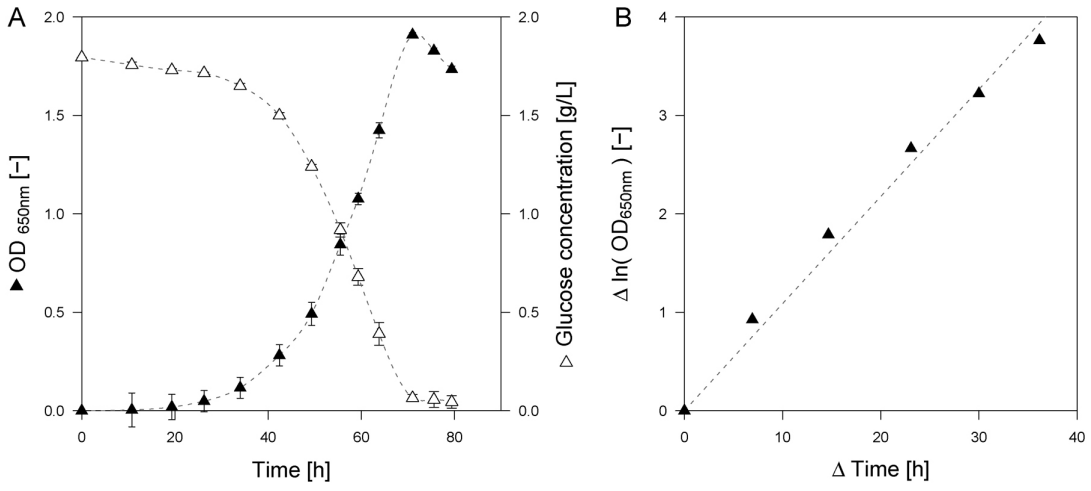

Figure 4.6.: Cultivation profile of *D. shibae* on SWM with glucose as carbon source grown in permanent darkness (A). The linear dependency of the natural logarithm of the optical density on time indicated exponential growth (B).

Table 4.5.: Growth kinetics and stoichiometry of *D. shibae*, grown in minimal medium with 10 mM glucose as sole carbon source at permanent darkness. Data include the specific growth rate (μ), the biomass yield $Y_{X/S}$, the specific substrate uptake rate (q_S). Data represent mean values with standard deviations (n = 3).

Illumination	μ [h^{-1}]	$Y_{X/S}$ [g mol^{-1}]	$Y_{X/S}$ [g $Cmol^{-1}$]	q_S [mmol g^{-1} h^{-1}]
Glucose dark	0.11 ± 0.00	70.3 ± 1.0	11.7 ± 0.2	1.59 ± 0.17

This fulfilled an important prerequisite for ^{13}C metabolic flux analysis. Metabolic steady state was indicated by constant growth stoichiometry, i.e. the linear correlation between biomass production and glucose consumption (Figure: 4.7 A). The constant ^{13}C labeling pattern of proteinogenic amino acids over time confirmed isotopic steady state (Figure: 4.7 B).

The biomass composition was then analyzed to great detail at the level of cell protein, DNA, RNA, Lipids, carbohydrates and other storage compounds (Table: 4.6). Interestingly, analysis revealed that polyhydroxybutyric acid (PHB) was a major biomass component, constituted 8 % of the total biomass during exponential growth phase and up to 28 % in stationary phase. This is not uncommon among marine bacteria (Arun et al. 2009). Especially for *Dinoroseobacter* species grown on glucose, PHB contents of up to 68 % have been found (Xiao et al. 2011). No further other carbohydrate storage compounds like glycogen, were identified. In total, 94.9 % of the total biomass

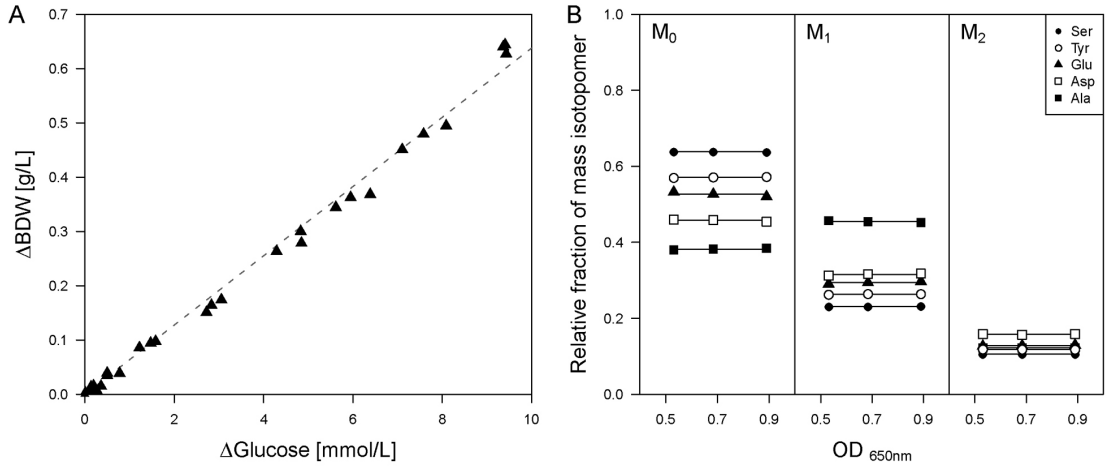

Figure 4.7.: Biomass yield as indicator for metabolic steady state (A) and stable isotopic labeling patterns of several amino acids at different optical densities as indicator for isotopic steady state (B) for *D. shibae* grown in SWM with 10 mM glucose at permanent dark. Data represent the mean values with standard deviations (n = 3).

Table 4.6.: Macromolecular biomass composition of *D. shibae* grown on minimal medium with 10 mM glucose as sole carbon source at permanent dark. Values given for Protein, PHB, Lipids, RNA and DNA were determined in total [g] and related to the produced biomass [g]. Data represent the mean values with standard deviations for three biological replicates.

Component	Protein	PHB	Lipids	RNA	DNA	Total
Amount [%]	64.6 ± 2.8	7.6 ± 1.5	5.4 ± 2.2	10.1 ± 0.7	7.3 ± 0.4	94.9 ± 8.3

could be recovered. To resolve the corresponding precursor demand, the monomeric composition of the macromolecules was investigated. Amino acids obtained from hydrolyzed protein of the protein fraction were measured by HPLC (Table: 4.7). The pool of glutamate/glutamine displayed the largest amino acid fraction (18.5 %), followed by alanine (11.7 %), glycine (9.7 %) and aspartate/asparagine (8.9 %). These amino acids belong also to the major fractions in *E. coli* (Neidhardt et al. 1990) or *C. glutamicum* (Marx et al. 1996). Cysteine, methionine and tryptophane could not be measured due to their degradation during hydrolysis of the protein. Therefore, published values from

Table 4.7.: Amino acid composition of the cell protein from *D. shibae* grown on glucose as sole carbon source at permanent light for the determination of the precursor demand. The values were determined in cooperation with Samuel Hauf during his bachelor thesis. Data represent the mean values with standard deviations (n = 3)

Amino acid	Amount [µmol l^{-1}]	Share of protein fraction [%]
Alanine	156.3 ± 20.2	11.75 ± 0.02
Arginine	61.7 ± 8.7	4.63 ± 0.14
Aspartate/Asparagine	118.9 ± 15.7	8.94 ± 0.09
Cysteine	-	1.71[a]
Glutamate/Glutamine	246.6 ± 32.8	18.53 ± 0.24
Glycine	128.6 ± 15.2	9.68 ± 0.11
Histidine	22.3 ± 2.6	1.68 ± 0.04
Isoleucine	55.0 ± 7.3	4.14 ± 0.11
Leucine	98.9 ± 13.4	7.43 ± 0.13
Lysine	57.5 ± 7.3	4.32 ± 0.09
Methionine	-	2.87[a]
Phenylalanine	42.4 ± 5.2	3.19 ± 0.06
Proline	35.5 ± 7.1	2.68 ± 0.44
Serine	58.6 ± 6.8	4.41 ± 0.06
Threonine	66.3 ± 8.9	4.98 ± 0.05
Tryptophan	-	1.06[a]
Tyrosine	22.6 ± 2.9	1.70 ± 0.03
Valine	83.6 ± 11.0	6.29 ± 0.03

[a] values for *E. coli* (Neidhardt et al. 1990)

E. coli were used for these selected compounds (Neidhardt et al. 1990). The monomeric composition of the DNA, was based on the GC content (Wagner-Döbler et al. 2010). The demand of nucleotides for RNA was obtained from the sequence of th rRNA genes Dshi_6006, Dshi_6009, Dshi_6010, Dshi_6013, Dshi_6016 and Dshi_6017, the main RNA fraction. Other minor components, like lipopolysaccharides (Neumann et al. 1995), photosynthetic pigments (Biebl et al. 2006), cell wall components and polyamines (Neidhardt et al. 1990), as well as the lipid composition (Biebl et al. 2005) were obtained from literature. The values are given in the appendix (Table: A.1). The overall anabolic precursor demand of *D. shibae* is summarized in Table 4.8. Interestingly, the flux from acetyl-CoA to biomass is the highest, whereas the demand for glucose-6 phosphate is small because the major storage compound (PHB) was produced from acetyl-CoA, whereas the cells did not contain glycogen.

Table 4.8.: Precursor demand for *D. shibae* grown on glucose in permanent dark calculated from biomass composition in µmol g^{-1} with a definite biomass yield ($Y_{X/S}$ = 70.3 g mol^{-1}). The determined precursor were glucose 6-phosphate (G6P), fructose 6-phosphate (F6P), ribose 5-phosphate (R5P), erythrose 4-phosphate (E4P), glycerinaldehyde 3-phosphate (GAP), 3-phosphoglycerate (PGA), phosphoenolpyruvate(PEP), pyruvate (PYR), acetyl-CoA(AcCoA), oxaloacetate (OAA), oxoglutarate (AKG).

precursor	G6P	F6P	R5P	E4P	GAP	PGA	PEP	PYR	AcCoA	OAA	AKG	NADPH
amount [µmol g^{-1}]	27	38	661	303	65	1222	565	2465	3098	2031	1410	13574

4.1.2. Metabolic model generation for *D. shibae*.

Previous studies provided first interesting insights into the glucose catabolism of selected members of the *Roseobacter* clade (Fürch et al. 2009, Tang et al. 2009, Reisch et al. 2013). A major finding was the exclusive use of the Entner-Doudoroff pathway (EDP) for glucose assimilation (Fürch et al. 2009), which was coincided with a lack enzymatic activity of phosphofructokinase, the key enzyme of glycolysis. Furthermore, high activity of 6-phosphogluconate dehydratase and of KDPG aldolase within the Entner-Doudoroff pathway were detected.

The first draft of the central carbon metabolism of *D. shibae* (Figure: 4.8) considered the information based on functional annotation of genome data published on KEGG (Kyoto Encyclopedia of Genes and Genomes) and IMG of the JGI (Integrated Microbial Genomes of DOE Joint Genome Institute). Surprisingly, 6-phosphogluconate dehydrogenase, the key enzyme of the pentose phosphate pathway was not annotated.

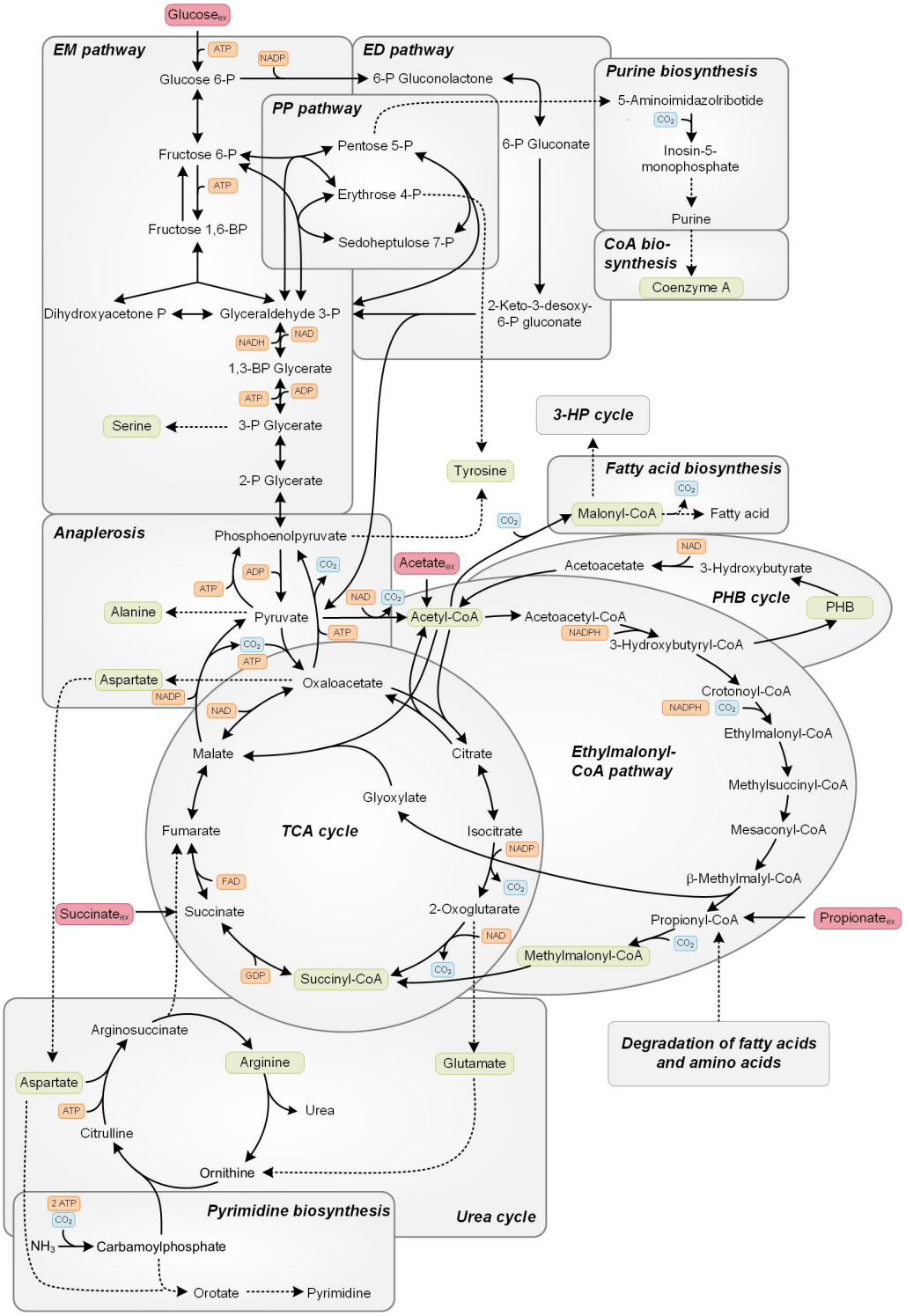

Figure 4.8.: Central metabolic pathways of *D. shibae* comprising the Embden-Meyerhof-Parnas pathway (EMP pathway), the Entner-Doudoroff pathway (ED pathway), the pentose phosphate pathway (PP pathway), anaplerosis, the tricarboxylic acid cycle (TCA cycle), the urea cycle, the polyhydroxybutyric acid cycle (PHB cycle) and the ethylmalonyl-CoA pathway based on annotated genomic information. Metabolites shown in green were determined in labeling studies, metabolites given in red were used as substrates, CO_2 (given in blue) shows incorporated and released carbon dioxide, while reduction equivalents are shown in orange.

Moreover, it was interesting to note that the isocitrate lyase was not annotated, while the ethylmalonyl-CoA pathway for the assimilation of acetate was completely annotated (Figure: 4.8).

For subsequent flux calculations, all reactions were implemented into the software platform OpenFlux (Table: A.2). This comprised the Embden-Meyerhof-Parnas pathway , the Entner-Doudoroff pathway and the pentose phosphate pathway as well as the anaplerotic reactions and the TCA cycle. Additionally, analysis of the degradation of DMSP in *R. pomeroyi* revealed an involvement of the ethylmalonyl-CoA pathway in acetate metabolism (Reisch et al. 2013). Therefore this pathway was also considered. Where needed, the presence of specific enzymes was validated by enzymatic activity assays (Table: 4.9). This confirmed the lack of 6-phosphogluconate dehydrogenase (oxidative PP pathway), because no *in vitro* activity was observed. In contrast, the glucose 6-phosphate dehydrogenase as well as the 6-phosphogluconate dehydratase and the KDPG aldolase within the Entner-Doudoroff pathway were found active. This suggested an inactive oxidative PPP. Interestingly, the glucose 6-phosphate dehydrogenase, the 6-phosphogluconate dehydratase and the KDPG aldolase showed high activity suggesting a high possible flux through the ED pathway. As shown before (Fürch et al. 2009), no PFK activity was detected indicating an inactive EMP pathway. Low activity of fructose bisphosphatase (22 %) suggested a possible small gluconeogenetic backflux and cycling through the ED pathway, which is also found for *R. sphaeroides* (Fuhrer et al. 2005) and seems to be common for AAnP bacteria (Tang et al. 2011). A high activity of isocitrate dehydrogenase pointed to an extensive use of the TCA cycle. A potential flux through

Table 4.9.: *In vitro* activity of glucose 6-phosphate dehydrogenase (G6P-DH), 6-phosphogluconate dehydrogenase (6PG-DH), 6-phosphogluconate dehydratase and KDPG aldolase the enzymes of the Entner Doudoroff Pathway (EDP-E), phosphofructokinase (PFK), fructose bisphosphatase (FBPase), isocitrate dehydrogenase (ICI-DH), malic enzyme (MAL-E) and isocitrate lyase. For the analysis *D. shibae* was grown on SWM with glucose as carbon source. Data represent mean values with standard deviations (n = 3) and the resulting maximum flux, given as relative enzymatic activity, normalized to the specific glucose uptake rate.

Enzyme	Enzymatic activity [U mg^{-1}_{Prot}]	Relative enzymatic activity [%]
G6P-DH	0.057 ± 0.001	139.0
6PG-DH	< 0.001	0
EDP-E	0.040 ± 0.004	97.5
PFK	< 0.001	0
FBPase	0.009 ± 0.001	21.9
ICI-DH	0.246 ± 0.008	599.7
MAL-E	0.008 ± 0.000	19.5
ICI-LY	< 0.001	0

the glyoxylate shunt, as shown for *P. aeruginosa* (Berger et al. 2014), was not detected, because of the inactivity of isocitrate lyase.
Further metabolome analysis revealed, that intermediates of all major pathways could be detected by LC-MS/MS analysis (Table: A.9). Only the intermediates of the PP pathway, succinyl-CoA, glyceraldyhyde 3-phosphate and glyoxylate were under the limit of detection. An determined AEC of 0.86 showed a good energy handling.

4.1.3. Systems-wide pathway analysis of *D. shibae*.

D. shibae was grown in grown in SWM supplemented with 1-^{13}C-glucose and the incorporation of this labeled glucose into cell protein was measured by analysing TBDMS derivated amino acid fragments with GC-MS (Table: A.3). Based on the experimental data of growth physiology (Table: 4.5) and amino acid labeling data (Table: A.3) and the metabolic network of *D. shibae* (Figure: 4.8), the global flux distribution was then computed, considering full stoichiometric and isotopomer balancing (Table: A.2). Fluxes were determined with high precision, as reflected by the narrow 90 % confidence intervals (Figure: 4.10) and the excellent agreement of calculated and measured mass isotopomer fractions of the amino acids from hydrolyzed cell protein (Figure: 4.9). The corresponding raw data from measurement and simulation are given in the appendix (Table: A.4).
Obviously, *D. shibae* channeled the complete carbon into the ED pathway. The oxidative pentose phosphate pathway (PP pathway) and the Emden-Meyerhoff-Parnas pathway (EMP pahway) were, in contrast, inactive. This agreed with the lack of phosphofructokinase and 6-phosphogluconate dehydrogenase (Table: 4.9). The anabolic demand for

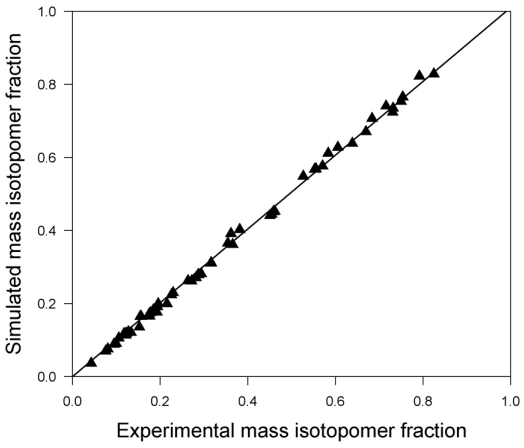

Figure 4.9.: Experimental and simulated mass isotopomer fractions of the labeling experiment of *D. shibae*, cultivated on glucose minimal medium in the dark.

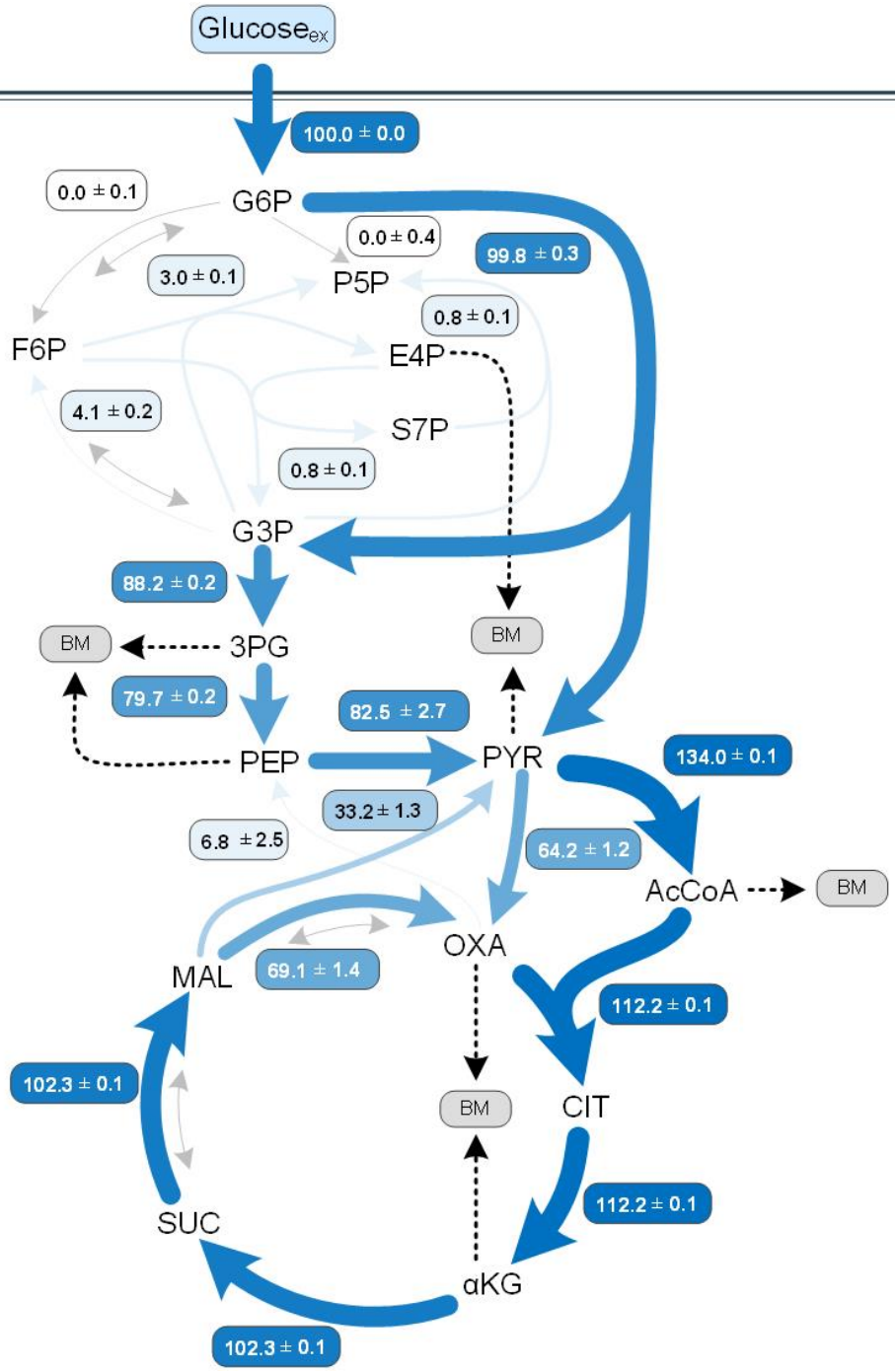

Figure 4.10.: Intracellular flux distribution of *D. shibae* grown in SWM with 10 mM glucose. The fluxes are given in molar percentage of the mean specific glucose uptake rate (q_S = 1.59 mmol g^{-1} h^{-1}, set to 100 %). The corresponding errors were determined by Monte-Carlo analysis, and display the 90 % confidence intervals.

erythrose 4-phosphate and ribulose 5-phosphate, was completely covered by the regenerative PP pathway. In most other bacteria, grown on glucose, with a fully functioning PP pathway, the flux through transketolase 1 and 2, and transaldolase was thereby in-

verted. Similarly, this has been proposed for *R. denitrificans* and for other organisms, lacking the 6-phosphogluconate dehydrogenase (Tang et al. 2009). Glyceraldehyde 3-phosphate (GAP), formed in the ED pathway, was mainly recruited to feed the pyruvate pool through the lower glycolysis. However, a small fraction also entered gluconeogenesis mainly to supply fructose 6-phosphate for anabolism. A gluconeogenetic flux through the ED pathway was not observed.
High flux resulted for the lower glycolytic chain and the TCA cycle. A flux was withdrawn from the acetyl-CoA pool into PHB synthesis. Anaplerotic replenishment of the TCA cycle occurred via pyruvate carboxylase. The metabolic flux estimation further revealed *in vivo* activity of PEP carboxykinase and malic enzyme. Overall this resulted in an exchange flux between the C_3 and C_4 metabolites of glycolysis and TCA cycle.
The prevalence of the ED pathway for glucose assimilation seems common for AAnP (Tang et al. 2011) and *Roseobacteria* (Tang et al. 2009). Such a metabolism is also observed for *Pseudomonas*, lacking phosphofructokinase (Fuhrer et al. 2005, Chavarría et al. 2013, Berger et al. 2014). The high activity of the ED pathway provides an increased NADPH amount, which was found to mediate oxidative stress tolerance (Chavarría et al. 2013). The use of the ED pathway might give *D. shibae* an advantage to survive in its marine environment, where it typically has to deal with photo-oxidative stress (Alonso-Sáez et al. 2006).

4.2. Analysis of succinic acid metabolism of *D. shibae* at permanent darkness.

Another interesting and common carbon source in the marine environment is succinic acid, often released in algal blooms (Biebl et al. 2005), and this carbon source has been widely used to study *D. shibae* (Tomasch et al. 2011, Wiegmann et al. 2014, Doi et al. 1991, Soora et al. 2013).

4.2.1. Growth physiology of *D. shibae* on succinic acid.

Cultivation of *D. shibae* on SWM with 10 mM succinic acid as sole carbon source could be established with a high reproducibility (Figure: 4.11). *D. shibae* grew exponentially with a specific growth rate of $\mu = 0.21\ h^{-1}$, nearly twice as fast as on glucose. A maximum optical density (OD_{650}) of 1.3 was reached after 30 h (Figure: 4.11), which coincided with the depletion of succinic acid. A quantification of the biomass yield of 42.2 g mol^{-1} revealed a rather efficient carbon utilization for anabolism (Table: 4.10). The fact that, next to biomass only low levels of fumarate were formed confirmed this observation.

Metabolic steady state during the exponential growth was validated by constant growth stoichiometry, i.e. linear correlation between biomass production and succinic acid consumption (Figure: 4.12 A). The constant ^{13}C labeling pattern of diverse proteinogenic

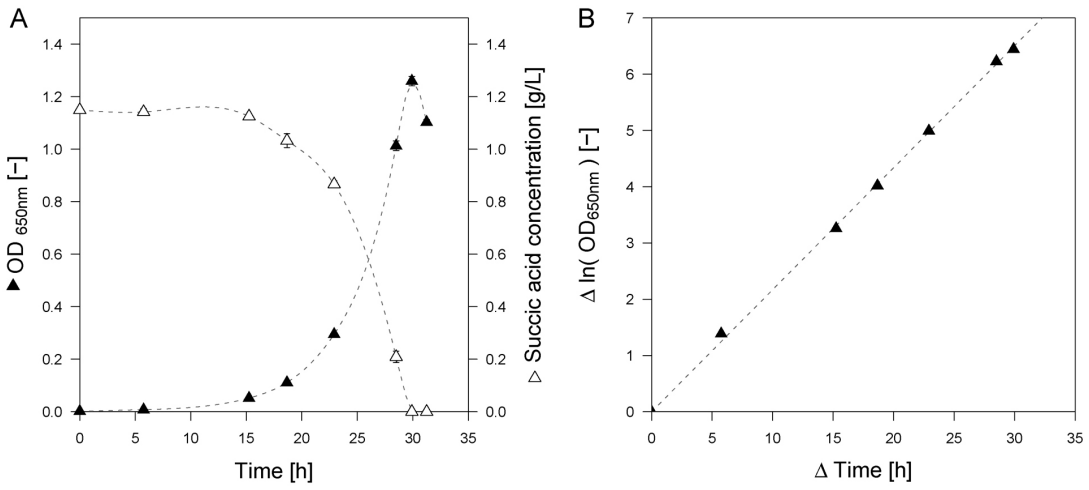

Figure 4.11.: Cultivation profile of *D. shibae* on SWM with succinic acid as carbon source grown in permanent darkness (A). The linear dependency of the natural logarithm of the optical density on time indicated exponential growth (B)

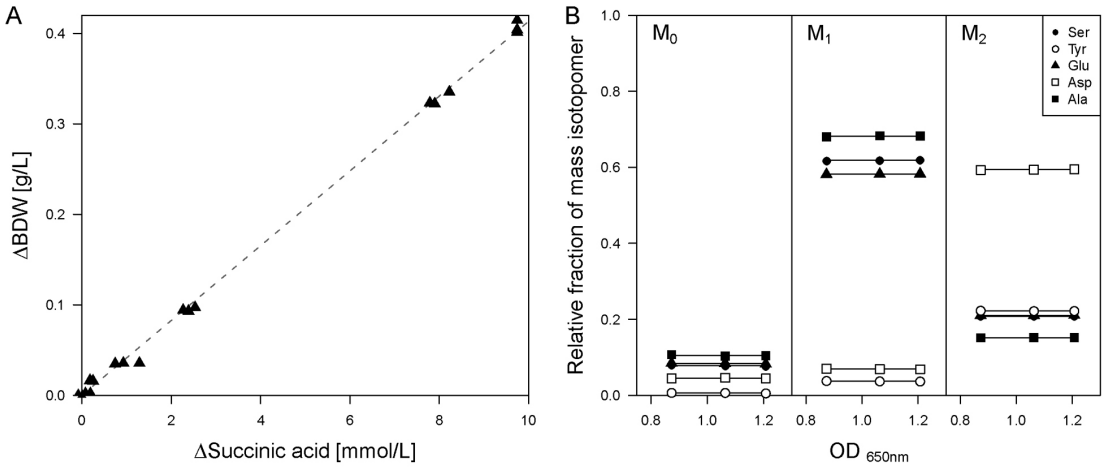

Figure 4.12.: Biomass yield as indicator for metabolic steady state (A) isotopic labeling pattern of amino acids as indicator for isotopic steady state (B) for *D. shibae* grown in SWM with 10 mM succinic acid at permanent dark. Data represent the mean values with standard deviations (n=3)

amino acids over time confirmed isotopic steady state (Figure: 4.7 B). The macromolecular composition was then quantified to subsequently implement the anabolic demand in the metabolic model. For this purpose the amount of DNA, RNA, protein, lipids and PHB in the cell was determined (Table: 4.11). Interestingly, the amount of polyhydroxybutyric acid (50.2 %) was much higher than for glucose. This high PHB content was live visible under the microscope. Corresponding to the high PHB content, other macromolecules were less present. Remarkable was the relatively low protein content (40.6 %).

The monomeric precursor demand for the anabolism was determined as described for glucose (Table: A.5). For a cultivation of *D. shibae* on SWM with 10 mM succinic acid, the resulted fluxes for the metabolites in permanent dark were displayed in Table 4.12.

Table 4.10.: Growth kinetics and stoichiometry of *D. shibae*, grown in minimal medium with 10 mM succinic acid as sole carbon source at permanent darkness. Data include the specific growth rate (μ), the biomass yield $Y_{X/S}$, the specific substrate uptake rate (q_S). Data represent mean values with standard deviations (n = 3).

Illumination	μ [h^{-1}]	$Y_{X/S}$ [g mol^{-1}]	$Y_{X/S}$ [g $Cmol^{-1}$]	q_S [mmol g^{-1} h^{-1}]
Succinic acid dark	0.21 ± 0.00	42.2 ± 0.3	10.6 ± 0.1	5.09 ± 0.23

Table 4.11.: Macromolecular biomass composition of *D. shibae* grown on minimal medium with 10 mM succinic acid as sole carbon source at permanent dark. Values given for Protein, PHB, Lipids, RNA and DNA were determined in total [g] and related to the produced biomass [g]. Data represent the mean values with standard deviations for three biological replicates.

component	protein	PHB	lipids	RNA	DNA	Total
amount [%]	40.6 ± 4.8	50.2 ± 5.3	4.0 ± 1.3	6.7 ± 1.0	4.6 ± 0.6	106.2 ± 12.9

4.2.2. Metabolic model generation for *D. shibae*.

All previous studies of *Roseobacter* species considered glucose, pyruvate, acetate, MMPA or DMSP to analyze the catabolism (Fürch et al. 2009, Tang et al. 2009, Reisch et al. 2013). To date, nothing is known in detail about the metabolism of succinic acid, despite this compound is a preferred substrate for this organisms (Soora et al. 2013, Tomasch et al. 2011, H. Wang et al. 2014, Laass et al. 2014, Rex et al. 2013, Ebert et al. 2013, Biebl et al. 2006, Holert et al. 2011). As for glucose the specific activity of key enzymes was validated by enzymatic assays (Table: 4.13). This allowed to draw first conclusions on the metabolism of *D. shibae*

Here, only small activities for fructose bisphosphatase, glucose 6-phosphate dehydrogenase as well as for enzymes of the EDP (Glucose 6-phosphate dehydratase and KDPG aldolase) were observed. This indicated rather small fluxes through these pathways, which likely only covered precursor demand for biomass formation, but were not major supplier of NADPH. As noted for glucose, the oxidative part of the PP pathway was inactive and thus, did not contribute to NADPH supply. A high activity of isocitrate dehydrogenase suggested an extensive use of the TCA cycle. Surprisingly, the activity of malic enzyme was very low. As a consequence, the quantity of pyruvate required for PHB synthesis was created by phosphoenolpyruvate carboxykinase and pyruvate kinase

Table 4.12.: Precursor demand for *D. shibae* grown on succinic acid in permanent dark calculated from biomass composition µmol g^{-1} with a definite biomass yield ($Y_{X/S}$ = 42.2 g mol^{-1}). The determined precursor were glucose 6-phosphate (G6P), fructose 6-phosphate (F6P), ribose 5-phosphate (R5P), erytrose 4-phosphate (E4P), glycerinaldehyde 3-phosphate (GAP), 3-phosphoglycerate (PGA), phosphoenolpyruvate(PEP), pyruvate (PYR), acetyl-CoA(AcCoA), oxaloacetate (OAA), oxoglutarate (AKG).

precursor	G6P	F6P	R5P	E4P	GAP	PGA	PEP	PYR	AcCoA	OAA	AKG	NADPH
amount [µmol g^{-1}]	27	38	430	190	49	812	361	1566	10858	979	922	13325

Table 4.13.: *In vitro* enzymatic activity for *D. shibae* grown on SWM with succinic acid as carbon source, determined for the key enzymes glucose 6-phosphate dehydrogenase (G6P-DH), 6-phosphogluconate dehydrogenase (6PG-DH), 6-phosphogluconate dehydratase and KDPG aldolase the enzymes of the Entner Doudoroff Pathway (EDP-E), fructose bisphosphatase (FBPase), isocitrate dehydrogenase (ICI-DH), malic enzyme (MAL-E). Data represent the mean values with standard deviations (n = 3) and the maximum possible flux as relative enzymatic activity.

Enzyme	Enzymatic activity [mU mg^{-1}_{Prot}]	Relative enzymatic activity [%]
G6P-DH	0.013 ± 0.001	6.2
6PG-DH	< 0.001	0.0
EDP-E	0.006 ± 0.002	2.9
FBPase	0.013 ± 0.001	6.2
ICI-DH	0.287 ± 0.001	137.4
MAL-E	0.011 ± 0.000	5.3

while the major NADPH production was carried out by isocitrate dehydrogenase.
Further metabolome analysis revealed, that intermediates of the major pathway, TCA cycle, could be detected by LC-MS/MS analysis (Table: A.9). Only few intermediates of the glyconegenesis and ED pathway over the limit of detection. An determined AEC of 0.74 showed a also good energy handling.

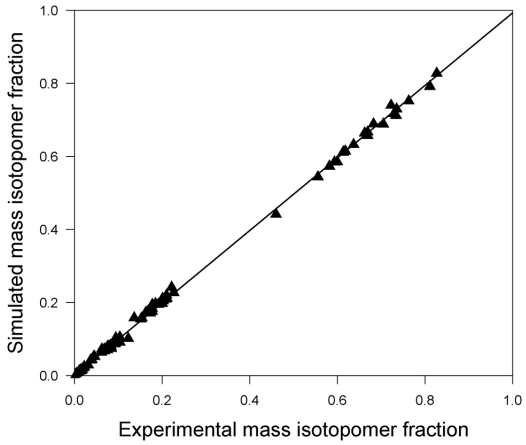

Figure 4.13.: Experimental and simulated mass isotopomer fractions of the labeling experiment of *D. shibae* cultivated on succinic acid minimal medium in the dark. A linear correlation with an slope of 1 stood for precise determination of the flux distribution by the used model.

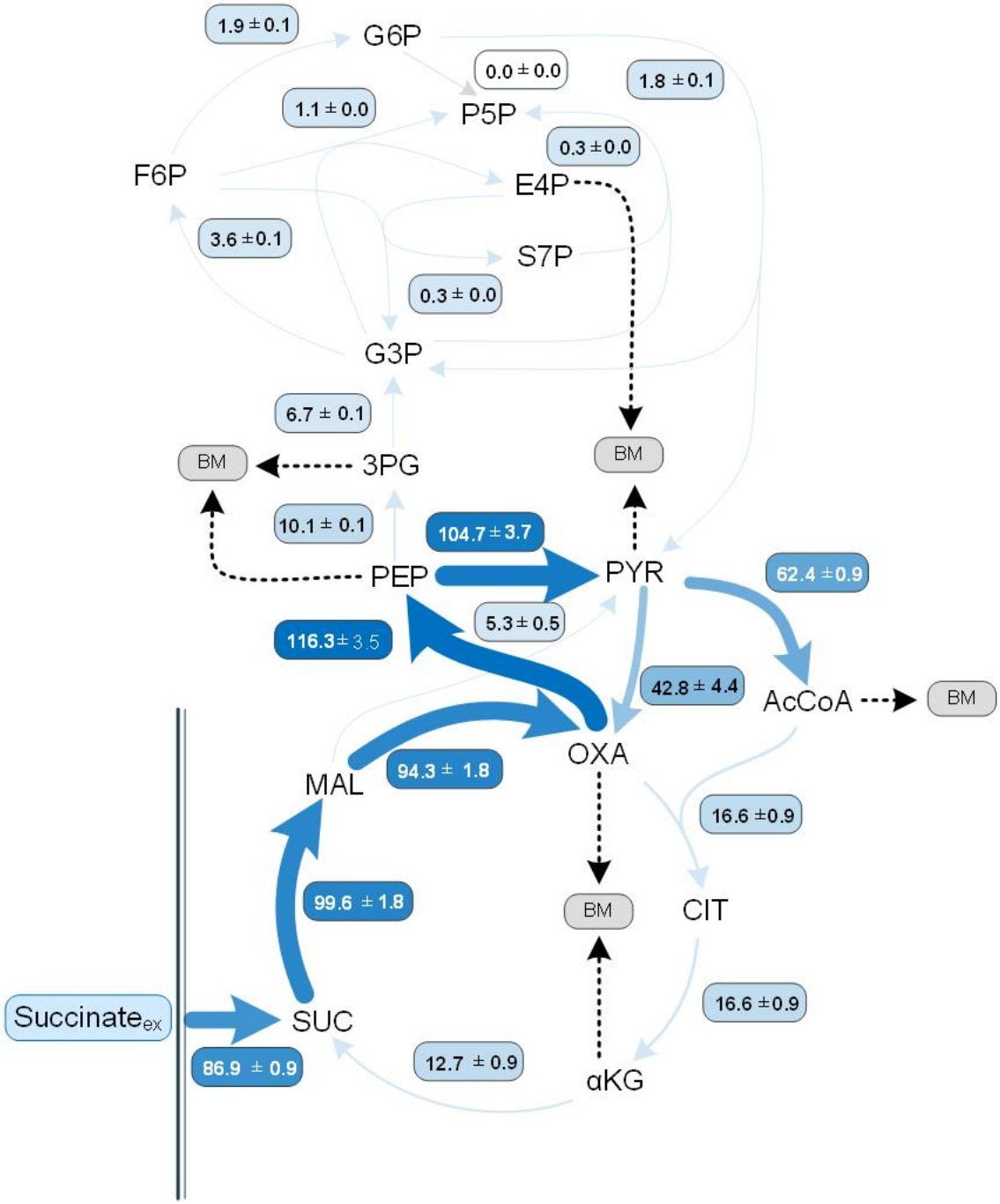

Figure 4.14.: Fluxmap for *D. shibae* in SWM with 10 mM succinic acid. The *in vivo* flux distribution were given in as molar percentage of the mean specific succinic acid uptake rate q_S = 5.09 mmol g^{-1} h^{-1} set to 100 %. The corresponding error were determined by Monte-Carlo analysis with 90 % confidence interval.

4.2.3. Systems-wide pathway analysis of *D. shibae*.

For the system wide pathway analysis with succinic acid as carbon source, the incorporation of 1,4-$^{13}C_2$-succinic acid into the cell protein was measured by analysing TBDMS

derivated amino acid fragments with GC-MS (Table: A.7). Combined with the experimental data on growth physiology (Table: 4.10) and the metabolic network of *D. shibae* (4.8), the global flux distribution was then computed involving full stoichiometric and isotopomer balancing (Table: A.6). Fluxes were determined with high precision as reflected by the narrow 90 % confidence intervals (Figure: 4.14) and the excellent agreement of the calculated and measured mass isotopomer fractions of the amino acids from hydrolyzed cell protein (Figure: 4.13). The raw data from measurement and simulation of mass isotopomer fractions are depicted in the appendix (Table: A.8).
In contrast to glucose, the complete carbon flux entered the metabolism at the level of succinic acid, an intermediate of the TCA cycle. However, only a small flux circled through the entire TCA cycle. At the level of oxaloacetate a huge flux was directed to phosphoenolpyruvate and the pyruvate pool. Partly, it was re-channeled to oxaloacetate, but the major fraction of carbon was channeled into PHB production. From phosphoenolpyruvate only a small flux through gluconeogenesis was able, which obviously satisfied the anabolic demand. The lack of the oxidative PPP and the inverted flux through the reductive PPP were similar as observed on glucose. It is interesting to note that the gluconeogenetic flux was re-channeled through the EDP to pyruvate again.
The small flux through the ED pathway might prepare the organism to cope with fast changes in nutrient level, often seen in marine environments (Hahnke et al. 2013). Similarly, a maintained activity of G6P-DH might facilitate the change of the carbon metabolism from organic acid, to sugar, or to increase NADPH formation, i. e. oxidative stress condition (Bériault et al. 2007). High amounts of acetyl-CoA were provided during growth on succinic acid, mostly stored in high intracellular PHB concentration as back-up for starving conditions.

4.3. Analysis of oxidative stress of *D. shibae*.

Oxidative stress is a wide spread phenomenon in the oceans, so that marine microorganism need efficient mechanisms to protect against damage caused by such stress (Lesser 2006). As described recently for *P. putida* (Chavarría et al. 2013) the ED pathway can have a positive influence on the robustness against oxidative stress. This is due to high NADPH levels, provided through this pathway. Generally, four enzymes are involved in NADPH generation: glucose 6-phosphate dehydrogenase, 6-phosphogluconate dehydrogenase, isocitrate dehydrogenase and malic enzyme (Berger et al. 2014). It was therefore interesting to study their contribution to the NADPH metabolism in *D. shibae*.

Capability of *D. shibae* to produce NADPH

In order to integrate metabolic *in vivo* fluxes with *in vitro* enzymatic activities, the latter values were related to the bio dry weight of the cells (protein content for glucose grown cells: 64.6 g g_{BDW}^{-1} / for succinic acid grown cells: 40.6 g g_{BDW}^{-1}). Similarly, the metabolic fluxes were normalized to the substrate uptake rate (q_S [mmol g^{-1} min^{-1}] for glucose: 0.0265; for succinic acid: 0.0848), to get the molecular flux values. The relation then directly showed the capacity of utilization. In case the *in vitro* activity of the enzyme exceeded the real flux, this would indicate that the enzyme could potentially provide more NADPH. Figure 4.15 shows the data for *D. shibae*. Malic enzyme showed low levels of activity, which were nearly identical for both conditions. The flux and enzymatic activity determined for G6P-DH were significantly higher as for malic enzyme and were dependent on the substrate used. On glucose, the enzymatic activity was seven times higher than of succinic acid. Generally, this enzyme operated never with its full capacity. Among all enzymes, isocitrate dehydrogenase was an exception. On both substrates high *in vitro* activity was observed (glucose: 159 U g_{BDW}^{-1} succinic acid: 116 U g_{BDW}^{-1}), which strongly exceeded the *in vivo* flux. As a consequence, ICl-DH appeared as the most potent reaction to deliver additional NADPH under stress conditions.
Subsequently NADPH consuming and generating reactions were balanced (Berger et al. 2014). The NADPH supply of *D. shibae* using glucose as substrate was calculated to 245.2 %, while the demand for anabolism was only 95.4 % (Chapter: 4.1.3), resulting a high apparent overproduction of NADPH under these growth conditions. For succinic acid grown cells, this was completely different. Here The ED pathway was nearly inactive, and also, the TCA cycle carried much lower flux than on glucose (Chapter: 4.2.3). Accordingly, the NADPH supply was 23.7 %, while the demand was 56.2 %. The apparent imbalance of NADPH supply and demand suggests, that likely a compensating

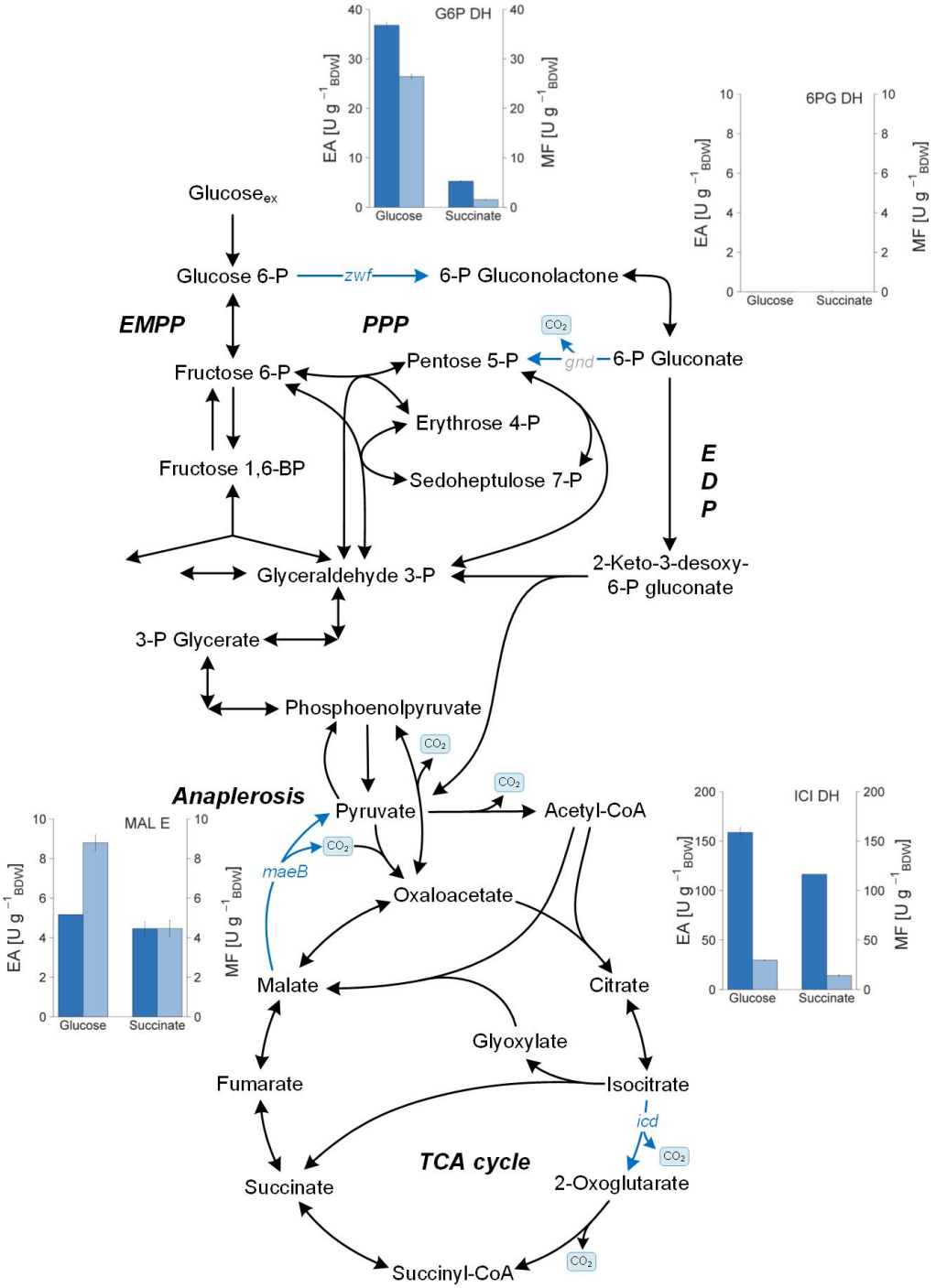

Figure 4.15.: Analysis of enzymatic activities and metabolic fluxes of *D. shibae*, involved in NADPH production. The enzymatic activities (EA in blue) and metabolic fluxes (MF in light blue), related to bio dry weight, were determined for glucose 6-phosphate dehydrogenase (G6P DH), 6-phosphogluconate dehydrogenase (6PG DH), isocitrate dehydrogenase (ICI DH) and malic enzyme (ME), all providing NADPH.

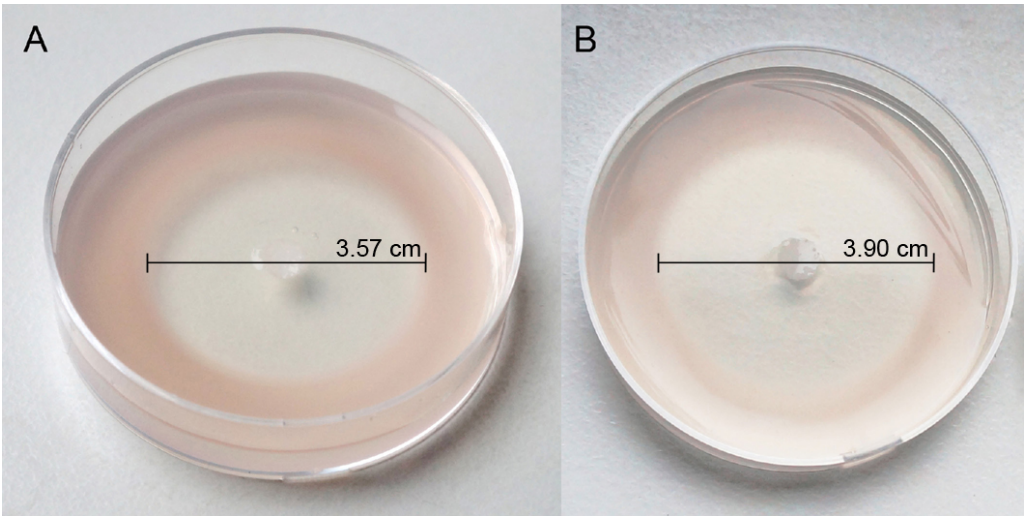

Figure 4.16.: Oxidative stress test of *D. shibae* on SWM agar plates supplemented with succinic acid (A) and glucose (B) treated with filter immersed with 0.11 g l^{-1} diamide solution. The diameter of growth inhibition is used as direct measurement of the robustness against oxidative stress, determined to 3.90 cm for glucose and 3.57 cm for succinic acid.

mechanism is involved. In this regard, NADPH is the nicotinamide adenine dinucleotide (phosphate) transhydrogenase is annotated for *D. shibae* and it appears likely for the flux data, that this enzyme plays an important role to balance the redox metabolism in *D. shibae*.

Agar plate based assay

To determine the ability of *D. shibae* to tolerate oxidative stress, cells were treated with diamide. Diamide oxidizes sulphydryl bonds in the cytoplasm which then are reduced by enzymes using NADPH as cofactor (Chavarría et al. 2013, Cumming et al. 2004). In a plate-based assay with SWM and 10 mM substrate (glucose or succinic acid), *D. shibae* was treated with a filter immersed with 0.11 g l^{-1} diamide solution. On glucose supplemented medium, a zone of inhibition of 3.9 cm could be observed around the filter (Figure: 4.16 B), while succinic acid resulted in a smaller zone of inhibition of 3.6 cm (Figure: 4.16 A). The diameter was taken as direct measure of the sensitivity against diamide and the robustness to oxidative stress.

Microtiter plate based assay

Next, oxidative stress resistance was monitored in a microtiter plate experiment. Here, diamide was added in different concentrations to growing *D. shibae* cells on SWM with glucose. The growth inhibition and diamide degradation was then recovered on-line.

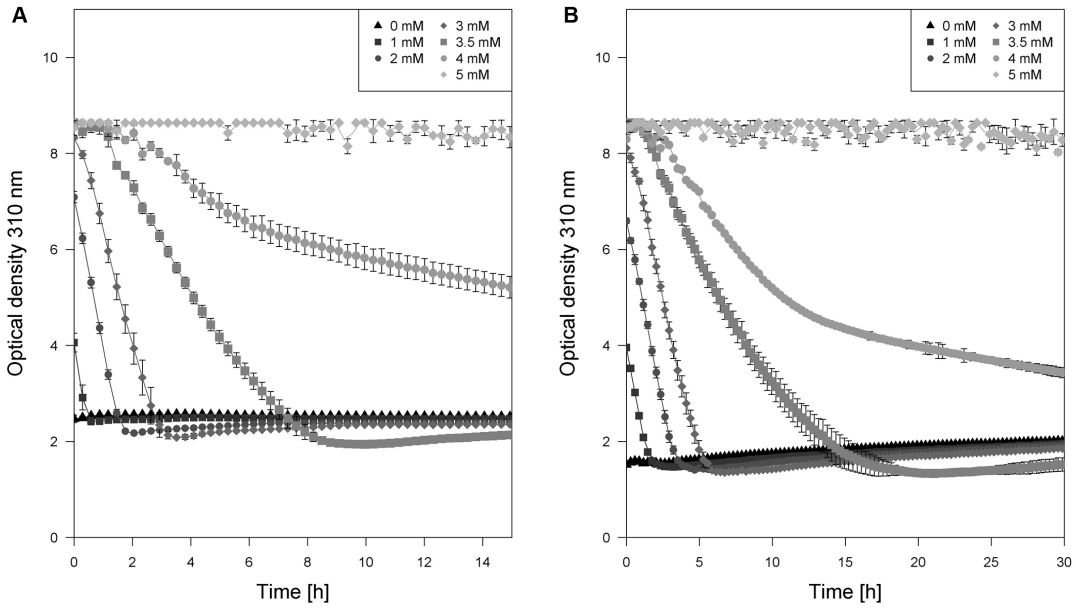

Figure 4.17.: Diamide degradation as indicator for oxidative stress defense of *D. shibae* grown on SWM with succinic acid (A) and glucose (B) as carbon source. The cultivations were conducted with different diamide concentrations (0 mM, 1 mM, 2 mM, 3 mM, 3.5 mM, 4 mM, 5 mM).

While bacterial growth was determined at 650 nm, the diamide degradation was monitored at 310 nm. The degradation of diamide by glucose grown cells is shown in Figure 4.17 B. With higher diamide concentrations added, the time of degradation increased. For concentrations of 4 mM diamide the degradation was not complete. For 5 mM diamide no degradation could be observed at all. No bacterial growth was observed at both concentrations. At lower levels, between 1 mM and 3.5 mM diamide the time of degradation corresponded to the lag phase of growth. This time was used to calculate the specific degradation rate for diamide. The microtiterplate experiment with *D. shibae* cultures, growing on SWM with succinic acid, showed a similar result. The degradation of diamide by succinic acid grown cells is depicted in Figure 4.17 A. Here the degradation of diamide also increased in correlation to its concentrations.

Glucose-grown *D. shibae* showed a specific diamide degradation rate of 4.9 mmol g^{-1} h^{-1}, while succinic acid grown cells had a degradation rate of 3.7 mmol g^{-1} h^{-1}. As control, *P. putida* showed a degradation rate of only 1.5 mmol g^{-1} h^{-1} (data not shown).

D. shibae is able to reduce diamide and handle oxidative stress

In the oceans, damages caused by reduced oxygen species are wide spread and resistance mechanisms in marine organisms are necessary (Lesser 2006). A positive effect of the

EDP on oxidative stress tolerance was recently proposed for *P. putida* by Chavarría et al. (2013). Similarly, *P. aeruginosa* exhibits high NADPH supply, which likely enhances its tolerance against oxidative stress imposed by the host (Berger et al. 2014). Also, *P. aeruginosa* it is also known to use the ED pathway exclusively (Berger et al. 2014). Regarding stoichiometry, the EMP pathway (Equation: 2.1) provides more ATP, but no NADPH in contrast to the ED pathway (Equation: 2.3). NADPH is involved in different defense mechanisms (Pollak et al. 2007, Krömer et al. 2008). Recently, it has been revealed for *P. fluorescens*, that especially the NADPH producing enzymes ICI-DH and G6P-DH show higher activities under oxidative stress conditions (Bériault et al. 2007), opposite to the other two NADPH producing enzymes 6PG-DH and MAL-E (Bériault et al. 2007).

As shown, *D. shibae* is able to reduce diamide during growth. The specific degradation rate for *D. shibae* (4.88 mmol g_{BDW}^{-1} h^{-1}) was more effective in oxidative stress defense than for *P. putida* (1.47 mmol g_{BDW}^{-1} h^{-1}). Regarding the supplied capacity of ICI-DH and G6P-DH, *D. shibae* also might profit from the high potential activity of these two enzymes producing high amounts of NADPH (Bériault et al. 2007).

All together *D. shibae* showed a high robustness against oxidative stress for both substrates tested, although differences in metabolic fluxes occurred. A highly used ED pathway and TCA cycle were shown for glucose, while for succinic acid grown cellsonly show small fluxes over ED pathway and TCA cycle, revealing in a different NADPH generation. The use of a transhydrogenase enabled the fast adaptation on different conditions and provided reduction equivalents missing. Furthermore, different other mechanisms (e.g. Superoxide dismutase) can have a positive impact on oxidative stress response.

4.4. Influence of environmental changes on metabolic pathways of *D. shibae*

Interesting questions for marine environments revolve around their response to environmental changes. In the next chapter, growth of *D. shibae* under different light regimes as well as on different substrates was investigated to address these questions.

4.4.1. Growth physiology of *D. shibae* under environmental changes

In a first act of experiments, cells were cultivated under different light conditions, i.e. permanent light, permanent dark and dark-light-cycles of 20 h each to simulate day and night, respectively. Furthermore, different carbon sources were tested: succinic acid as common carbon source and acetate and propionate as more reduced carbon sources with a higher potential to incorporate inorganic carbon(McKinlay et al. 2011, McKinlay et al. 2010). To investigate potential incorporation of inorganic carbon, high bicarbonate levels were chosen for these cultivations. In addition, the ability for autotrophic growth was tested.

Growth physiology of *D. shibae* under different light regimes

The illumination conditions strongly affected the pigmentation of *D. shibae*. When cells grew under permanent light, they exhibited a pale beige color (Figure: 4.18 A). The pigmentation was dark red, when the cultivation was under permanent dark or under dark-light cycles. At high carbon concentrations (50 mM succinate and 2.3 mM $NaHCO_3$), the cultivation profile of *D. shibae* appeared rather similar in the light and

Table 4.14.: Kinetics and stoichiometry of *D. shibae* grown in a mineral salt medium with succinate as the sole carbon source. Data comprise the specific growth rate (μ), the biomass yield ($Y_{X/S}$) and the specific substrate uptake rate (q_S) for three different illumination settings comprising permanent light, permanent dark, and dark-light cycles of 20 h, each. Data represent the mean values with corresponding standard deviations (n = 3).

Illumination	μ [h^{-1}]	$Y_{X/S}$ [g mol^{-1}]	q_S [mmol g^{-1} h^{-1}]
Light	0.18 ± 0.00	43.4 ± 1.0	4.19 ± 0.05
Dark	0.18 ± 0.00	46.3 ± 0.6	3.95 ± 0.19
Dark-light	0.18 ± 0.00	46.3 ± 0.9	3.93 ± 0.07

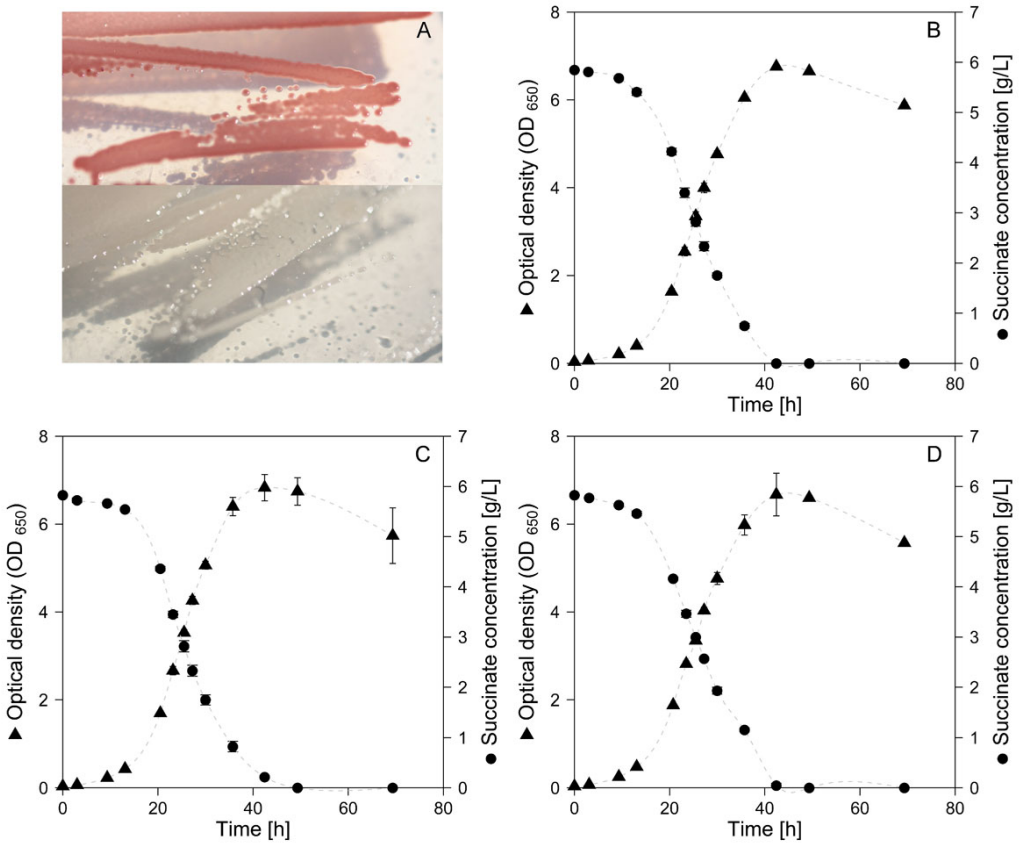

Figure 4.18.: Cultivation profile of *D. shibae* grown in permanent light (B), dark-light cycles (C) or permanent dark (D). Experiments were conducted using a mineral salt medium with succinate as the carbon source, and the data represent mean values with corresponding standard deviations (n = 3). Biomass was the only product formed. Photographs (A) show cells from five days old agar plates that have been grown at permanent dark (red colonies) or at permanent light (beige colonies).

in the dark, despite the strong change in color (Figure: 4.18 A-D). For all illumination conditions, *D. shibae* exhibited a specific growth rate of 0.18 h^{-1}. At an OD_{650} of 4, growth slowed down slightly until a maximum OD_{650} of 6.7 was reached after 42 h, which coincided with the depletion of the supplied succinate. Increasing the bicarbonate concentration to 42 mM – as later required for the labeling studies – had no significant influence on the growth performance of *D. shibae*, as indicated by the unaffected growth rate of 0.18 h^{-1}. Independent cultivations without succinate revealed that *D. shibae* was not able to grow on bicarbonate alone. Quantification of the biomass yield revealed slight differences in growth efficiency depending on the light settings (Table: 4.14). In permanent light, a biomass yield of 44.9 g mol^{-1} was achieved. This was somewhat lower than the biomass yield of 47.9 g mol^{-1} in permanent dark or the dark-light cycles. Biomass was the only product that was formed during the cultivation. None of the cultures secreted extracellular products, as verified by HPLC analysis. On glucose and

Table 4.15.: Kinetics and stoichiometry of *D. shibae* grown in a mineral salt medium with glucose, succinate, acetate and propionate, respectively, as the sole carbon source. Data denote the specific growth rate (μ), the biomass yield ($Y_{X/S}$) and the specific substrate uptake rate (q_S) for growth in permanent dark. Data represent the mean values with standard deviations (n = 3).

Substrate	μ [h^{-1}]	$Y_{X/S}$ [g mol^{-1}]	$Y_{X/S}$ [g C-mol^{-1}]	q_S [mmol g^{-1} h^{-1}]
Glucose	0.11 ± 0.00	70.3 ± 1.0	11.7 ± 0.2	1.59 ± 0.17
Succinate	0.18 ± 0.00	46.3 ± 0.6	11.6 ± 0.2	3.95 ± 0.19
Propionate	0.16 ± 0.00	50.5 ± 0.9	16.8 ± 0.3	3.18 ± 0.18
Acetate	0.15 ± 0.00	20.6 ± 0.4	10.3 ± 0.2	7.46 ± 0.36

propionate no differences in growth rate and only small changes in biomass yield and specific substrate uptake rate were observed (Table: 4.15).

Growth physiology of *D. shibae* on different carbon sources

D. shibae grows on a wide range of carbon sources, especially organic acids (Biebl et al. 2005). To investigate carbon uptake of *D. shibae* in more detail, reduced carbon sources were chosen in addition to succinate and glucose. As Hädicke et al. (2011) described for purple non-sulfur bacteria, the CO_2 production rate correlates with the carbon oxidation state of the substrate in the media. Succinate as well as acetate led to a netto CO_2 efflux, while propionate showed a netto CO_2 influx. The calculated carbon oxidation/reduction states for the three different substrates are shown in Table 4.16. Succinate was the only carbon source with an positive carbon oxidation/reduction state: i.e. a value of +0.5 per carbon atom. Acetate and glucose are neutral, while propionate was chosen as example for a negative state of –0.67. All together, propionate as substrate might be the most possible candidate for carbon incorporation in *D. shibae*, while succinate is too oxidized.

Prior to labeling studies, *D. shibae* was cultivated at high carbon (2.3 mM $NaHCO_3$)

Table 4.16.: Oxidation/reduction state of the carbon in substrates for the analysis of inorganic carbon incorporation of *D. shibae*. The relative values were averaged by dividing the value of the carbon oxidation/reduction state by the number of carbon atoms (McKinlay et al. 2011).

Substrate	Formula	Carbon oxidation state	Relative carbon oxidation state
Succinate	$C_4H_6O_4$	+2	+0.5
Acetate	$C_2H_4O_2$	0	0
Glucose	$C_6H_{12}O_6$	0	0
Propionate	$C_3H_6O_2$	-2	-0.67

and substrate concentrations (5.9 g/L succinate, 1.8 g/L glucose, 3 g/L acetate or 3.7 g/L propionate). All cultivations unraveled an exponential growth behavior. The highest specific growth rate (0.18 h^{-1}) was observed on succinic acid, followed by propionate (0.16 h^{-1}). On acetate, the cells grew with a specific growth rate of 0.15 h^{-1}. The slowest growth rate (0.11 h^{-1}) was observed on glucose (Table: 4.16).
Quantification of the C-mol dependent biomass yield showed the highest value on propionate (16.8 g C-mol^{-1}), which indicated that 73 % of this substrate were used for biomass formation. The biomass yields for succinate (11.6 g C-mol^{-1}), acetate (10.3 g C-mol^{-1}) and glucose (11.7 g C-mol^{-1}) were lower and corresponded to only 34-39 % of substrate use. Probably unlike to its reduced state, cells grown on propionate produced the highest amount of biomass per C-Atom. This indicated an effective use of propionate as carbon source, nearly twice as high as the other tested substrates.

4.4.2. Potential carbondioxide incorporation in *D. shibae* grown on succinic acid

It was now interesting to see, to which extent carbon dioxide fixation contributed to the growth of *D. shibae*. The inspection of the genomic repertoire of *D. shibae* revealed an extended set of annotated genes that are potentially involved in autotrophic and anaplerotic CO_2 fixation. Most key genes of the putative 3-HP cycle (Tomasch et al. 2011) are annotated, including acetyl-CoA carboxylase and propionyl-CoA carboxylase, putative involved in CO_2 fixation. Acetyl-CoA carboxylase is also part of fatty acid production pathway and the propionyl-CoA carboxylase also belongs to the overlapping ethylmalonyl-CoA pathway (EMC pathway). In addition, all genes of this pathway were identified, especially the second CO_2 fixating enzyme crotonyl-CoA carboxylase (Table: 2.1), which can be taken as a marker for the presence of the EMC pathway (Erb et al. 2009). Two of the three key enzymes of the reductive TCA cycle, another autotrophic CO_2 fixation route in photosynthetic bacteria, i.e. oxoglutarate synthase and fumarate reductase were not annotated. This indicated rather no activity of this cycle in *D. shibae*. Also known to incorporate inorganic carbon is pyruvate carboxylase, an anaplerotic enzyme at the entry into the TCA cycle. Moreover, incorporation of inorganic carbon during carboxylation reactions occurred in the biosynthetic pathways involving purine and pyrimidine bases, and the amino acid arginine.

Carbon dioxide incorporation into cellular polymers of *D. shibae*

To investigate the general ability of *D. shibae* to assimilate inorganic carbon from CO_2, isotope tracer experiments were conducted with 41 mM $NaH^{13}CO_3$. In parallel, reference experiments with $NaHCO_3$, having the natural isotope composition, were conducted. Cells were then analyzed for ^{13}C incorporation into the two major biomass constituents, i.e., cell protein and PHB. Most obviously, ^{13}C incorporation occurred for amino acids of the aspartate- and glutamate-family, originating from TCA cycle intermediates (Table: 4.17). Compared with the reference on non-labeled $NaHCO_3$, the amino acids aspartate, threonine, glutamate, lysine, and arginine significantly contained ^{13}C. The ^{13}C labeling exclusively referred to the single-labeled amino acids (Table: 4.17). This was a first hint concerning the functional contribution of anaplerotic pyruvate carboxylase, which is closely connected to the pool of TCA cycle intermediates. Arginine was the only exception. Here, also the double-labeled mass isotopomer occurred, most likely due to incorporation via the urea cycle (Fig. 4.8). However, the single-labeled mass isotopomer represented the major fraction. Aromatic amino acids and amino acids, that were derived from glycolytic C_3 precursors such as pyruvate, phosphoenolpyruvate and 3-phosphoglycerate, respectively, did not reveal an altered labeling pattern between the tracer and the reference cultivation (Table: 4.17). Regarding PHB biosynthesis, the monomer building block, hydroxybutyrate, displayed no ^{13}C incorporation (Table: 4.17). Overall, the results revealed the general ability of *D. shibae* to fix inorganic carbon by assimilating carbon dioxide. The ^{13}C pattern of all metabolites was independent of the illumination settings of the culture.

Experimental design – portfolio of intracellular metabolites to resolving CO_2 fixation fluxes

The contribution of different pathways to carbon fixation from CO_2 was next resolved in detail by dynamic labeling studies. This required the measurement of key intermediates to obtain pathway-specific information. As displayed in Figure 4.8, the different pathways, potentially contributing to CO_2 fixation, include specific metabolites. As a first step, metabolite profiling of *D. shibae* was conducted to clarify, if these analytes of interest were accessible in sufficient amounts for quantitative determination of ^{13}C incorporation. Key intermediates of the 3-HP cycle comprised different CoA esters (Zarzycki et al. 2009). Several of them were detected by LC-MS in suitable amounts for all light conditions (Figure: 4.19 A-B). This included malonyl-CoA, acetyl-CoA, succinyl-CoA, and methylmalonyl-CoA. Malonyl-CoA also allowed studying fatty acid biosynthesis. Other

Table 4.17.: Relative mass isotopomer fractions of amino acids and of hydroxybutyrate from hydrolyzed cells of succinate-grown *D. shibae*. The medium was supplemented with non-labeled $NaHCO_3$ and labeled $NaH^{13}CO_3$, respectively. Tracer studies were performed in permanent dark and permanent light conditions. Derivatisation of GC-MS analysis was conducted with MBDSTFA. Standard values refer to MBDSTFA-derivatives of the pure substances. M_0 denotes the non-labeled and M_1 the single-labeled mass isotopomer. Higher numbers accordingly refer to higher labeling. Data are given as the mean values (n = 2). The relative deviation for the mass isotopomer fractions was ≤ 2 %. As related to the small signal intensity of arginine, the relative error was somewhat higher (≤ 4 %).

		Non-labeled		labeled	
Analyte	**Standard**	**Dark**	**Light**	**Dark**	**Light**
Alanine (m/z 260)					
M_0	0.746	0.748	0.746	0.734	0.729
M_1	0.172	0.171	0.172	0.182	0.186
M_2	0.072	0.071	0.072	0.073	0.074
Serine (m/z 390)					
M_0	0.643	0.648	0.647	0.637	0.623
M_1	0.225	0.223	0.223	0.231	0.240
M_2	0.107	0.105	0.106	0.107	0.110
Aspartate (m/z 418)					
M_0	0.632	0.636	0.633	0.559	0.563
M_1	0.227	0.226	0.227	0.275	0.272
M_2	0.110	0.107	0.108	0.122	0.122
Glutamate (m/z 432)					
M_0	0.623	0.627	0.623	0.562	0.567
M_1	0.231	0.230	0.231	0.272	0.268
M_2	0.111	0.109	0.111	0.121	0.121
Arginine (m/z 442)					
M_0	0.622	0.585	0.594	0.276	0.171
M_1	0.238	0.224	0.229	0.413	0.446
M_2	0.107	0.102	0.103	0.193	0.216
Tyrosine (m/z 466)					
M_0	0.605	0.604	0.606	0.579	0.570
M_1	0.246	0.245	0.246	0.262	0.265
M_2	0.112	0.111	0.111	0.117	0.119
PHB (m/z 275)					
M_0	0.741	0.730	0.727	0.735	0.725
M_1	0.174	0.180	0.181	0.177	0.182
M_2	0.072	0.076	0.077	0.074	0.078

CoA-esters were hardly detectable (Figure: 4.19 A-B). Their ^{13}C enrichment could not be quantified properly, related to their small pool sizes. This included intermediates of the ECM pathway (Erb et al. 2009). Beyond the CoA thioesters, the successful measurement of coenzyme A itself allowed insights into coenzyme A biosynthesis and related reactions of the purine pathway (Figure: 4.8). To determine the contribution of remaining pathways to carbon dioxide assimilation, free intracellular amino acids were

used. In particular, amino acids of the aspartate family provided insights into a potential contribution of anaplerotic carboxylation activity. Arginine enabled a functional analysis of the urea cycle. For the aspartate- and glutamate-derived amino acids, adequate signal sizes for the free intracellular pools allowed quantitative ^{13}C analysis and thus dynamic labeling studies (Figure: 4.19 C-D). Lysine and arginine, however, only yielded sufficient signals for cells grown in the dark-light cycle. Overall, the spectrum of measurable metabolites provided a substantial basis to unravel the functional contribution of the proposed pathways to CO_2 fixation using dynamic labeling studies.

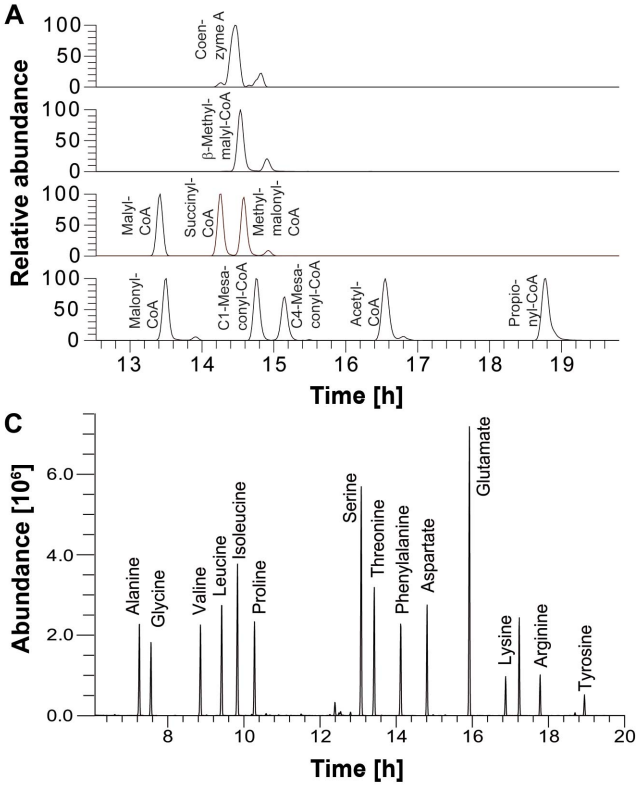

B

Metabolite	Dark	Light	Dark-light
Malyl-CoA	-	-	-
Malonyl-CoA	+	+	+
Succinyl-CoA	+	+	+
Methylmalonyl-CoA	+	+	+
Coenzyme A	+	+	+
β-Methylmalyl-CoA	-	-	-
C1-Mesaconyl-CoA	(+)	(+)	(+)
C4-Mesaconyl-CoA	(+)	(+)	(+)
Acetyl-CoA	+	+	+
Propionyl-CoA	(+)	(+)	(+)
Hydroxybutyryl-CoA	(+)	(+)	(+)
Ethylmalonyl-CoA	(+)	(+)	(+)
Methylsuccinyl-CoA	(+)	(+)	(+)
Mesaconyl-CoA	(+)	(+)	(+)
Methylmalyl-CoA	(+)	(+)	(+)

D

Metabolite	Dark	Light	Dark-light
Alanine	+	+	+
Glycine	+	+	+
Valine	+	+	+
Leucin	-	-	-
Isoleucine	-	-	-
Proline	-	-	-
Serine	+	+	+
Threonine	+	+	+
Phenylalanine	(+)	(+)	+
Aspartate	+	+	+
Glutamate	+	+	+
Lysine	(+)	-	+
Arginine	-	-	+
Tyrosine	-	-	+

Figure 4.19.: Metabolite profiling of intracellular CoA esters and free amino acids in *D. shibae*. Pool sizes were analyzed with regard to their suitability for dynamic labeling studies. Appropriate pool sizes allowing quantitative analysis of ^{13}C enrichment are indicated by '+'. The label '(+)' denotes detection of the metabolites but not sufficient data quality to quantify ^{13}C enrichment. Metabolites that could not be detected are indicated by '-'. To account for potential light-dependent deviations, the metabolite profiling was conducted for the three relevant illumination conditions (n = 2). The LC-MS results were determined in cooperation with Dr. Patrick Kiefer (ETH Zürich).

Dynamic $^{13}CO_2$ incorporation into CoA esters

To investigate the *in vivo* activity of the 3-HP cycle, the sequential incorporation of the ^{13}C-labeling into the corresponding key CoA ester intermediates was analyzed. This revealed a time-dependent increase of the ^{13}C enrichment as shown in Figure 4.20 A. The labeling increased rather slowly until a plateau after 4 h. It became obvious that the labeling dynamics were identical for almost all investigated CoA esters and also for the coenzyme A molecule itself (Figure: 4.20 A). For each compound, the maximal ^{13}C enrichment after 4 h of incubation corresponded to the presence of 70 % of the single-labeled thioester or coenzyme A, respectively. No multi-labeled mass isotopomer fractions were detected. In this regard, malonyl-CoA represented a unique exception. Both the time course of label incorporation as well as the overall ^{13}C enrichment differed from the other thioesters. Within the first hours, ^{13}C incorporation was significantly faster compared with the other analytes (Figure: 4.20 A). Still, it took 4 h until the labeling pattern of malonyl-CoA became constant. The final ^{13}C enrichment was approximately twice as high as that of coenzyme A and the other thioesters (Figure: 4.20 A). The illumination conditions did not influence the pattern or dynamics of the ^{13}C incorporation, for all tested analytes. The ^{13}C labeling profile for cells grown in permanent light or permanent dark was identical to the profile for dark-light cycles (Figure: 4.20 A).

Dynamic ^{13}C incorporation into amino acids

Beyond the stationary ^{13}C experiment, labeling dynamics were assessed for free intracellular amino acids representing the C_3-family, the aspartate family and the glutamate family. The time profile of the label incorporation immediately revealed different dynamics compared with the CoA esters (Figure: 4.20 B). This was mainly reflected by a saturation of ^{13}C enrichment within only 1 - 2 h. This labeling enrichment determined for the maximum ^{13}C enrichment of the free amino acid pools was identical with the protein-bound amino acids. These results indicated sufficient supply of the ^{13}C bicarbonate throughout the entire tracer cultivation. For free aspartate and glutamate, only the single-labeled mass isotopomer fraction was detected. In addition, for arginine, however, the amount of the double-labeled molecules significantly increased. The labeling profile of alanine and serine, representatives for the C_3-derived amino acids, did not reveal any ^{13}C incorporation. As already found for the CoA esters, the different light regimes did not influence the labeling profiles. In general, the relative ^{13}C enrichment was lower compared with the CoA esters.

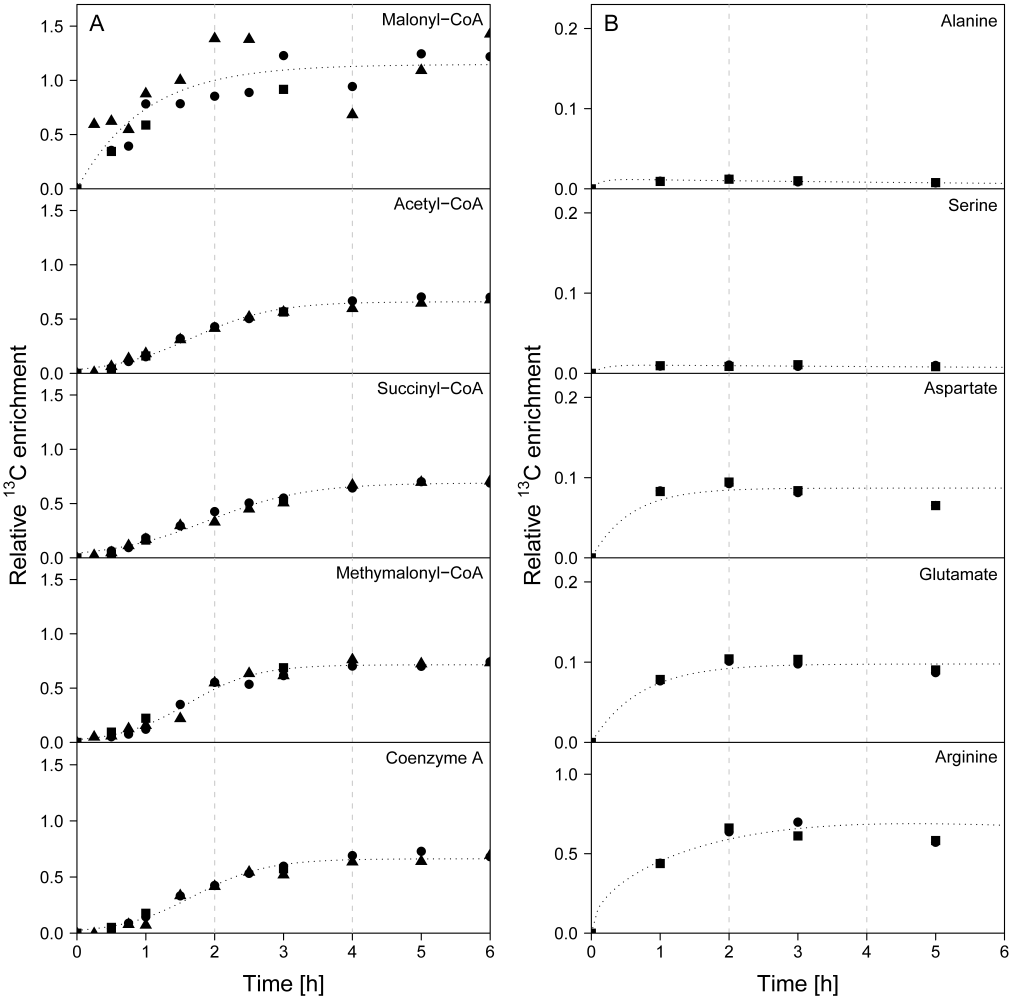

Figure 4.20.: Dynamic ^{13}C incorporation from carbon dioxide into CoA thioesters (left, n = 3) and free intracellular amino acids (right, n = 2). Dynamic labeling profiles are displayed for cells grown at dark-light cycles. Independent experiments are indicated by different symbols. The dynamic ^{13}C profiles were identical for cells grown in permanent light or permanent dark (data not shown).

The 3-HP cycle does not contribute to CO_2 fixation in succinate-grown *D. shibae*

At first glance, the increase of the ^{13}C labeling into the CoA esters suggested a functional contribution of the 3-HP cycle to CO_2 fixation, a picture that faded upon closer inspection of the ^{13}C labeling dynamics. Obviously, the time profile for all investigated intermediates of this pathway was identical. In contrast, subsequent incorporation of the labeled carbon into the different metabolites along their position within the pathway would be expected for full *in vivo* activity, as previously observed for methanol assimilation via the ethylmalonyl-CoA pathway by *M. extorquens* (Peyraud et al. 2009).

Furthermore, the time for label incorporation into the CoA esters was much longer than the values expected for such low intracellular pool sizes. Indeed, it required several hours to achieve constant labeling. In *M. extorquens*, though, ^{13}C incorporation results within a few seconds (Peyraud et al. 2009). The most obvious proof for ^{13}C incorporation, independent from 3-HP cycle was the labeling enrichment of coenzyme A itself, which was identical to all investigated thioesters. Without doubt, the ^{13}C labeling within the thioester originated from the CoA backbone, but not from the CoA-bound metabolites. As displayed in Figure 4.8, the CoA biosynthesis involves CO_2 incorporation by phosphoribosylaminoimidazole carboxylase as part of the purine pathway (Michal 1999), which is the reason for the observed ^{13}C enrichment.

In summary, the proposed 3-HP cycle does not contribute to CO_2 fixation under the investigated conditions. Together with the fact that two metabolites weren't detected at all and one gene of the 3-HP cycle has not been identified to date; thus, it is possible that the cells do not have a functional 3-HP cycle (Figure: 4.8). Still, it was interesting to see that most of the related metabolites were present in *D. shibae*. It can believed that they most likely belong to pathways with other functions like the ethylmalonyl-CoA pathway lately described for *R. pomeroyi*, another *Roseobacter* (Reisch et al. 2013). For growth on acetate or dimethylsulfoniopropionate (DMSP) medium, this pathway is used in organisms, lacking the isocitrate lyase, as alternative route for the glyoxylate shunt and as part of the DMSP degradation route (Reisch et al. 2013, Alber et al. 2006,Erb et al. 2010). Accordingly, the corresponding genes could encode part of the DMSP utilization pathway. DMSP is regarded as an important nutrient for the *Roseobacter* clade, due to their symbiosis with DMSP-producing algae (Curson et al. 2011). It is interesting to note that DMSP formation by macro algae is induced in light (Karsten et al. 1990). The light-induced expression of the corresponding genes might thus reflect a fine-tuned response of a symbiotic bacterium to the nutrient supply by its partner. This hypothesis, however, has to be tested. *D. shibae* is not a mixotroph, i.e., does not co-metabolize carbon dioxide and organics, as shown for other photosynthetic marine bacteria (Muñoz-Marín et al. 2013). However, it cannot fully be excluded, that the 3-HP cycle under environmental conditions different from our experiments might be active. In this study, higher levels of CO_2 and succinate were used. Organic excess in the sea is observed under certain conditions such as algal blooms or eutrophic coastal waters (Anderson et al. 2002), but such conditions are not representative for the marine environment, which is widely deprived in nutrients (Sharp 1993).

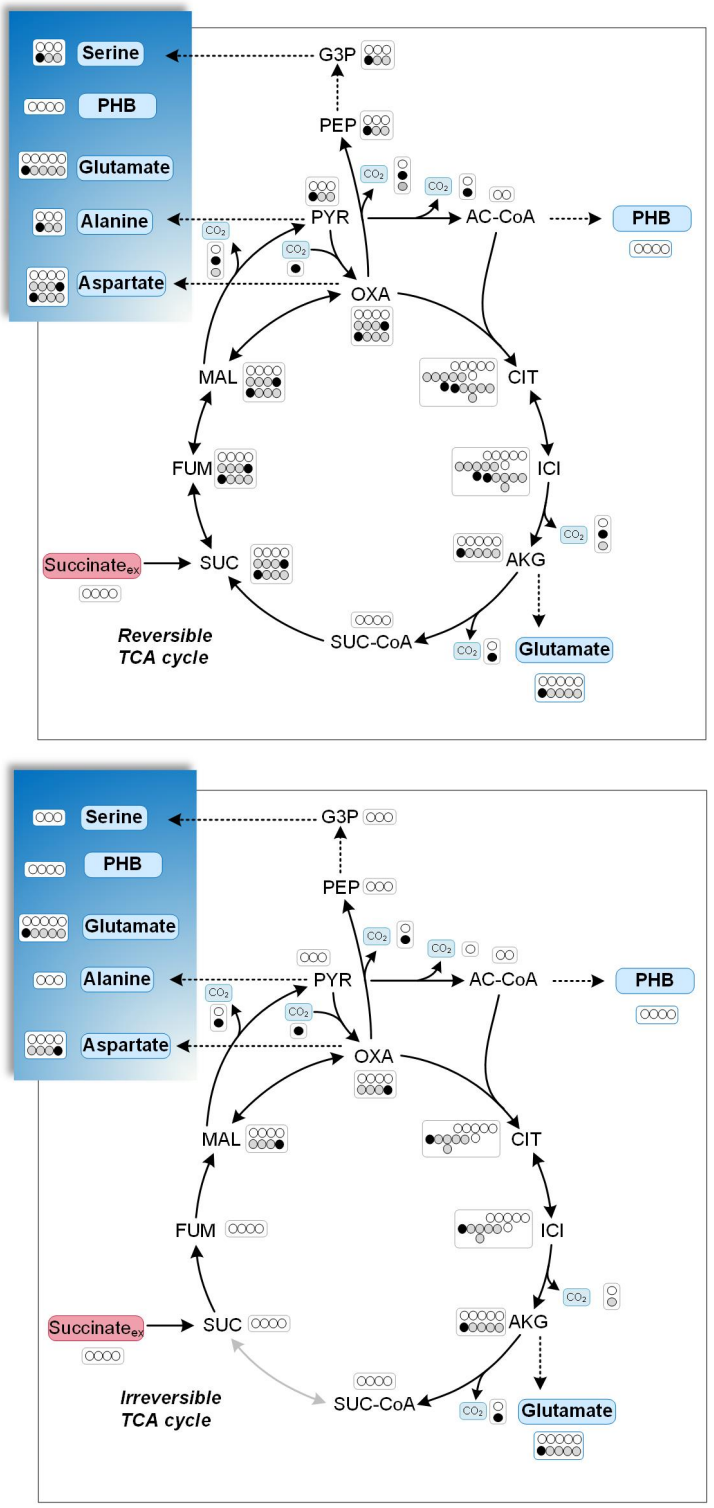

Figure 4.21.: Carbon transition resulting from the oxidative TCA cycle with reversible (A) and irreversible (B) interconversion of C_4 intermediates while growing on unlabeled succinate and ^{13}C-labeled carbonate. The closed circles indicate ^{13}C-labeled carbon atoms, open circles indicate non-labeled carbon atoms.

Anaplerotic carboxylation significantly contributes to carbon dioxide fixation

labeling profiling of free intracellular metabolites revealed ^{13}C incorporation into amino acids of the aspartate and glutamate family. C_3-derived amino acids were, however, unlabeled. Therefore, carbon dioxide fixation is likely linked to the activity of C_3-carboxylating enzymes. Given the existing genome annotation (Wagner-Döbler et al. 2010), the presence of different reactions for C_3/C_4 interconversion, including pyruvate carboxylase, malic enzyme and phosphoenolpyruvate (PEP) carboxykinase, is expected. Previous studies of a spectrum of phylogenetically diverse organisms disclosed that they generally catalyse the decarboxylation of oxaloacetate (OAA) and malate (Becker et al. 2008, Sauer et al. 2005, Petersen et al. 2000). Here, this is likely related to the utilization of succinate as a carbon source, requiring gluconeogenesis. The major role for anaplerotic carboxylation in *D. shibae* was, thus, attributed to pyruvate carboxylase, thereby forming single-labeled OAA. This is a direct precursor of aspartate and related amino acids, which, as a result, exhibit ^{13}C labeling (Figure: 4.21). Through the activity of citrate synthase and isocitrate dehydrogenase, the glutamate precursor 2-oxoglutarate originates from OAA, whereby the ^{13}C-labeling is conserved and is, thus, found in glutamate (Figure: 4.21). Still, a substantial portion of aspartate and glutamate was unlabeled. These results indicate that the major OAA pool was fed by the externally supplied carbon source, succinate. This is also confirmed by metabolic flux analysis revealing 94 % flux from succinate and only 43 % from pyruvate through carboxylation.

Carbon dioxide fixation is linked to biosynthetic routes

As illustrated above for coenzyme A, specific biosynthetic reactions contributed to carbon dioxide fixation. Indeed, the label incorporation during coenzyme A formation was attributed to purine biosynthesis (Figure: 4.8). Related to this, all purine-based metabolites including the DNA and RNA building blocks as well as energy compounds such as ATP or GTP rely on carbon dioxide. From the dynamic labeling incorporation into the CoA thioesters it became obvious that the ^{13}C enrichment in malonyl-CoA was significantly higher than that in other CoA-bound metabolites. This indicated additional carbon fixation during malonyl-CoA formation. Malonyl-CoA is formed in the first reaction of the fatty acid biosynthesis via the activity of acetyl-CoA carboxylase, assimilating inorganic CO_2 (Michal 1999). However, in the next step, the condensation with acetyl-CoA, this CO_2 is released again. Consequently, the malonyl-CoA based molecules, i.e., fatty acids, lipids and polyhydroxyalkanoate (PHA) in some species, did not contain incorporated CO_2 (Escapa et al. 2012). In this regard, it is interesting that *D. shibae* can accumulate up to 72 % polyhydroxybutyrate (PHB) (Xiao et al. 2011), a C_4 PHA. As ex-

pected, ^{13}C enrichment in the monomer building block of PHB was not detected (Table: 4.17). For this reason, for *D. shibae*, a malonyl-CoA independent PHB biosynthesis via acetoacetyl-CoA seems likely, as described for *Ralstonia eutropha* (Escapa et al. 2012). The lack of ^{13}C incorporation into PHB additionally indicated that the accumulation of storage compounds in *D. shibae* strictly depends on the presence of organic carbon. The cells appear to be unable to take benefit from assimilating inorganic carbon to bridge phases of starvation. labeling analysis of the proteogenic amino acids revealed a clear contribution of pyruvate carboxylase to carbon dioxide fixation as discussed above. The high labeling enrichment observed for arginine, however, might be attributed not to this reaction, but to biosynthesis in the urea cycle and, thus, carbon dioxide fixation via carbamoylphosphate synthase (Figure: 4.8). This is also one of the initial steps for the biosynthesis of pyrimidines (Figure: 4.8). Consequently, these building blocks of DNA and RNA also rely on CO_2 fixation as already discussed above for the purine precursors. As anticipated before, the absence of the rTCA cycle becomes obvious from the labeling pattern of several amino acids. Its contribution would have yielded double-labeled oxaloacetate derived amino acids, i.e. aspartate and threonine, as well as single-labeled amino acids, originating from pyruvate (Figure: 4.21). However, these were not found, which yet confirms the absence of the cycle.

Carbon dioxide fixation accounts for 1.4 % of total carbon assimilation in *D. shibae*

Based on the macromolecular biomass composition (Table: 4.18), pathway stoichiometry and ^{13}C enrichment of the individual building blocks, i.e., amino acids, nucleotides, and fatty acids, the overall contribution of CO_2 to biomass formation was determined to be 1.4 % (Table: 4.18). The dominating fraction of the cell was, thus, built from organic carbon. In the context of carbon dioxide assimilation by the marine biota and global carbon cycle, this is an important finding. So far, it has been speculated that the *Roseobacter* clade, especially the bacteria able to perform aerobic anoxygenic photosynthesis, play a substantial role in marine CO_2 fixation and cycling of organic and inorganic carbon (Kolber et al. 2001). This work provides evidence that, despite their dominant presence within the marine ecosystem, the *Roseobacter* clade only contributes to a minor extent to carbon dioxide assimilation. In the conditions tested, the growth of *D. shibae* can, indeed, not be stimulated or boosted by CO_2, but almost exclusively relies on the presence of organic carbon. This might explain the symbiotic growth with dinoflagellates, which may provide organic carbon, often observed in the natural habitat (Biebl et al. 2005).

4.4.3. Differences in the central metabolic pathways under environmental changes

The next interesting questions were the carbon dioxide incorporation subjected to changing environmental conditions and which pathways might then be activated. The most obvious alteration was the coloration of the cells under different light regimes. It seemed to be also interesting to know how the carbon oxidation state was involved in carbon dioxide incorporation and which pathways were used to metabolize other substrates.

labeling studies for the investigation of related pathways for assimilating different carbon sources

Isotope tracer experiments were conducted for different substrates (glucose, acetate, propionate) as described above (Chapter 4.4.2). Table: 4.19 summarizes the corrected

Table 4.18.: Macromolecular biomass composition of succinate-grown *D. shibae*. Data are given as the mean values with corresponding standard deviation (n = 3). In addition, the relative CO_2 incorporation for each compound is given. This was calculated from the monomeric composition of the corresponding polymer fraction and the fractional ^{13}C enrichment. The latter was determined experimentally (amino acids, PHB) or was deduced from pathway stoichiometry (lipids, nucleotides).

Polymer Component	Biomass fraction [g g^{-1}]	Metabolites	Polymer fraction [g $g^{-1}_{Polymer}$]	Fractional ^{13}C enrichment	Relative CO_2 incorporation [%]
Protein[a]	0.406 ± 0.048	Aspartate[b]	0.20	0.094	1.43
		Threonine	0.05	0.130	
		Glutamate[c]	0.21	0.103	
		Arginine	0.05	0.655	
PHB	0.502 ± 0.053	3-hydroxybutyrate	1.00	0.000	0.00
Lipids[a]	0.040 ± 0.013	3OH 10:0 fatty acid	0.02	0.004	0.00
		12:1 fatty acid	0.03	0.005	
		3OH 14:1 fatty acid	0.03	0.005	
		18:1w7c fatty acid	0.53	0.068	
		18:0 fatty acid	0.04	0.005	
		cyclo 19:0 fatty acid	0.03	0.003	
DNA	0.047 ± 0.006	Purine	0.50	0.069	7.25[d]
		Pyrimidine	0.50	0.076	
RNA	0.067 ± 0.010	Purine	0.56	0.069	7.20[d]
		Pyrimidine	0.44	0.076	
Others	0.042 ± 0.015				–
Sum of organics	**1.105 ± 0.144**				**1.41**

[a] monomeric composition was taken from Neidhardt et al. (1990)
[b] given as lumped pool of aspartate and thereof derived amino acids methionine and isoleucine
[c] given as lumped pool of glutamate and proline
[d] given as relative fraction of the purine ring and pyrimidine ring, respectively. Relative fraction of purines and pyrimidines was determined from the GC content (Wagner-Döbler et al. 2010).

relative mass isotopomer fractions of amino acids and of hydroxybutyrate from hydrolyzed cells of *D. shibae* grown on the different substrates. In all cases, the medium was supplemented with labeled $NaH^{13}CO_3$ and the tracer studies were performed in permanent dark conditions.

To get an insight into the total labeling of cells, grown on different substrates, the summed fractional labeling was calculated (Table: 4.20). The results presented in Table 4.19 demonstrated, that the incorporation of inorganic carbon into amino acids was higher on glucose, acetate and propionate, than on succinic acid. For glucose, the most pronounced ^{13}C incorporation occurred for amino acids of the aspartate- and glutamate-family built from TCA cycle intermediates. In total, aspartate, threonine, glutamate, lysine, and arginine significantly contained ^{13}C labeled molecules, when grown in presence of $NaH^{13}CO_3$. This was even more obvious for the calculated summed fractional labeling (Table: 4.20). Here, the total labeling of aspartate and glutamate was 5 and 3 times higher, respectively, as for succinic acid. For glutamate, the ^{13}C labeling exclusively referred to the single-labeled amino acid (Table: 4.19), while the other amino acids showed also double-labeled patterns. Again, the labeling in all TCA cycle derived amino acids referred to the functional contribution of anaplerotic pyruvate carboxylase. The m+2 labeling for aspartate and threonine, both derived from oxaloacetate, indicated flux reversibility of the TCA cycle reactions between succinic acid and oxaloacetate. For arginine, the double-labeled mass isotope indicated an incorporation via the urea cycle (Figure: 4.8). Aromatic amino acids and amino acids that were derived from glycolytic C_3 precursors, such as pyruvate, phosphoenolpyruvate and 3-phosphoglycerate as well as PHB, did not reveal an altered labeling pattern between the tracer cultivation on glucose and on succinic acid. They were all unlabeled (Table: 4.19 and 4.20). In conclusion 5.3 % of the carbon atoms from the protein fraction was labeled, which was 3.7 times higher as for succininc acid (Table: 4.21).

Regarding acetate-grown cells, an equal distribution of the labeling for all amino acids was observed (Table: 4.19). In total, 3.1 % of the carbon atoms from the protein fraction were labeled (Table: 4.21). As exception, PHB was unlabeled. Obviously, also C_3 derived amino acids like alanine, valine, serine and glycine showed an incorporation of $NaH^{13}CO_3$. Here, the C_1 carbon atom of the molecules was labeled, which was not released as CO_2 by malic enzyme or phosphoenolpyruvate carboxykinase and was incorporated before entering the TCA cycle. More apparent was the ^{13}C incorporation into the aspartate- and glutamate-family amino acids, derived from the TCA cycle. For glutamate, nearly the same mass isotopomer fractions were found as for succinic acid grown cells, while aspartate showed a ^{13}C enrichment, which was twice as high (Table: 4.19 and 4.20).

Table 4.19.: Corrected relative mass isotopomer fractions of amino acids and of hydroxybutyrate from hydrolyzed cells of *D. shibae* grown on different substrates. The medium was supplemented with labeled $NaH^{13}CO_3$ and the tracer studies were performed in permanent dark conditions. Derivatisation prior to GC-MS analysis was conducted with MBDSTFA. Standard values refer to MBDSTFA-derivatives of the pure substances. M_0 denotes the non-labeled and M_1 the single-labeled mass isotopomer. Higher numbers accordingly refer to higher labeling. Data are given as the mean values (n = 2). The relative deviation for the mass isotopomer fractions was ≤ 2 %. As related to the small signal intensity of arginine, the relative error was somewhat higher (≤ 4 %).

Analyte	Standard	Succinate	Glucose	Acetate	Propionate
Alanine (m/z 260)					
M_0	0.965	0.950	0.949	0.879	0.658
M_1	0.032	0.049	0.050	0.118	0.335
M_2	0.002	0.001	0.000	0.002	0.007
Valine (m/z 288)					
M_0	0.948	0.933	0.930	0.859	0.619
M_1	0.050	0.065	0.069	0.136	0.365
M_2	0.002	0.002	0.001	0.005	0.015
Serine (m/z 390)					
M_0	0.964	0.952	0.948	0.859	0.637
M_1	0.033	0.046	0.051	0.139	0.356
M_2	0.003	0.001	0.000	0.002	0.007
Glycine (m/z 246)					
M_0	0.977	0.958	0.947	0.850	0.634
M_1	0.022	0.042	0.052	0.148	0.362
Aspartate (m/z 418)					
M_0	0.956	0.846	0.469	0.780	0.351
M_1	0.041	0.148	0.457	0.207	0.600
M_2	0.004	0.006	0.072	0.012	0.047
Glutamate (m/z 432)					
M_0	0.944	0.850	0.618	0.857	0.627
M_1	0.052	0.143	0.368	0.138	0.359
M_2	0.004	0.007	0.013	0.004	0.014
Arginine (m/z 442)					
M_0	0.949	0.425	0.121	0.321	0.127
M_1	0.051	0.496	0.564	0.589	0.532
M_2	0.000	0.072	0.301	0.087	0.324
Tyrosine (m/z 466)					
M_0	0.911	0.853	0.900	0.705	0.303
M_1	0.084	0.121	0.095	0.255	0.430
M_2	0.003	0.010	0.004	0.037	0.221
PHB (m/z 275)					
M_0	0.959	0.951	0.962	0.959	0.958
M_1	0.041	0.047	0.038	0.040	0.041
M_2	0.001	0.003	0.000	0.000	0.000

The highest labeling incorporation resulted for the cultivation on propionate, supplemented with $NaH^{13}CO_3$, where 10.6 % of the carbon atoms from the protein fraction

was labeled, which was 7.6 times higher than for succinic acid (Table: 4.21). All amino acids showed similar high labeling enrichments of the M+1 fragment (Table: 4.19). This might be caused by propionyl-CoA carboxylase, catalyzing the first carboxylation step of the assimilation of propionate. The molecule then enters the TCA cycle via succinyl-CoA. As described for acetate, the next step was the hydrolysis catalyzed by succinyl-CoA synthase to succinic acid. Since succinic acid is a symmetric molecule, the

Table 4.20.: Summed fractional labeling of amino acids and of hydroxybutyrate from hydrolyzed cells of *D. shibae* grown on succinate, glucose, acetate and propionate. The medium was supplemented with labeled $NaH^{13}CO_3$ and the tracer studies were performed in permanent dark. The sum fractional labeling was then calculated from corrected relative mass isotopomer fractions as described before (Wittmann 2007). The values were corrected for natural labeling and higher numbers accordingly refer to higher labeling. Data are given as the mean values (n = 3). The relative deviation for the mass isotopomer fractions was ≤ 2 %. As related to the small signal intensity of arginine, the relative error was somewhat higher (≤ 4 %).

Analyte	Succinate	Glucose	Acetate	Propionate
Alanine (m/z 260)	0.015	0.015	0.086	0.312
Valin (m/z 390)	0.015	0.018	0.092	0.344
Serine (m/z 390)	0.010	0.014	0.105	0.331
Glycin (m/z 390)	0.019	0.030	0.128	0.345
Aspartate (m/z 418)	0.113	0.560	0.185	0.651
Glutamate (m/z 432)	0.097	0.335	0.087	0.327
Arginine (m/z 442)	0.618	1.160	0.723	1.187
Tyrosine (m/z 466)	0.105	0.005	0.238	0.911
PHB (m/z 275)	0.010	0.000	0.000	0.000

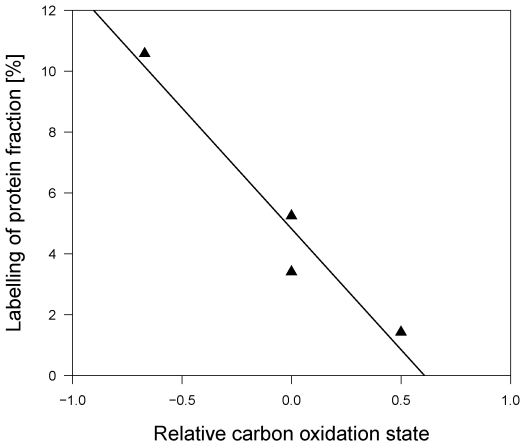

Figure 4.22.: Total labeling of carbon atoms of the protein fraction for *D. shibae* in relation to the relative oxidation state of the used substrate.

Table 4.21.: Relative CO_2 incorporation in the protein fraction of *D. shibae* cells grown on different carbon sources. This was calculated from the monomeric composition of the protein fraction and the fractional ^{13}C enrichment. The amino acids were determined experimentally.

	Succinate	Glucose	Acetate	Propionate
total labeling of carbon atoms of the protein fraction [%]	1.43	5.25	3.41	10.58

incorporated labeled carbon atom can be found on either the C_1 or C_4 of this molecule. The labeling would further be spread by anaplerosis and could be found again in amino acids derived from glycolytic C_3 precursors. Analysis exposed that only arginine showed a slightly higher total labeling in the same amount as for glucose (Table: 4.20).
Overall, the results revealed the general ability of *D. shibae* to incorporate inorganic carbon into cell protein by assimilating carbon dioxide. Obviously, the ability to incorporate inorganic carbon shows a dependency on the carbon oxidation state of the used carbon source (Figure: 4.22). The higher reduced the used carbon source for growth is, the more carbon dioxide is incorporated into cell protein. Furthermore it turned out, that the ^{13}C pattern of all metabolites, were independent of the illumination settings of the culture.

Enzymatic assays for the unravelling of the assimilation route used for acetate metabolism

Different pathways for aerobic acetate assimilation are known, the glyoxylate shunt, the ethylmalonyl-CoA pathway and the methylaspartate cycle (Erb 2011). Here, it should be analysed which pathways were active in *D. shibae*. While for the ethyl-CoA pathway all genes were annotated, the isocitrate lyase, the key enzyme from glyoxylate shunt, was missing (Figure: 4.8). But as seen in the previous chapter, the labeling pattern fits for both pathways. To validate the absence of the isocitrate lyase and therefore the inactivity of the glyoxylate shunt, enzymatic assays for both key enzymes, malate synthase and isocitrate lyase, were established. *C. glutamicum* was used as positive control for the functionality of the assay for the isocitrate lyase.
As expected by analyzing the genomic repertoire of *D. shibae*, no activity for isocitrate lyase was determined for growth on minimal medium supplemented with acetate (Figure: 4.23), while the positive control depicted an activity of 55 mU mg^{-1}_{Prot} also grown on acetate medium. In contrast, for malate synthase an activity of 222 mU mg^{-1}_{Prot} was measured. This corresponds to 93.6 % of the substrate uptake rate and is part of both

possible metabolic pathways. Taken together, the ethylmalonyl-CoA pathway seems to be the pathway, that is involved in acetate assimilation in *D. shibae*.

The incorporation of inorganic carbon depends on the metabolized substrate

Bacteria use different pathways for the assimilation of different carbon sources and therefore the incorporation of inorganic carbon changes. It was shown that during growth on succinic acid, only anaplerotic reactions lead to incorporation of ^{13}C bicarbonate (Table: 4.19). When the cells were cultivated on glucose, however, the metabolic pathways used were different. When carbon entered the citrate cycle from the pyruvate node, the activity of pyruvate carboxylase increases significantly to fill up the TCA cycle with the intermediate oxaloacetate (Sauer et al. 2005). The results showed furthermore an higher enrichment in labeling of TCA cycle derived amino acids than for succinic acid grown cells indicating an increased activity of pyruvate carboxylase, since it is the only possible enzyme for labeling incorporation (Figure: 4.24). This observation is especially important, regarding the growth behavior of a pyruvate carboxylase knockout mutant (Δ PYC). On glucose, no growth could be observed, while the cells were still able to grow on succinic acid, but without labeling incorporation (data not shown). The phosphoenolpuruvate carboxylase, another possible enzyme to replenish the citrate cycle, is not annotated for *D. shibae* and it also seems not to be expressed under these conditions. In conclusion for growth on glucose, pyruvate carboxylase is essential in *D. shibae* and responsible for the main labeling incorporation. For *B. subtilis*, pyruvate carboxylase was also reported as

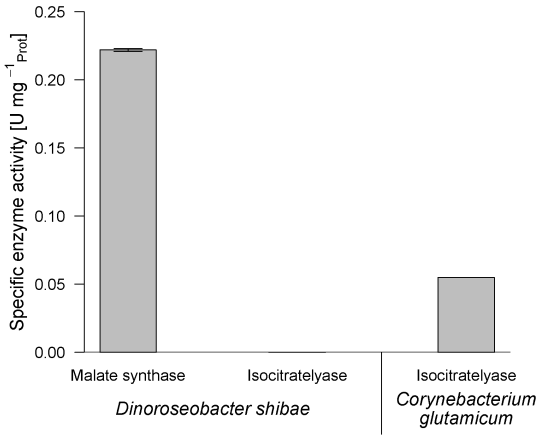

Figure 4.23.: Enzymatic activity for the key enzymes of the glyoxylate shunt, malate synthase and isocitrate lyase for *D. shibae* grown on acetate minimal medium. As positive control the activity for the isocitrate lyse of *C. glutamicum* was determined in the same way.

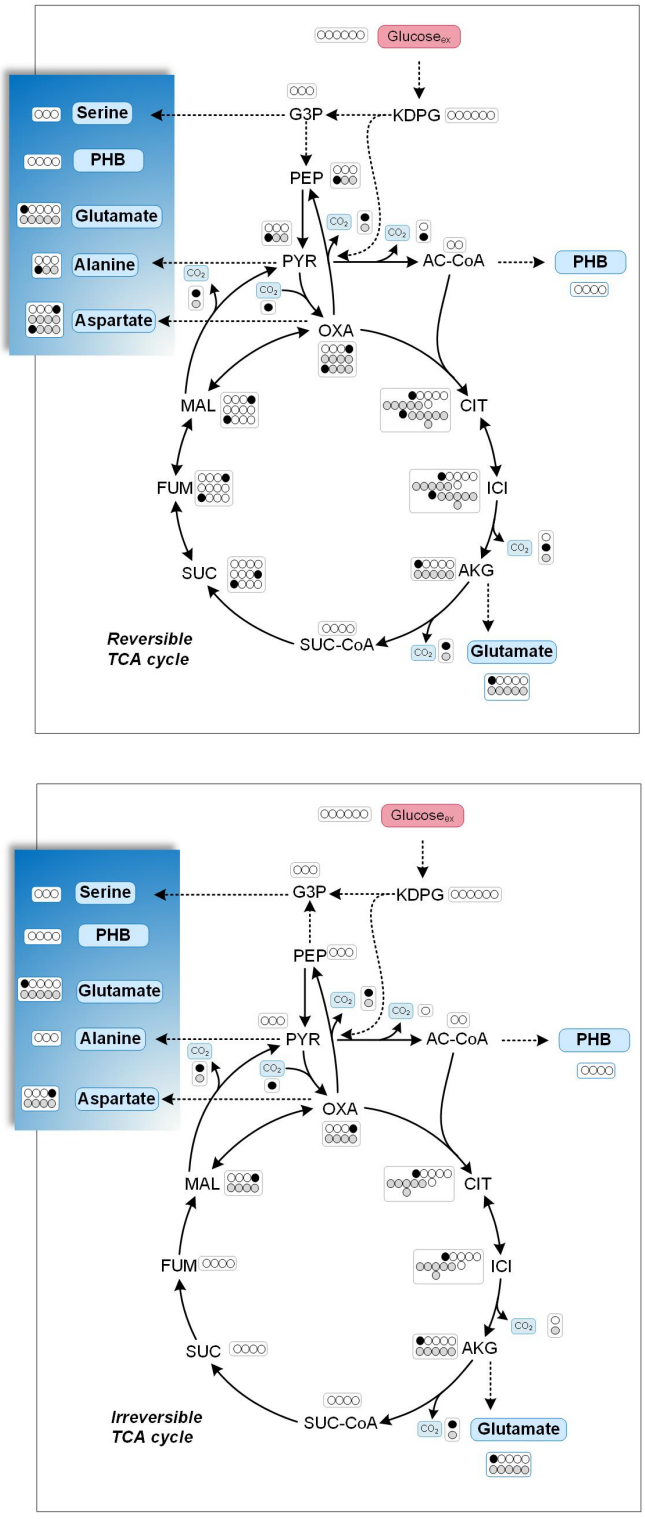

Figure 4.24.: Carbon transition resulting from the oxidative TCA cycle with reversible (A) and irreversible (B) interconversion of C_4 intermediates while growth on unlabeled glucose and ^{13}C-labeled carbonate. The closed circles indicate ^{13}C-labeled carbon atoms, open circles indicate non-labeled carbon atoms.

essential enzyme for bacterial growth in the absence of phosphoenolpyruvate carboxylase and was mainly responsible for carbonate incorporation (Diesterhaft et al. 1973). It is interesting to note that alanine was unlabeled. This indicated a nearly fully inactivity of malic enzyme and phosphoenolpyruvate carboxykinase during growth on glucose.
As most potential carbon source to incorporate inorganic carbon, propionate was studied. Since on propionate the highest biomass yield was achieved, it seemed reasonable that this might also result in the highest amount of fixed inorganic carbon. Propionate usually enters the TCA cycle at succinyl-CoA, as shown for *R. palustris* (Wampler et al. 2005). Previous to this reaction one carboxylation step is involved, so that every molecule entering the TCA cycle would be single labeled (Figure: 4.25). This labeling was then spread over the TCA cycle equally distributed to the C_1 and C_4 based on the symmetry of succinate. By anaplerotic reactions, labeling reached also the upper part of glycolysis. As a result, the highest labeling incorporation for all tested substrates was determined.

In conclusion, anaplerotic carboxylation and biosynthetic reactions contribute to in-

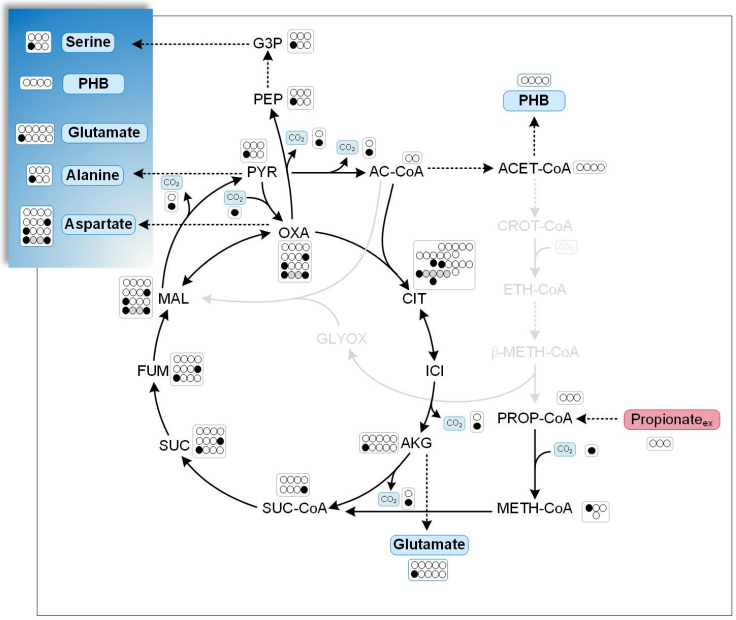

Figure 4.25.: Carbon transition resulting from the oxidative TCA cycle with reversible (A) and irreversible (B) interconversion of C_4 intermediates while growth on unlabeled propionate and ^{13}C-labeled carbonate. The closed circles indicate ^{13}C-labeled carbon atoms, open circles indicate non-labeled carbon atoms.

corporation of inorganic CO_2 for all tested substrates. This was already proposed by Swingley et al. (2007) and Tang et al. (2009). The most efficient growth and the highest inorganic carbon incorporation could be found for propionate, as expected from the carbon oxidation state of the molecule.

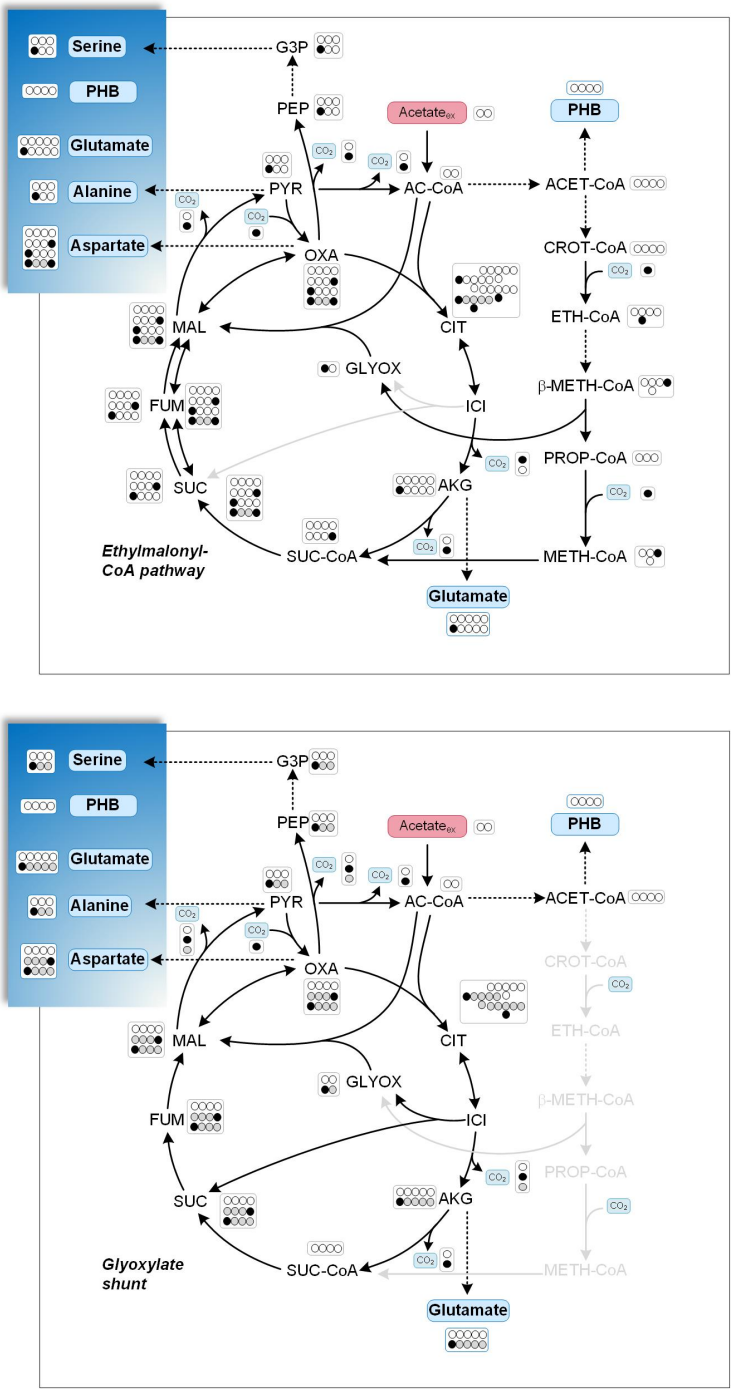

Figure 4.26.: Carbon transition resulting from the oxidative TCA cycle with reversible (A) and irreversible (B) interconversion of C_4 intermediates while growth on unlabeled acetate and ^{13}C-labeled carbonate. The closed circles indicate ^{13}C-labeled carbon atoms, open circles indicate non-labeled carbon atoms.

D. shibae uses the ethylmalonyl-CoA pathway for acetate assimilation

For the assimilation of acetate different pathways were known (Erb 2011). Most interesting for *D. shibae* was the EMC pathway, known as alternative to the glyoxylate shunt for organisms lacking the isocitrate lyase (Alber et al. 2006, Erb et al. 2010). As described in the previous chapters, a lot of metabolites of the EMC pathway could be found by LC-MS/MS analysis for *D. shibae*. Especially ethylmalonyl-CoA, mesaconyl-CoA and β-methylmalyl-CoA, the pathway specific intermediates, could be detected (Peyraud et al. 2009), even on succinate as carbon source. Theoretical analysis revealed a complete annotation of this pathway using KEGG database. Thus, its activity for acetate grown cells was suggested. Labeling studies of *D. shibae* with ^{13}C bicarbonate and acetate as carbon source revealed a single labeling of pyruvate, oxoglutarate and 3-phosphoglycerate derived amino acids of one C atom, while oxaloacetate derived amino acids were labeled either on C_1 or C_4. Figure 4.26 demonstrated, that these labeling pattern fit for EMC pathway and glyoxylate shunt (Figure: 4.26). The theoretical labeling incorporation for the glyoxylate shunt exclusively came from pyruvate carboxylase during anaplerotic reactions. For the EMC pathway, incorporation additionally occurred by crotonoyl-CoA reductase/carboxylase and propionylCoA carboxylase. While the glyoxylate shunt would result in similar enrichment as succinate, the increased incorporation of CO_2 unravels functional contribution of the EMC pathway to acetate assimilation in *D. shibae*. These results were confirmed by enzymatic inactivity of the isocitrate lyase, the key enzyme of the glyoxylate shunt.
Investigations of the metabolism of *R. pomeroyi* revealed that the EMC pathway might also play a role by DMSP degradation and is assumed to be used for acetate assimilation (Reisch et al. 2013) in this *Roseobacter*. Interestingly, *R. sphaeroides*, located in the same family of *Rhodobacteraceae*, also uses the EMC pathway (Alber 2011, Alber et al. 2006). The lack of isocitrate lyase seems to be wide spread under *Roseobacteria* and the EMC pathway might be a carbon saving strategy of this group for acetate assimilation.

The light-dependent metabolism of *D. shibae* does not involve increased carbon dioxide assimilation

The difference in pigmentation (Figure: 4.18) and biomass formation (Table: 4.14) indicates that the metabolism of *D. shibae* differs in the light. Indeed, light plays an important role for this *Roseobacter* member. Dark-light cycles are required to enable photosynthesis (Holert et al. 2011) and globally influence the expression of genes in *D. shibae* (Tomasch et al. 2011). Moreover, *D. shibae* is able to change its energetic

status in response to the light regime (Holert et al. 2011). Under conditions of nutrient limitation in a chemostat, *D. shibae* reacts to illumination by instantaneous reduction of aerobic respiration and an increase in biomass (Tomasch et al. 2011). The previous results indicate that *D. shibae* did not use other carbon dioxide assimilation pathways than those required for anaplerotic reactions, and these were independent of the illumination conditions. It can be concluded that the light adapted metabolism of this marine bacterium is completely independent from carbon dioxide fixation. The reduced growth yield in constant light was most likely caused by oxidative stress. The more efficient growth, observed during dark-light cycles (Table: 4.14), might here been stimulated by extra ATP, generated by photosynthesis. However, the exact reason for the equally effective growth in permanent darkness remains unclear. Comparative investigations with non-pigmented and pigmented cells in dark conditions are, so far, not available for *D. shibae* (Holert et al. 2011), but might give new insights into its metabolic adaptation. Overall, *D. shibae* differs from the photosynthetic bacterium *Acidiphilium rubrum*, which exhibits an enhanced CO_2 fixation capacity under lighted conditions (Kishimoto et al. 1995). Carbon dioxide fixation, at least on the level of pyruvate carboxylase, appears to be more similar to that of *R. denitrificans*, another AAnP member, where it is also light-independent (Tang et al. 2009). There is evidence that the *Roseobacter* clade relies on a mixed, flexible combination of different energy sources and benefits (Swingley et al. 2007). The most important sources are organic nutrients, which are complemented by light and CO oxidation (Moran et al. 2007b). However, no evidence for the costly fixation of CO_2 has been obtained so far. The macromolecular biomass composition of *D. shibae* revealed strong formation of PHB. PHB formation is a well-known strategy of different organisms for carbon storage, particularly when inorganic nutrients are limiting. As example, PHB synthesis is triggered or initiated by nitrogen or phosphate starvation (Poblete-Castro et al. 2012, Johnson et al. 2010). In contrast, *D. shibae* used a substantial fractions of carbon for PHB formation even during non-limited exponential growth. Obviously, the cells constitutively accumulate an intracellular carbon and energy reservoir, relying on organic nutrients. This might be a strategy of the bacterium, relying on organic nutrients, to survive in its natural habitat, which is typically low in organic carbon (Sharp 1993). Still, there are phases with increased nutrient availability. The uptake and storage of the additionally available carbon as PHB might be advantageous for *D. shibae*, as it could facilitate survival of the cells during subsequent starvation phases. Considering the dominance of the *Roseobacter* clade among the marine bacterial community, constitutive carbon storage may represent yet another feature of this microbial group.

4.5. Changes in the central metabolic pathways for quorum sensing mutants.

Quorum sensing is a common technique, wide spread under *Roseobacters*, regulating cell populations and their physiologies (Cude et al. 2013). In *D. shibae* several new long chain AHLs could be identified being involved in quorum sensing (Wagner-Döbler et al. 2005). These were responsible for changes in morphology of *D. shibae* from small rods to long filamentous cells with several copies of the chromosome (Patzelt et al. 2013). Deletions of genes involved in the AHL production could re-establish the standard morphology of small rods (Patzelt et al. 2013). *luxI* and *luxR* genes were further investigated and deletion mutants showed differences in growth behavior (Patzelt et al. 2013). This interesting fact might have also influence on metabolic traits. By analysis of the *in vivo* fluxes, the communication of the cell population should be investigated on a metabolic level.

4.5.1. Metabolic flux analysis reveals only slight changes in central carbon fluxes

The adaptation of the established procedure for metabolic flux analysis of *D. shibae* was conducted with 1-^{13}C glucose as carbon source for the two mutant strains Δ*luxI* and Δ*luxR*. Growth experiments revealed no big changes in growth characteristic parameters (Table: 4.22) as seen in Patzelt et al. (2013) for growth on succinic acid. The Δ*luxI* mutant showed the same growth rate as the wild-type strain, while Δ*luxR* was slightly faster. In addition, biomass yield and substrate uptake rate were nearly identical. Both mutant strains also showed exponential growth and the maximal optical density coincided with the depletion of glucose (Figures: A.1 and A.2). The reproducibility is given

Table 4.22.: Growth characteristic parameters for *D. shibae* and two Δ*lux* mutants grown in minimal medium with 10 mM glucose as sole carbon source at permanent dark. Data denote the specific growth rate (μ), the biomass yield $Y_{X/S}$, The biomass yield $Y_{X/S}$ divided by the number of C-atoms from the substrate and the specific substrate uptake rate q_S. Data represent the mean values with standard deviations (n = 3).

Illumination	μ [h^{-1}]	$Y_{X/S}$ [g mol^{-1}]	$Y_{X/S}$ [g $Cmol^{-1}$]	q_S [mmol g^{-1} h^{-1}]
WT	0.11 ± 0.00	70.3 ± 1.0	11.7 ± 0.2	1.59 ± 0.17
Δ*luxI*	0.11 ± 0.00	70.6 ± 2.8	11.8 ± 0.5	1.52 ± 0.03
Δ*luxR*	0.12 ± 0.00	69.7 ± 3.0	11.6 ± 0.5	1.72 ± 0.04

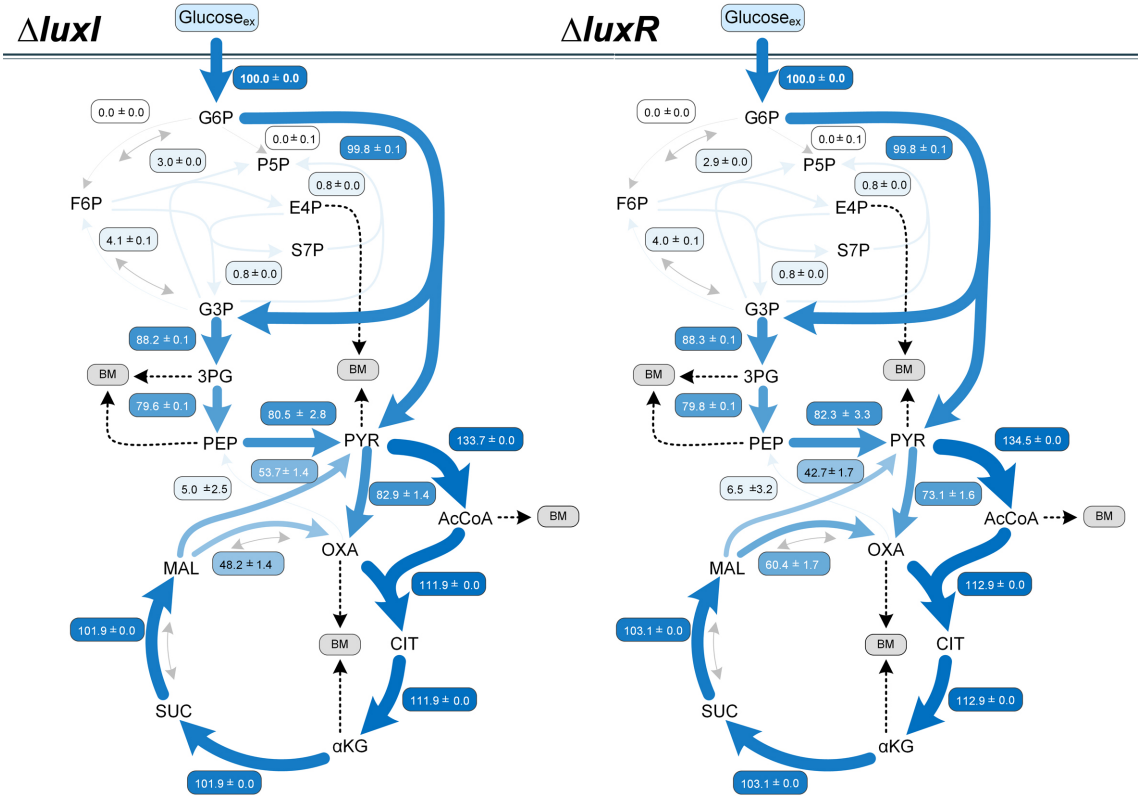

Figure 4.27.: Fluxmap for *D. shibae* Δ*luxI* on the left and Δ*luxR* on the right in SWM supplemented with 10 mM glucose. The *in vivo* flux distribution were given in as molar percentage of the mean specific glucose uptake rates q_S set to 100 %. The corresponding error were determined by Monte-Carlo analysis with 90 % confidence interval.

by small standard deviations for both strains from three cultivations. As required for metabolic flux analysis, metabolic and isotopic steady state was verified (Figures: A.1 and A.2) showing no time dependent changes for biomass formation from glucose (B) and for the labeling pattern (C).

Flux analysis of the mutant strains revealed that the complete carbon, entering the metabolism at the glucose 6-phophate node, was channeled through the ED pathway as seen for the wild-type strain. In contrast, the oxidative pentose phosphate pathway (PP pathway) and the Emden-Meyerhoff-Parnas pathway (EMP pathway) were found inactive. Changes were only observed in the variable part of the anaplerotic reactions. Both strains showed a slightly minor flux through malic enzyme going with with an increased flux through pyruvate carboxylase and phosphoenolpyruvate carboxykinase. In bacteria, this phosphoenolpyruvate-pyruvate-oxaloacetate node is used to distribute the carbon flux among the catabolic, anabolic and energy supply pathways (Sauer et al. 2005). The anaplerotic replenishment occurred only via pyruvate carboxylase and was 10 % higher

for Δ*luxR* and 23 % for Δ*luxI* mutants. The *in vivo* activity of PEP carboxykinase, resulting in an exchange flux between the C_3 and C_4 metabolites of glycolysis and TCA cycle, was further increased by 10 % for Δ*luxR* and 23 % for Δ*luxI* mutants.
Production of long chain AHL causes changes in morphology for *D. shibae* (Patzelt et al. 2013, Wagner-Döbler et al. 2010, Wagner-Döbler et al. 2005), which might have resulted in an augmented usage of anaplerotic reactions. Knocking out the autoinducer *luxI* increased fluxes towards anaplerosis in a greater manner than for the knock-out of the regulator *luxR* for AHL production. This is interesting, because the *luxI* deficient mutants showed a complete inactivation of AHL production which changed their morphology to normal shape again (Patzelt et al. 2013). This high variability of the anaplerotic node seems to be advantageous for *D. shibae* to adapt to different situation and shows the high conservation of the remaining pathways.

5. Conclusions and Outlook

The marine environment is one of the largest habitats on earth, but the investigation of life in such a variable environment is still in the beginning. Although the nutrient supply is usually weak and environmental changes hamper living conditions, various bacterial communities can be found. One of the dominant groups is the *Roseobacter* clade, showing interesting habits linked to the carbon core metabolism. *Dinoroseobacter shibae* is one of the model organisms belonging to this group of *Alphaproteobacteria*, known for either planktonic or biofilm forming growth attached to algae. This organism seems to be a good candidate for investigations of metabolism, because it further belongs to the group of aerobic anoxigenic phototrophs. Challenges for living in marine environments are versatile, especially under enormous changes of the nutrient level and under oxidative stress caused by radiation or photosynthesis of algae.

In the present work, the central carbon metabolism of *D. shibae* was investigated, referring to changes in the environment and oxidative stress by using systems biological techniques. To unravel the use of the central carbon core metabolism on glucose and succinic acid, both prevalent carbon sources in the oceans, ^{13}C metabolic flux analysis were performed. Detailed flux maps of *in vivo* reaction rates combined with enzymatic assays elucidated the carbon core metabolism and gave information about the enormous success of this bacterial group.

The results of the ^{13}C metabolic flux analysis revealed a highly conserved glucose metabolism, allowing degradation solely via the Entner-Doudoroff pathway. The phosphofructokinase, key enzyme of the Embden-Meyerhof-Parnas pathway, showed no activity under the tested conditions and the 6-phosphogluconate dehydrogenase, key enzyme of the oxidative pentose phosphate pathway, was neither annotated nor showed any enzymatic activity. The non-oxidative part of the pentose phosphate pathway was only used for the generation of anabolic precursors. Furthermore, degradation via anaplerotic reactions and TCA cycle was more flexible. For replenishment of TCA cycle, mainly the two anaplerotic enzymes pyruvate carboxylase and phosphoenolpyruvate carboxykinase were responsible, while malic enzyme exposed only weak activities. The highly used TCA cycle was generating reduction equivalents for energy supply as well as precursors for anabolic demands. The NADPH demand was satisfied by glucose-6-phosphate and

isocitrate dehydrogenase being highly used. As storage compound, *D. shibae* produces polyhydroxybutyrate which results in high fluxes to acetyl-CoA, generating reduction equivalents as well. Other by-products were not produced revealing a highly efficient metabolism.

Using succinic acid as carbon source changed the metabolism entirely, because it enters the central carbon metabolism directly at the TCA cycle. From oxaloacetate the fluxes split into anaplerotic reactions and to further degradation via TCA cyle. Thus, only small fluxes remained. For anaplerosis, pyruvate carboxylase and phosphoenolpyruvate carboxykinase were still used resulting in high fluxes in the direction of acetyl-CoA. This was due to PHB contents of over 50 % cell dry weight, not uncommon for *Roseobacteria* and AAnP bacteria. The non-oxidative part of the pentose phosphate pathway was still generating precursors while small fluxes over the Entner-Doudoroff pathway revealed its ability to react fast on environmental changes. For this reason, the organism is able to reactivate sugar metabolism as soon as needed.

Regarding the high production rate for NADPH and the unused capacity of the NADPH generating enzymes, glucose-6-phosphate and isocitrate dehydrogenase, *D. shibae* showed good abilities to handle oxidative stress. Experiments using diamide to induce oxidative stress revealed good tolerance and a positive effect of the mainly used Entner-Doudoroff pathway. Additionally, the resistance against oxidative stress was independent from the substrate used for bacterial growth.

Labeling studies under different environmental changes showed no influence of changing light regimes on the central carbon metabolism. This was curious because the pigmentation changed from dark red, when cultivated in the dark, to light beige for cells grown in permanent light. During night the establishment of a photosynthesis complex, including bacteriochlorophyll *a* production, colored the cells. Additionally, no changes in heterotrophic carbon incorporation could be detected under different light conditions. For the proposed carbon fixation via 3-hydroxypropionate cycle no activity was determined under nutrient rich conditions as well as changing light regimes. But it was shown that *D. shibae* used heterotrophic carbon incorporation via anaplerotic reactions. As a result different amounts of incorporated inorganic carbon were provided dependent on the metabolized substrate. While with succinic acid only small amount were incorporated, the growth on glucose and acetate revealed higher amounts. The most effective carbon fixation occurred using propionate as sole carbon source. Further analysis of the acetate metabolism discovered the use of the ethylmalonyl-CoA pathway instead of glyoxylate shunt for assimilation shown by enzymatic activity assays and labeling studies, known to be active for AAnP.

The analysis of quorum sensing mutants, which do not produce AHL at all, revealed only

small changes in central carbon metabolism. Only slight variations in use of anaplerotic reactions occurred, while the main degradation routes were used equally. Consequently, *D. shibae* seemed to be highly adapted to the marine environment and able to react flexible on changing environmental conditions.
In future research it would be interesting to investigate the central carbon fluxes under further changes of environmental conditions. As described before, times of low nutrient contents were common for marine environments, but the influence on metabolism is not understood very well. For this reason analysis on multi-omics level for starving conditions would be very elucidating. Maybe carbon fixation pathways will be up-regulated and used under these condition.
Another interesting topic could be the investigation of stress conditions in more detail. Oxidative and salt stress are very common in marine environments and organisms from these habitats could provide more information on mechanisms for protection. These analysis combined with multi-omics data could lead to a better understanding of the great success of bacteria belonging to the *Roseobacter* clade in marine environments.
To better understand the relations of algae and bacteria analysis regarding the symbiosis would be fascinating. Substances provided by the algae host could be analyzed with metabolic flux analysis for incorporation in bacterial metabolism and clarify the profits for the bacteria in this symbiosis. Combining these analysis with investigations on substances flowing back from bacteria to algal host will provide new insights into the symbiotic relationship.

6. References

Alber, B. E. (2011). "Biotechnological potential of the ethylmalonyl-CoA pathway". *Applied Microbiology and Biotechnology* 89.1, pp. 17–25.

Alber, B. E., Spanheimer, R., Ebenau-Jehle, C., and Fuchs, G. (2006). "Study of an alternate glyoxylate cycle for acetate assimilation by Rhodobacter sphaeroides". *Molecular Microbiology* 61.2, pp. 297–309.

Allgaier, M., Uphoff, H., Felske, A., and Wagner-Döbler, I. (2003). "Aerobic Anoxygenic Photosynthesis in Roseobacter Clade Bacteria from Diverse Marine Habitats". *Applied and Environmental Microbiology* 69.9, pp. 5051–5059.

Alonso, C. and Pernthaler, J. (2006). "Roseobacter and SAR11 dominate microbial glucose uptake in coastal North Sea waters". *Environmental Microbiology* 8.11, pp. 2022–2030.

Alonso-Sáez, L., Gasol, J. M., Lefort, T., Hofer, J., and Sommaruga, R. (2006). "Effect of natural sunlight on bacterial activity and differential sensitivity of natural bacterioplankton groups in northwestern Mediterranean coastal waters". *Applied and Environmental Microbiology* 72.9, pp. 5806–5813.

Aluwihare, L. I., Repeta, D. J., and Chen, R. F. (2002). "Chemical composition and cycling of dissolved organic matter in the Mid-Atlantic Bight". *Deep Sea Research Part II: Topical Studies in Oceanography* 49.20, pp. 4421–4437.

Amon, R. M. and Benner, R. (2003). "Combined neutral sugars as indicators of the diagenetic state of dissolved organic matter in the Arctic Ocean". *Deep Sea Research Part I: Oceanographic Research Papers* 50.1, pp. 151–169.

Anderson, D. M., Glibert, P. M., and Burkholder, J. M. (2002). "Harmful algal blooms and eutrophication: Nutrient sources, composition, and consequences". *Estuaries* 25.4, pp. 704–726.

Antoniewicz, M. R. (2013). "13C metabolic flux analysis: optimal design of isotopic labeling experiments". *Current Opinion in Biotechnology* 24.6, pp. 1116–1121.

Antoniewicz, M. R., Kelleher, J. K., and Stephanopoulos, G. (2007a). "Elementary metabolite units (EMU): a novel framework for modeling isotopic distributions". *Metabolic Engineering* 9.1, pp. 68–86.

Antoniewicz, M. R., Kraynie, D. F., Laffend, L. A., González-Lergier, J., Kelleher, J. K., and Stephanopoulos, G. (2007b). "Metabolic flux analysis in a nonstationary system: fed-batch fermentation of a high yielding strain of E. coli producing 1,3-propanediol". *Metabolic Engineering* 9.3, pp. 277–292.

Arun, A., Arthi, R., Shanmugabalaji, V., and Eyini, M. (2009). "Microbial production of poly-β-hydroxybutyrate by marine microbes isolated from various marine environments". *Bioresource Technology* 100.7, pp. 2320–2323.

Bar-Even, A., Noor, E., Lewis, N. E., and Milo, R. (2010). "Design and analysis of synthetic carbon fixation pathways". *Proceedings of the National Academy of Sciences* 107.19, pp. 8889–8894.

Becker, J., Klopprogge, C., and Wittmann, C. (2008). "Metabolic responses to pyruvate kinase deletion in lysine producing Corynebacterium glutamicum". *Microbial Cell Factories* 7.1, p. 8.

Becker, J., Reinefeld, J., Stellmacher, R., Schäfer, R., Lange, A., Meyer, H., Lalk, M., Zelder, O., Abendroth, G. v., Schröder, H., Haefner, S., and Wittmann, C. (2013). "Systems-wide analysis and engineering of metabolic pathway fluxes in bio-succinate producing Basfia succiniciproducens". *Biotechnology and Bioengineering* 110.11, pp. 3013–3023.

Becker, J., Zelder, O., Häfner, S., Schröder, H., and Wittmann, C. (2011). "From zero to hero — Design-based systems metabolic engineering of Corynebacterium glutamicum for l-lysine production". *Metabolic Engineering* 13.2, pp. 159–168.

Berger, A., Dohnt, K., Tielen, P., Jahn, D., Becker, J., Wittmann, C., and Fong, S. S. (2014). "Robustness and Plasticity of Metabolic Pathway Flux among Uropathogenic Isolates of Pseudomonas aeruginosa". *PLoS ONE* 9.4, e88368.

Bergh, O., Børsheim, K. Y., Bratbak, G., and Heldal, M. (1989). "High abundance of viruses found in aquatic environments". *Nature* 340.6233, pp. 467–468.

Berghoff, B. A., Glaeser, J., Nuss, A. M., Zobawa, M., Lottspeich, F., and Klug, G. (2011). "Anoxygenic photosynthesis and photooxidative stress: a particular challenge for Roseobacter". *Environmental Microbiology* 13.3, pp. 775–791.

Bériault, R., Hamel, R., Chenier, D., Mailloux, R. J., Joly, H., and Appanna, V. D. (2007). "The overexpression of NADPH-producing enzymes counters the oxidative stress evoked by gallium, an iron mimetic". *Biometals* 20.2, pp. 165–176.

Biebl, H., Allgaier, M., Tindall, B. J., Koblizek, M., Lünsdorf, H., Pukall, R., and Wagner-Döbler, I. (2005). "Dinoroseobacter shibae gen. nov., sp. nov., a new aerobic phototrophic bacterium isolated from dinoflagellates". *International journal of systematic and evolutionary microbiology* 55.3, pp. 1089–1096.

Biebl, H. and Wagner-Döbler, I. (2006). "Growth and bacteriochlorophyll a formation in taxonomically diverse aerobic anoxygenic phototrophic bacteria in chemostat culture: Influence of light regimen and starvation". *Process Biochemistry* 41.10, pp. 2153–2159.

Biersmith, A. and Benner, R. (1998). "Carbohydrates in phytoplankton and freshly produced dissolved organic matter". *Marine Chemistry* 63.1-2, pp. 131–144.

Bolten, C. J. and Wittmann, C. (2008). "Appropriate sampling for intracellular amino acid analysis in five phylogenetically different yeasts". *Biotechnology Letters* 30.11, pp. 1993–2000.

Borodina, I., Scholler, C., Eliasson, A., and Nielsen, J. (2005). "Metabolic Network Analysis of Streptomyces tenebrarius, a Streptomyces Species with an Active Entner-Doudoroff Pathway". *Applied and Environmental Microbiology* 71.5, pp. 2294–2302.

Brinkhoff, T., Bach, G., Heidorn, T., Liang, L., Schlingloff, A., and Simon, M. (2004). "Antibiotic Production by a Roseobacter Clade-Affiliated Species from the German Wadden Sea and Its Antagonistic Effects on Indigenous Isolates". *Applied and Environmental Microbiology* 70.4, pp. 2560–2565.

Brinkhoff, T., Giebel, H.-A., and Simon, M. (2008). "Diversity, ecology, and genomics of the Roseobacter clade: a short overview". *Archives of microbiology* 189.6, pp. 531–539.

Bruhn, J. B., Gram, L., and Belas, R. (2007). "Production of Antibacterial Compounds and Biofilm Formation by Roseobacter Species Are Influenced by Culture Conditions". *Applied and Environmental Microbiology* 73.2, pp. 442–450.

Buchan, A. and González, J. M. (2010). "Roseobacter". In: *Handbook of Hydrocarbon and Lipid Microbiology*. Ed. by K. N. Timmis. Berlin and Heidelberg: Springer Berlin Heidelberg, pp. 1335–1343.

Buchan, A., Gonzalez, J. M., and Moran, M. A. (2005). "Overview of the Marine Roseobacter Lineage". *Applied and Environmental Microbiology* 71.10, pp. 5665–5677.

Buschke, N., Becker, J., Schäfer, R., Kiefer, P., Biedendieck, R., and Wittmann, C. (2013a). "Systems metabolic engineering of xylose-utilizing Corynebacterium glutamicum for production of 1,5-diaminopentane". *Biotechnology Journal* 8.5, pp. 557–570.

Buschke, N., Schäfer, R., Becker, J., and Wittmann, C. (2013b). "Metabolic engineering of industrial platform microorganisms for biorefinery applications - Optimization of substrate spectrum and process robustness by rational and evolutive strategies". *Bioresource Technology* 135, pp. 544–554.

Carducci, C., Birarelli, M., Nola, M., and Antonozzi, I. (1999). "Automated high-performance liquid chromatographic method for the determination of homocysteine in plasma samples". *Journal of chromatography A* 846.1-2, pp. 93–100.

Chavarría, M. N. P. I., Pérez-Pantoja, D., and Lorenzo, V. d. (2013). "The Entner-Doudoroff pathway empowers Pseudomonas putida KT2440 with a high tolerance to oxidative stress". *Environmental Microbiology* 15.6, pp. 1772–1785.

Christensen, B. and Nielsen, J. (2000). "Metabolic network analysis. A powerful tool in metabolic engineering". *Advances in Biochemical Engineering / Biotechnology* 66, pp. 209–231.

Conway, T. (1992). "The Entner-Doudoroff pathway: history, physiology and molecular biology". *FEMS Microbiology Reviews* 9.1, pp. 1–27.

Cude, W. N. and Buchan, A. (2013). "Acyl-homoserine lactone-based quorum sensing in the Roseobacter clade: complex cell-to-cell communication controls multiple physiologies". *Frontiers in microbiology* 4.

Cumming, R. C., Andon, N. L., Haynes, P. A., Park, M., Fischer, W. H., and Schubert, D. (2004). "Protein disulfide bond formation in the cytoplasm during oxidative stress". *The Journal of biological chemistry* 279.21, pp. 21749–21758.

Cunliffe, M. (2011). "Correlating carbon monoxide oxidation with cox genes in the abundant Marine Roseobacter Clade". *The ISME Journal* 5.4, pp. 685–691.

Curson, A. R. J., Todd, J. D., Sullivan, M. J., and Johnston, A. W. B. (2011). "Catabolism of dimethylsulphoniopropionate: microorganisms, enzymes and genes". *Nature reviews. Microbiology* 9.12, pp. 849–859.

Dauner, M., Bailey, J. E., and Sauer, U. (2001). "Metabolic flux analysis with a comprehensive isotopomer model in Bacillus subtilis". *Biotechnology and Bioengineering* 76.2, pp. 144–156.

Dauner, M. and Sauer, U. (2000). "GC-MS analysis of amino acids rapidly provides rich information for isotopomer balancing". *Biotechnology progress* 16.4, pp. 642–649.

Diesterhaft, M. D. and Freese, E. (1973). "Role of pyruvate carboxylase, phosphoenolpyruvate carboxykinase, and malic enzyme during growth and sporulation of Bacillus subtilis". *The Journal of biological chemistry* 248.17, pp. 6062–6070.

Dogs, M., Voget, S., Teshima, H., Petersen, J., Davenport, K., Dalingault, H., Chen, A., Pati, A., Ivanova, N., Goodwin, L. A., Chain, P., Detter, J. C., Standfest, S., Rohde, M., Gronow, S., Kyrpides, N. C., Woyke, T., Simon, M., Klenk, H.-P., Göker, M., and Brinkhoff, T. (2013). "Genome sequence of Phaeobacter inhibens type strain (T5T), a secondary metabolite producing representative of the marine Roseobacter clade, and emendation of the species description of Phaeobacter inhibens". *Standards in Genomic Sciences* 9.2, pp. 334–350.

Doi, M. and Shioi, Y. (1991). "Enhancement of denitrifying activity in cells of Roseobacter denitrificans grown aerobically in the light". *Plant and cell physiology* 32.3, pp. 365–370.

Don, C., Hanselmann, K. W., Peduzzi, R., and Bachofen, R. (1994). "Biomass composition and methods for the determination of metabolic reserve polymers in phototrophic sulfur bacteria". *Aquatic Science* 56.1, pp. 1–15.

Driouch, H., Roth, A., Dersch, P., and Wittmann, C. (2010). "Optimized bioprocess for production of fructofuranosidase by recombinant Aspergillus niger". *Applied Microbiology and Biotechnology* 87.6, pp. 2011–2024.

Ebert, M., Laass, S., Burghartz, M., Petersen, J., Kossmehl, S., Wohlbrand, L., Rabus, R., Wittmann, C., Tielen, P., and Jahn, D. (2013). "Transposon Mutagenesis Identified Chromosomal and Plasmid Genes Essential for Adaptation of the Marine Bacterium Dinoroseobacter shibae to Anaerobic Conditions". *Journal of Bacteriology* 195.20, pp. 4769–4777.

Erb, T. J. (2011). "Carboxylases in Natural and Synthetic Microbial Pathways". *Applied and Environmental Microbiology* 77.24, pp. 8466–8477.

Erb, T. J., Frerichs-Revermann, L., Fuchs, G., and Alber, B. E. (2010). "The Apparent Malate Synthase Activity of Rhodobacter sphaeroides Is Due to Two Paralogous Enzymes, (3S)-Malyl-Coenzyme A (CoA)/β-Methylmalyl-CoA Lyase and (3S)- Malyl-CoA Thioesterase". *Journal of Bacteriology* 192.5, pp. 1249–1258.

Erb, T. J., Berg, I. A., Brecht, V., Müller, M., Fuchs, G., and Alber, B. E. (2007). "Synthesis of C5-dicarboxylic acids from C2-units involving crotonyl-CoA carboxylase/reductase: The ethylmalonyl-CoA pathway". *Proceedings of the National Academy of Sciences of the United States of America* 104.25, pp. 10631–10636.

Erb, T. J., Fuchs, G., and Alber, B. E. (2009). "(2S)-Methylsuccinyl-CoA dehydrogenase closes the ethylmalonyl-CoA pathway for acetyl-CoA assimilation". *Molecular Microbiology* 73.6, pp. 992–1008.

Erb, T. J., Rétey, J., Fuchs, G., and Alber, B. E. (2008). "Ethylmalonyl-CoA mutase from Rhodobacter sphaeroides defines a new subclade of coenzyme B12-dependent acyl-CoA mutases". *The Journal of biological chemistry* 283.47, pp. 32283–32293.

Escapa, I. F., García, J. L., Bühler, B., Blank, L. M., and Prieto, M. A. (2012). "The polyhydroxyalkanoate metabolism controls carbon and energy spillage in Pseudomonas putida". *Environmental Microbiology* 14.4, pp. 1049–1063.

Fuhrer, T., Fischer, E., and Sauer, U. (2005). "Experimental Identification and Quantification of Glucose Metabolism in Seven Bacterial Species". *Journal of Bacteriology* 187.5, pp. 1581–1590.

Fürch, T., Preusse, M., Tomasch, J., Zech, H., Wagner-Döbler, I., Rabus, R., and Wittmann, C. (2009). "Metabolic fluxes in the central carbon metabolism of Dinoroseobacter shibae and Phaeobacter gallaeciensis, two members of the marine Roseobacter clade". *BMC Microbiology* 9.1, p. 209.

Giebel, H.-A., Brinkhoff, T., Zwisler, W., Selje, N., and Simon, M. (2009). "Distribution of Roseobacter RCA and SAR11 lineages and distinct bacterial communities from the subtropics to the Southern Ocean". *Environmental Microbiology* 11.8, pp. 2164–2178.

Gram, L., Grossart, H.-P., Schlingloff, A., and Kiorboe, T. (2002). "Possible Quorum Sensing in Marine Snow Bacteria: Production of Acylated Homoserine Lactones by Roseobacter Strains Isolated from Marine Snow". *Applied and Environmental Microbiology* 68.8, pp. 4111–4116.

Hädicke, O., Grammel, H., and Klamt, S. (2011). "Metabolic network modeling of redox balancing and biohydrogen production in purple nonsulfur bacteria". *BMC Systems Biology* 5.1, p. 150.

Hahnke, S., Brock, N. L., Zell, C., Simon, M., Dickschat, J. S., and Brinkhoff, T. (2013). "Physiological diversity of Roseobacter clade bacteria co-occurring during a phytoplankton bloom in the North Sea". *Systematic and Applied Microbiology* 36.1, pp. 39–48.

Halliwell, B. and Gutteridge, J. M. (1984). "Oxygen toxicity, oxygen radicals, transition metals and disease". *The Biochemical journal* 219.1, pp. 1–14.

Holert, J., Hahnke, S., and Cypionka, H. (2011). "Influence of light and anoxia on chemiosmotic energy conservation in Dinoroseobacter shibae". *Environmental microbiology reports* 3.1, pp. 136–141.

Hörl, M., Schnidder, J., Sauer, U., and Zamboni, N. (2013). "Non-stationary 13C-metabolic flux ratio analysis". *Biotechnology and Bioengineering* 110.12, pp. 3164–3176.

Hügler, M. and Sievert, S. M. (2011). "Beyond the Calvin cycle: autotrophic carbon fixation in the ocean". *Annual review of marine science* 3, pp. 261–289.

Imam, S., Noguera, D. R., and Donohue, T. J. (2013). "Global insights into energetic and metabolic networks in Rhodobacter sphaeroides". *BMC Systems Biology* 7.1, p. 89.

Johnson, K., Kleerebezem, R., and Loosdrecht, M. C. van (2010). "Influence of ammonium on the accumulation of polyhydroxybutyrate (PHB) in aerobic open mixed cultures". *Journal of Biotechnology* 147.2, pp. 73–79.

Jordà, J., Suarez, C., Carnicer, M., Pierick, A. t., Heijnen, J. J., Gulik, W. van, Ferrer, P., Albiol, J., and Wahl, A. (2013). "Glucose-methanol co-utilization in Pichia pastoris studied by metabolomics and instationary 13C flux analysis". *BMC Systems Biology* 7.1, p. 17.

Kao, K. C. (2005). "A Global Regulatory Role of Gluconeogenic Genes in Escherichia coli Revealed by Transcriptome Network Analysis". *Journal of Biological Chemistry* 280.43, pp. 36079–36087.

Karsten, U., Wiencke, C., and Kirst, G. O. (1990). "The effect of light intensity and daylength on the β-dimethylsulphoniopropionate (DMSP) content of marine green macroalgae from Antarctica*". *Plant, Cell and Environment* 13.9, pp. 989–993.

Kind, S., Becker, J., and Wittmann, C. (2013). "Increased lysine production by flux coupling of the tricarboxylic acid cycle and the lysine biosynthetic pathway — Metabolic engineering of the availability of succinyl-CoA in Corynebacterium glutamicum". *Metabolic Engineering* 15, pp. 184–195.

Kind, S., Jeong, W. K., Schröder, H., Zelder, O., and Wittmann, C. (2010). "Identification and elimination of the competing N-acetyldiaminopentane pathway for improved production of diaminopentane by Corynebacterium glutamicum". *Applied and Environmental Microbiology* 76.15, pp. 5175–5180.

Kind, T. and Fiehn, O. (2007). "Seven Golden Rules for heuristic filtering of molecular formulas obtained by accurate mass spectrometry". *BMC Bioinformatics* 8.1, p. 105.

Kirst, G. O. (1990). "Salinity tolerance of eukaryotic marine algae". *Annual review of plant biology* 41.1, pp. 21–53.

Kishimoto, N., Fukaya, F., Inagaki, K., Sugio, T., Tanaka, H., and Tano, T. (1995). "Distribution of bacteriochlorophyll a among aerobic and acidophilic bacteria and light-enhanced CO2-incorporation in Acidiphilium rubrum". *FEMS Microbiology Ecology* 16.4, pp. 291–296.

Klingner, A., Bartsch, A., Dogs, M., Wagner-Döbler, I., Jahn, D., Simon, M., Brinkhoff, T., Becker, J., and Wittmann, C. (2015). "Large-scale 13C-flux profiling reveals conservation of the Entner-Doudoroff pathway as glycolytic strategy among glucose-using marine bacteria". *Applied and Environmental Microbiology* 81.7, pp. 2408–2422.

Koblížek, M. (2011). "Role of photoheterotrophic bacteria in the marine carbon cycle". *Microbial carbon pump in the ocean*, pp. 49–51.

Kohlstedt, M., Becker, J., and Wittmann, C. (2010). "Metabolic fluxes and beyond — systems biology understanding and engineering of microbial metabolism". *Applied Microbiology and Biotechnology* 88.5, pp. 1065–1075.

Kohlstedt, M., Sappa, P. K., Meyer, H., Maaß, S., Zaprasis, A., Hoffmann, T., Becker, J., Steil, L., Hecker, M., van Dijl, Jan Maarten, Lalk, M., Mäder, U., Stülke, J., Bremer, E., Völker, U., and Wittmann, C. (2014). "Adaptation of Bacillus subtilis carbon core metabolism to simultaneous nutrient limitation and osmotic challenge: a multi-omics perspective". *Environmental Microbiology* 16.6, pp. 1898–1917.

Kolber, Z. S., Plumley, F. G., Lang, A. S., Beatty, J. T., Blankenship, R. E., VanDover, C. L., Vetriani, C., Koblizek, M., Rathgeber, C., and Falkowski, P. G. (2001). "Contribution of aerobic photoheterotrophic bacteria to the carbon cycle in the ocean". *Science* 292.5526, pp. 2492–2495.

Krömer, J. O., Bolten, C. J., Heinzle, E., Schröder, H., and Wittmann, C. (2008). "Physiological response of Corynebacterium glutamicum to oxidative stress induced by deletion of the transcriptional repressor McbR". *Microbiology* 154.Pt 12, pp. 3917–3930.

Krömer, J. O., Fritz, M., Heinzle, E., and Wittmann, C. (2005). "In vivo quantification of intracellular amino acids and intermediates of the methionine pathway in Corynebacterium glutamicum". *Analytical biochemistry* 340.1, pp. 171–173.

Krömer, J. O., Sorgenfrei, O., Klopprogge, K., Heinzle, E., and Wittmann, C. (2004). "In-depth profiling of lysine-producing Corynebacterium glutamicum by combined analysis of the transcriptome, metabolome, and fluxome". *Journal of Bacteriology* 186.6, pp. 1769–1784.

Kuntze, K., Kiefer, P., Baumann, S., Seifert, J., Bergen, M. v., Vorholt, J. A., and Boll, M. (2011). "Enzymes involved in the anaerobic degradation of meta-substituted halobenzoates". *Molecular Microbiology* 82.3, pp. 758–769.

Laass, S., Kleist, S., Bill, N., Drueppel, K., Kossmehl, S., Woehlbrand, L., Rabus, R., Klein, J., Rohde, M., Bartsch, A., Wittmann, C., Schmidt-Hohagen, K., Tielen, P., Jahn, D., and Schomburg, D. (2014). "Gene Regulatory and Metabolic Adaptation Processes of Dinoroseobacter shibae DFL12T during Oxygen Depletion". *The Journal of biological chemistry* 289.19, pp. 13219–13231.

Leighty, R. W. and Antoniewicz, M. R. (2012). "Parallel labeling experiments with [U-13C]glucose validate E. coli metabolic network model for 13C metabolic flux analysis". *Metabolic Engineering* 14.5, pp. 533–541.

Lenk, S., Moraru, C., Hahnke, S., Arnds, J., Richter, M., Kube, M., Reinhardt, R., Brinkhoff, T., Harder, J., Amann, R., and Mußmann, M. (2012). "Roseobacter clade bacteria are abundant in coastal sediments and encode a novel combination of sulfur oxidation genes". *The ISME Journal* 6.12, pp. 2178–2187.

Lesser, M. P. (2006). "Oxidative stress in marine environments: biochemistry and physiological ecology". *Annual review of physiology* 68, pp. 253–278.

Lesser, M. P. (2012). "Oxidative stress in tropical marine ecosystems". In: *Oxidative stress in aquatic ecosystems*. Ed. by D. Abele, J. P. Vazquez-Medina, and T. Zenteno-Savin. Chichester et al.: Wiley-Blackwell, pp. 9–19.

Liu, Z., Dreybrodt, W., and Wang, H. (2008). "A possible important CO2 sink by the global water cycle". *Chinese Science Bulletin* 53.3, pp. 402–407.

Marx, A., de Graaf, A A, Wiechert, W., Eggeling, L., and Sahm, H. (1996). "Determination of the fluxes in the central metabolism of Corynebacterium glutamicum by nuclear magnetic resonance spectroscopy combined with metabolite balancing". *Biotechnology and Bioengineering* 49.2, pp. 111–129.

Matyash, V., Liebisch, G., Kurzchalia, T. V., Shevchenko, A., and Schwudke, D. (2008). "Lipid extraction by methyl-tert-butyl ether for high-throughput lipidomics". *The Journal of Lipid Research* 49.5, pp. 1137–1146.

McKinlay, J. B. and Harwood, C. S. (2010). "Carbon dioxide fixation as a central redox cofactor recycling mechanism in bacteria". *Proceedings of the National Academy of Sciences* 107.26, pp. 11669–11675.

McKinlay, J. B. and Harwood, C. S. (2011). "Calvin Cycle Flux, Pathway Constraints, and Substrate Oxidation State Together Determine the H2 Biofuel Yield in Photoheterotrophic Bacteria". *mBio* 2.2, e00323–10.

Micale, G., Cipollina, A., and Rizzuti, L. (2009). "Seawater Desalination for Freshwater Production". In: *Seawater desalination*. Ed. by A. Cipollina, G. Micale, and L. Rizzuti. Green energy and technology. Heidelberg and New York: Springer, pp. 1–15.

Michal, G. (1999). *Biochemical pathways: Biochemie-Atlas*. Heidelberg and Berlin: Spektrum, Akad. Verl.

Michal, G. and Schomburg, D. (2012). *Biochemical Pathways*. Hoboken, NJ, and USA: John Wiley & Sons, Inc.

Moat, A. G., Foster, J. W., and Spector, M. P. (2002). *Microbial Physiology, Fourth Edition*. 4th ed. Hoboken and NJ: John Wiley & Sons.

Moran, M. A., Belas, R., Schell, M. A., Gonzalez, J. M., Sun, F., Sun, S., Binder, B. J., Edmonds, J., Ye, W., Orcutt, B., Howard, E. C., Meile, C., Palefsky, W., Goesmann, A., Ren, Q., Paulsen, I., Ulrich, L. E., Thompson, L. S., Saunders, E., and Buchan, A. (2007a). "Ecological Genomics of Marine Roseobacters". *Applied and Environmental Microbiology* 73.14, pp. 4559–4569.

Moran, M. A. and Miller, W. L. (2007b). "Resourceful heterotrophs make the most of light in the coastal ocean". *Nature reviews. Microbiology* 5.10, pp. 792–800.

Morano, K. A., Grant, C. M., and Moye-Rowley, W. S. (2012). "The response to heat shock and oxidative stress in Saccharomyces cerevisiae". *Genetics* 190.4, pp. 1157–1195.

Muñoz-Marín, M. d. C., Luque, I., Zubkov, M. V., Hill, P. G., Diez, J., and García-Fernández, J. M. (2013). "Prochlorococcus can use the Pro1404 transporter to take up glucose at nanomolar concentrations in the Atlantic Ocean". *Proceedings of the National Academy of Sciences* 110.21, pp. 8597–8602.

Neidhardt, F. C., Ingraham, J. L., and Schaechter, M. (1990). *Physiology of the bacterial cell: a molecular approach*. Sinauer Associates Sunderland, MA.

Netzer, R., Krause, M., Rittmann, D., Peters-Wendisch, P. G., Eggeling, L., Wendisch, V. F., and Sahm, H. (2004). "Roles of pyruvate kinase and malic enzyme in Corynebac-

terium glutamicum for growth on carbon sources requiring gluconeogenesis". *Archives of microbiology* 182.5, pp. 354–363.

Neumann, U., Mayer, H., Schiltz, E., Benz, R., and Weckesser, J. (1995). "Lipopolysaccharide and porin of Roseobacter denitrificans, confirming its phylogenetic relationship to the α-3 subgroup of Proteobacteria". *Microbiology* 141.8, pp. 2013–2017.

Nicolae, A., Wahrheit, J., Bahnemann, J., Zeng, A.-P., and Heinzle, E. (2014). "Non-stationary 13C metabolic flux analysis of Chinese hamster ovary cells in batch culture using extracellular labeling highlights metabolic reversibility and compartmentation". *BMC Systems Biology* 8.1, p. 50.

Nocon, J., Steiger, M. G., Pfeffer, M., Sohn, S. B., Kim, T. Y., Maurer, M., Rußmayer, H., Pflügl, S., Ask, M., Haberhauer-Troyer, C., Ortmayr, K., Hann, S., Koellensperger, G., Gasser, B., Lee, S. Y., and Mattanovich, D. (2014). "Model based engineering of Pichia pastoris central metabolism enhances recombinant protein production". *Metabolic Engineering* 24, pp. 129–138.

Nöh, K., Grönke, K., Luo, B., Takors, R., Oldiges, M., and Wiechert, W. (2007). "Metabolic flux analysis at ultra short time scale: isotopically non-stationary 13C labeling experiments". *Journal of Biotechnology* 129.2, pp. 249–267.

Okahashi, N., Kajihata, S., Furusawa, C., and Shimizu, H. (2014). "Reliable Metabolic Flux Estimation in Escherichia coli Central Carbon Metabolism Using Intracellular Free Amino Acids". *Metabolites* 4.2, pp. 408–420.

Patzelt, D., Wang, H., Buchholz, I., Rohde, M., Gröbe, L., Pradella, S., Neumann, A., Schulz, S., Heyber, S., Münch, K., Münch, R., Jahn, D., Wagner-Döbler, I., and Tomasch, J. (2013). "You are what you talk: quorum sensing induces individual morphologies and cell division modes in Dinoroseobacter shibae". *The ISME Journal* 7.12, pp. 2274–2286.

Peekhaus, N. and Conway, T. (1998). "What's for dinner?: Entner-Doudoroff metabolism in Escherichia coli". *Journal of Bacteriology* 180.14, pp. 3495–3502.

Pepper, I. L., Gerba, C. P., and Gentry, T. J. (2014). *Environmental microbiology*. Third edition.

Petersen, S., Graaf, A. A. d., Eggeling, L., Möllney, M., Wiechert, W., and Sahm, H. (2000). "In vivo quantification of parallel and bidirectional fluxes in the anaplerosis of Corynebacterium glutamicum". *The Journal of biological chemistry* 275.46, pp. 35932–35941.

Peyraud, R., Kiefer, P., Christen, P., Massou, S., Portais, J.-C., and Vorholt, J. A. (2009). "Demonstration of the ethylmalonyl-CoA pathway by using 13C metabolomics". *Proceedings of the National Academy of Sciences* 106.12, pp. 4846–4851.

Poblete-Castro, I., Escapa, I. F., Jäger, C., Puchalka, J., Chi Lam, C., Schomburg, D., Prieto, M., and Martins dos Santos, V. A. P. (2012). "The metabolic response of P. putida KT2442 producing high levels of polyhydroxyalkanoate under single- and multiple-nutrient-limited growth: Highlights from a multi-level omics approach". *Microbial Cell Factories* 11.1, p. 34.

Pócsi, I., Miskei, M., Karányi, Z., Emri, T., Ayoubi, P., Pusztahelyi, T., Balla, G., and Prade, R. (2005). "Comparison of gene expression signatures of diamide, H2O2 and menadione exposed Aspergillus nidulans cultures – linking genome-wide transcriptional changes to cellular physiology". *BMC Genomics* 6.1, p. 182.

Pollak, N., Dölle, C., and Ziegler, M. (2007). "The power to reduce: pyridine nucleotides–small molecules with a multitude of functions". *The Biochemical journal* 402.2, pp. 205–218.

Pradella, S., Allgaier, M., Hoch, C., Päuker, O., Stackebrandt, E., and Wagner-Döbler, I. (2004). "Genome organization and localization of the pufLM genes of the photosynthesis reaction center in phylogenetically diverse marine Alphaproteobacteria". *Applied and Environmental Microbiology* 70.6, pp. 3360–3369.

Quek, L.-E., Wittmann, C., Nielsen, L. K., and Krömer, J. O. (2009). "OpenFLUX: efficient modelling software for 13C-based metabolic flux analysis". *Microbial Cell Factories* 8.1, p. 25.

Reisch, C. R., Crabb, W. M., Gifford, S. M., Teng, Q., Stoudemayer, M. J., Moran, M. A., and Whitman, W. B. (2013). "Meatbolism of dimethyl sulphoniopropionate by Ruegeria pomeroyi DSS-3". *Molecular Microbiology* 89.4, pp. 774–791.

Rex, R., Bill, N., Schmidt-Hohagen, K., Schomburg, D., and Maranas, C. D. (2013). "Swimming in Light: A Large-Scale Computational Analysis of the Metabolism of Dinoroseobacter shibae". *PLoS Computational Biology* 9.10, e1003224.

Romano, A. H. and Conway, T. (1996). "Evolution of carbohydrate metabolic pathways". *Research in microbiology* 147.6-7, pp. 448–455.

Rutkis, R., Kalnenieks, U., Stalidzans, E., and Fell, D. A. (2013). "Kinetic modelling of the Zymomonas mobilis Entner-Doudoroff pathway: insights into control and functionality". *Microbiology* 159.Pt 12, pp. 2674–2689.

Sauer, U. (2006). "Metabolic networks in motion: 13C-based flux analysis". *Molecular Systems Biology)* 2, p. 62.

Sauer, U. and Eikmanns, B. J. (2005). "The PEP-pyruvate-oxaloacetate node as the switch point for carbon flux distribution in bacteria". *FEMS Microbiology Reviews* 29.4, pp. 765–794.

Schiefelbein, S., Fröhlich, A., John, G. T., Beutler, F., Wittmann, C., and Becker, J. (2013). "Oxygen supply in disposable shake-flasks: prediction of oxygen transfer rate,

oxygen saturation and maximum cell concentration during aerobic growth". *Biotechnology Letters* 35.8, pp. 1223–1230.

Schmidt, K., Nørregaard, L. C., Pedersen, B., Meissner, A., Duus, J. O., Nielsen, J. O., and Villadsen, J. (1999). "Quantification of intracellular metabolic fluxes from fractional enrichment and 13C-13C coupling constraints on the isotopomer distribution in labeled biomass components". *Metabolic Engineering* 1.2, pp. 166–179.

Schneider, K., Peyraud, R., Kiefer, P., Christen, P., Delmotte, N., Massou, S., Portais, J.-C., and Vorholt, J. A. (2012). "The ethylmalonyl-CoA pathway is used in place of the glyoxylate cycle by Methylobacterium extorquens AM1 during growth on acetate". *The Journal of biological chemistry* 287.1, pp. 757–766.

Seyedsayamdost, M. R., Case, R. J., Kolter, R., and Clardy, J. (2011). "The Jekyll-and-Hyde chemistry of Phaeobacter gallaeciensis". *Nature Chemistry* 3.4, pp. 331–335.

Sharp, J. H. (1993). "The dissolved organic carbon controversy: An update". *Oceanography* 6.2, pp. 45–50.

Shiba, T. (1991). "Roseobacter litoralis gen. nov., sp. nov., and Roseobacter denitrificans sp. nov., Aerobic Pink-Pigmented Bacteria which Contain Bacteriochlorophyll a". *Systematic and Applied Microbiology* 14.2, pp. 140–145.

Singh, R., Mailloux, R. J., Puiseux-Dao, S., and Appanna, V. D. (2007). "Oxidative stress evokes a metabolic adaptation that favors increased NADPH synthesis and decreased NADH production in Pseudomonas fluorescens". *Journal of Bacteriology* 189.18, pp. 6665–6675.

Soora, M. and Cypionka, H. (2013). "Light Enhances Survival of Dinoroseobacter shibae during Long-Term Starvation". *PLoS ONE* 8.12, e83960.

Stephanopoulos, G. (1999). "Metabolic fluxes and metabolic engineering". *Metabolic Engineering* 1.1, pp. 1–11.

Sternberg, N. L. and Maurer, R. (1991). "Bacteriophage-mediated generalized transduction in Escherichia coli and Salmonella typhimurium". *Methods in enzymology* 204, pp. 18–43.

Storz, G. and Imlay, J. A. (1999). "Oxidative stress". *Current opinion in microbiology* 2.2, pp. 188–194.

Storz, G., Tartaglia, L. A., Farr, S. B., and Ames, B. N. (1990). "Bacterial defenses against oxidative stress". *Trends in Genetics : TIG* 6.11, pp. 363–368.

Swingley, W. D., Sadekar, S., Mastrian, S. D., Matthies, H. J., Hao, J., Ramos, H., Acharya, C. R., Conrad, A. L., Taylor, H. L., Dejesa, L. C., Shah, M. K., O'huallachain, M. E., Lince, M. T., Blankenship, R. E., Beatty, J. T., and Touchman, J. W. (2007). "The complete genome sequence of Roseobacter denitrificans reveals a mixotrophic rather than photosynthetic metabolism". *Journal of Bacteriology* 189.3, pp. 683–690.

Szyperski, T. (1995). "Biosynthetically directed fractional 13C-labeling of proteinogenic amino acids. An efficient analytical tool to investigate intermediary metabolism". *European Journal of Biochemistry / FEBS* 232.2, pp. 433–448.

Tada, Y., Taniguchi, A., Nagao, I., Miki, T., Uematsu, M., Tsuda, A., and Hamasaki, K. (2011). "Differing Growth Responses of Major Phylogenetic Groups of Marine Bacteria to Natural Phytoplankton Blooms in the Western North Pacific Ocean". *Applied and Environmental Microbiology* 77.12, pp. 4055–4065.

Takahashi, T., Sutherland, S. C., Sweeney, C., Poisson, A., Metzl, N., Tilbrook, B., Bates, N., Wanninkhof, R., Feely, R. A., Sabine, C., et al. (2002). "Global sea–air CO2 flux based on climatological surface ocean pCO2, and seasonal biological and temperature effects". *Deep Sea Research Part II: Topical Studies in Oceanography* 49.9, pp. 1601–1622.

Tang, K.-H., Feng, X., Tang, Y. J., Blankenship, R. E., and Fugmann, S. D. (2009). "Carbohydrate Metabolism and Carbon Fixation in Roseobacter denitrificans OCh114". *PLoS ONE* 4.10, e7233.

Tang, K.-H., Le You, Blankenship, R. E., and Tang, Y. J. (2012). "Recent advances in mapping environmental microbial metabolisms through 13C isotopic fingerprints". *Journal of The Royal Society Interface* 9.76, pp. 2767–2780.

Tang, K.-H., Tang, Y. J., and Blankenship, R. E. (2011). "Carbon Metabolic Pathways in Phototrophic Bacteria and Their Broader Evolutionary Implications". *Frontiers in microbiology* 2, p. 165.

Tomasch, J., Gohl, R., Bunk, B., Diez, M. S., and Wagner-Döbler, I. (2011). "Transcriptional response of the photoheterotrophic marine bacterium Dinoroseobacter shibae to changing light regimes". *The ISME Journal* 5.12, pp. 1957–1968.

Wagner-Döbler, I., Ballhausen, B., Berger, M., Brinkhoff, T., Buchholz, I., Bunk, B., Cypionka, H., Daniel, R., Drepper, T., Gerdts, G., Hahnke, S., Han, C., Jahn, D., Kalhoefer, D., Kiss, H., Klenk, H.-P., Kyrpides, N., Liebl, W., Liesegang, H., Meincke, L., Pati, A., Petersen, J., Piekarski, T., Pommerenke, C., Pradella, S., Pukall, R., Rabus, R., Stackebrandt, E., Thole, S., Thompson, L., Tielen, P., Tomasch, J., Jan, M. v., Wanphrut, N., Wichels, A., Zech, H., and Simon, M. (2010). "The complete genome sequence of the algal symbiont Dinoroseobacter shibae: a hitchhiker's guide to life in the sea". *The ISME Journal* 4.1, pp. 61–77.

Wagner-Döbler, I., Thiel, V., Eberl, L., Allgaier, M., Bodor, A., Meyer, S., Ebner, S., Hennig, A., Pukall, R., and Schulz, S. (2005). "Discovery of complex mixtures of novel long-chain quorum sensing signals in free-living and host-associated marine alphaproteobacteria". *Chembiochem : a European journal of chemical biology* 6.12, pp. 2195–2206.

Wampler, D. A. and Ensign, S. A. (2005). "Photoheterotrophic Metabolism of Acrylamide by a Newly Isolated Strain of Rhodopseudomonas palustris". *Applied and Environmental Microbiology* 71.10, pp. 5850–5857.

Wang, B., Tan, T., and Shao, Z. (2009). "Roseovarius pacificus sp. nov., isolated from deep-sea sediment". *International journal of systematic and evolutionary microbiology* 59.Pt 5, pp. 1116–1121.

Wang, H., Ziesche, L., Frank, O., Michael, V., Martin, M., Petersen, J., Schulz, S., Wagner-Döbler, I., and Tomasch, J. (2014). "The CtrA phosphorelay integrates differentiation and communication in the marine alphaproteobacterium Dinoroseobacter shibae". *BMC Genomics* 15.1, p. 130.

Wiechert, W. (2001). "13C metabolic flux analysis". *Metabolic Engineering* 3.3, pp. 195–206.

Wiechert, W. and Nöh, K. (2013). "Isotopically non-stationary metabolic flux analysis: complex yet highly informative". *Current Opinion in Biotechnology* 24.6, pp. 979–986.

Wiegmann, K., Hensler, M., Wohlbrand, L., Ulbrich, M., Schomburg, D., and Rabus, R. (2014). "Carbohydrate Catabolism in Phaeobacter inhibens DSM 17395, a Member of the Marine Roseobacter Clade". *Applied and Environmental Microbiology* 80.15, pp. 4725–4737.

Wittmann, C. (2007). "Fluxome analysis using GC-MS". *Microbial Cell Factories* 6.1, p. 6.

Wittmann, C., Hans, M., and Heinzle, E. (2002). "In vivo analysis of intracellular amino acid labelings by GC/MS". *Analytical biochemistry* 307.2, pp. 379–382.

Wittmann, C. and Heinzle, E. (1999). "Mass spectrometry for metabolic flux analysis". *Biotechnology and Bioengineering* 62.6, pp. 739–750.

Wittmann, C., Krömer, J. O., Kiefer, P., Binz, T., and Heinzle, E. (2004). "Impact of the cold shock phenomenon on quantification of intracellular metabolites in bacteria". *Analytical biochemistry* 327.1, pp. 135–139.

Wittmann, C., Weber, J., Betiku, E., Krömer, J., Böhm, D., and Rinas, U. (2007). "Response of fluxome and metabolome to temperature-induced recombinant protein synthesis in Escherichia coli". *Journal of Biotechnology* 132.4, pp. 375–384.

Xiao, N. and Jiao, N. (2011). "Formation of Polyhydroxyalkanoate in Aerobic Anoxygenic Phototrophic Bacteria and Its Relationship to Carbon Source and Light Availability". *Applied and Environmental Microbiology* 77.21, pp. 7445–7450.

Yang, T. H., Heinzle, E., and Wittmann, C. (2005). "Theoretical aspects of 13C metabolic flux analysis with sole quantification of carbon dioxide labeling". *Computational Biology and Chemistry* 29.2, pp. 121–133.

Young, J. D., Walther, J. L., Antoniewicz, M. R., Yoo, H., and Stephanopoulos, G. (2008). "An elementary metabolite unit (EMU) based method of isotopically nonstationary flux analysis". *Biotechnology and Bioengineering* 99.3, pp. 686–699.

Yurkov, V. V. and Beatty, J. T. (1998). "Aerobic anoxygenic phototrophic bacteria". *Microbiology and molecular biology reviews : MMBR* 62.3, pp. 695–724.

Zan, J., Cicirelli, E. M., Mohamed, N. M., Sibhatu, H., Kroll, S., Choi, O., Choi, O., Uhlson, C. L., Wysoczynski, C. L., Wysoczinski, C. L., Murphy, R. C., Churchill, Mair E A, Hill, R. T., and Fuqua, C. (2012). "A complex LuxR-LuxI type quorum sensing network in a roseobacterial marine sponge symbiont activates flagellar motility and inhibits biofilm formation". *Molecular Microbiology* 85.5, pp. 916–933.

Zarzycki, J., Brecht, V., Müller, M., and Fuchs, G. (2009). "Identifying the missing steps of the autotrophic 3-hydroxypropionate CO2 fixation cycle in Chloroflexus aurantiacus". *Proceedings of the National Academy of Sciences* 106.50, pp. 21317–21322.

Zhang, W., Li, F., and Nie, L. (2010). "Integrating multiple 'omics' analysis for microbial biology: application and methodologies". *Microbiology* 156.2, pp. 287–301.

Zinger, L., Amaral-Zettler, L. A., Fuhrman, J. A., Horner-Devine, M. C., Huse, S. M., Welch, David B. Mark, Martiny, Jennifer B. H., Sogin, M., Boetius, A., Ramette, A., and Gilbert, J. A. (2011). "Global Patterns of Bacterial Beta-Diversity in Seafloor and Seawater Ecosystems". *PLoS ONE* 6.9, e24570.

A. Appendix

A.1. Precursor demand for glucose

Table A.1.: Building blocks for anabolic precursor demand for biomass synthesis in *D. shibae* in µmol g_{BTM}^{-1} for growth on SWM supplemented with 10 mM glucose as carbon source.

		µmol g_{BTM}^{-1}	G6P	F6P	R5P	E4P	GAP	PGA	PEP	PYR	AcCoA	OAA	AKG	NADPH
Amino acid		**5086**	**0**	**0**	**139**	**303**	**0**	**804**	**551**	**2424**	**378**	**1776**	**1314**	**9775**
Alanine	11.8	598								1				1
Arginine	4.6	235											1	4
Aspartate	8.9	454										1		1
Cysteine	1.7	87						1						1
Glutamate	18.5	942											1	1
Glycine	9.7	492						1						1
Histidine	1.7	85			1									1
Isoleucine	4.1	211								1		1		6
Leucine	7.4	378								2	1			2
Lysine	4.3	220								1		1		4
Methionine	2.9	146										1		4
Phenylalanine	3.2	162				1			2					2
Proline	2.7	136											1	3
Serine	4.4	225						1						1
Threonine	5.0	253										1		3
Tryptophane	1.1	54			1	1			1					3
Tyrosine	1.7	86				1			2					2
Valine	6.3	320								2				2
RNA		**294**	**0**	**0**	**294**	**0**	**0**	**165**	**0**	**0**	**0**	**129**	**0**	**203**
ATP	25	74			1			1						1
UTP	20	59			1							1		1
GTP	31	91			1			1						
CTP	24	71			1							1		1
DNA		**224**	**0**	**0**	**224**	**0**	**0**	**112**	**0**	**0**	**0**	**112**	**0**	**413**
dATP	17	38			1			1						2
dTTP	17	38			1							1		3
dGTP	33	74			1			1						1
dCTP	33	74			1							1		2
Lipids		**260**	**0**	**0**	**0**	**0**	**65**	**65**	**0**	**0**	**1129**	**0**	**0**	**1998**
Glycerine-P	25.0	65					1							1
Serine	25.0	65						1						1
3-OH 10:0	1.2	3									5			7
12:1	2.0	5									6			9
3-OH 14:1	2.4	6									7			10
18:1ω7c	39.9	104									9			15
18:0	2.7	7									9			16
Cyclo 19:0	1.9	5									10			15
	Average	*130*									*8.7*			*14.4*

		µmol g_{BTM}^{-1}	G6P	F6P	R5P	E4P	GAP	PGA	PEP	PYR	AcCoA	OAA	AKG	NADPH
LPS		71	27	10	3	0	0	4	0	0	93	0	0	137
Ribose	3.0	2			1									
Arabinose	1.4	1			1									
Mannose	9.9	7		1										
Glucose	9.7	7	1											
Glucosamine	28.7	20	1											
Glucosamine-6P	4.1	3		1										
Glycine	5.5	4						1						1
Alanine	0.2	0								1				1
KDO	0.0	0			1				1					
3-HD	9.6	7									5			7
3-oxo-TD	11.9	8									7			10
Peptidoglycan monomers		83	0	28	0	0	0	0	14	42	28	14	14	111
UDP-GlcNAc		14		1							1			
UDP-MurNAc		14		1					1		1			1
Alanine		28								1				1
DAP		14								1		1		4
Glutamate		14											1	1
PHB		733	0	0	0	0	0	0	0	0	1466	0	0	733
3-HB		733									2			1
Bacterio-chlorophyll		3	0	0	0	0	0	23	0	0	0	0	23	29
Bchl a		3						8					8	10
1-Carbon requirement		49	0	0	0	0	0	49	0	0	0	0	0	0
Serine		49						1						
Polyamines		59	0	0	0	0	0	0	0	0	0	0	59	176
ornithine eq.		59											1	3
Sum		6862	27	38	661	303	65	1222	565	2465	3098	2031	1410	13574

A.2. Reactions for pathway analysis on glucose

Table A.2.: Metabolic model for analysis of intracellular free fluxes of *D. shibae* with OpenFlux

rxnID	rxnEQ	cTrans	rates	type	basis	deviation
R01	GLC_EX = GLC6P	abcdef = abcdef		F	100	0
R02	GLC6P = F6P	abcdef = abcdef		F		
R03	F16P = F6P	abcdef = abcdef		F		
R04	F16P = DHAP + G3P	abcdef = cba + def		FR		
R05	DHAP + G3P = F16P	cba + def = abcdef		R	X	
R06	DHAP = G3P	abc = abc + def		FR		
R07	G3P = DHAP	abc + abc = abcdef		R	X	
R08	GLC6P = 6PG	abcdef = abcdef		F	X	
R09	6PG = PYR + G3P	abcdef = abc + def		F		
R10	6PG = P5P + CO2	abcdef = bcdef + a		F		
R11	P5P + P5P = S7P + G3P	abcde + fghij = fgabcde + hij		FR		
R12	S7P + G3P = P5P + P5P	fgabcde + hij = abcde + fghij		R	X	
R13	S7P + G3P = E4P + F6P	abcdefg + hij = defg + abchij		FR		
R14	E4P + F6P = S7P + G3P	defg + abchij = abcdefg + hij		R	X	
R15	E4P + P5P = F6P + G3P	abcd + efghi = efabcd + ghi		FR		
R16	F6P + G3P = E4P + P5P	efabcd + ghi = abcd + efghi		R	X	
R17	G3P = 3PG	abc = abc		FR		
R18	3PG = G3P	abc = abc		R	X	
R19	3PG = PEP	abc = abc		FR		
R20	PEP = 3PG	abc = abc		R	X	
R21	PEP = PYR	abc = abc		F		
R22	PYR = ACCOA + CO2	abc = bc + a		F		
R23	ACCOA + OAA = CIT	ab + cdef = fedbac		F		
R24	CIT = ICI	abcdef = abcdef		F		
R25	ICI = AKG + CO2	abcdef = abcde + f		F		
R26	AKG = 0.5 SUC + 0.5 SUC + CO2	abcde = 0.5 bcde + 0.5 edcb + a		F		
R27	SUC = MAL	abcd = abcd		F		
R28	MAL = OAA	abcd = abcd		F		
R29	PYR + CO2 = OAA	abc + d = abcd		F	X	
R30	MAL = PYR + CO2	abcd = abc + d		F	X	
R31	OAA = PEP + CO2	abcd = abc + d		F	X	
R32	GLC6P = GLC6P_B			B	0.193	0.002
R33	F6P = F6P_B			B	0.265	0.003
R34	P5P = P5P_B			B	4.646	0.046
R35	E4P = E4P_B	abcd = abcd		F	2.127	0.021
R36	G3P = G3P_B			B	0.457	0.005
R37	3PG = 3PG_B	abc = abc		F	8.590	0.086
R38	PEP = PEP_B	abc = abc		F	3.973	0.040
R39	PYR = PYR_B	abc = abc		F	17.331	0.173
R40	OAA = OAA_B	abcd = abcd		F	14.280	0.143
R41	ACCOA = ACCOA_B			B	21.780	0.218
R42	AKG = AKG_B			B	9.911	0.099
R43	E4P_B = E4P_BT			B		
R44	3PG_B = 3PG_BT			B		
R45	PEP_B = PEP_BT			B		
R46	PYR_B = PYR_BT			B		
R47	OAA_B = OAA_BT			B		
R48	3PG_B = SER	abc = abc		F		
R49	SER = GLYX + MTHF	abc = ab + c		F		
R50	OAA_B + PYR_B = 0.5 LYSX + 0.5 LYSX + 0.5 CO2 + 0.5 CO2	abcd + efg = 0.5 abcdfg + 0.5 efgdcb + 0.5 e + 0.5 a		F		
R51	PYR_B + PYR_B = VALX + CO2	abc + def = abefc + d		F		
R52	E4P_B + PEP_B = SHKM	abcd + efg = efgabcd		F		
R53	SHKM + PEP_B = CHRM	abcdefg + hij = abcdefghij		F		
R54	CHRM = TYRX + CO2	abcdefghij = hijbcdefg + a		F		
R55	CO2 = CO2_EX	a = a		FR		
R56	CO2_EX = CO2	a = a		R	X	
R57	0.492 GLYX + 0.086 TYRX + 0.320 VALX + 0.220 LYSX = BIOMASS			B	7.030	0.070
R58	PYR = ALAX	abc = abc		S		
R59	OAA = ASPX	abcd = abcd		S		
R60	AKG = GLUX	abcde = abcde		S		
R61	OAA = THR	abcd = abcd		S		

A.3. Metabolic flux analysis data for glucose

Table A.3.: Labelling data for *D. shibae* grown on SWM with glucose

Amino acid	Fragment	Measurement 1			Measurement 2			Measurement 3		
		M+0	M+1	M+2	M+0	M+1	M+2	M+0	M+1	M+2
Alanine	260	0.3797	0.4569	0.1221	0.3823	0.4545	0.1221	0.3846	0.4522	0.1222
	232	0.7540	0.1754		0.7536	0.1759		0.7530	0.1764	
Valine	288	0.3600	0.4532	0.1333	0.3615	0.4511	0.1336	0.3644	0.4491	0.1332
	260	0.7162	0.1927	0.0753	0.7155	0.1929	0.0756	0.7149	0.1936	0.0755
	186	0.7921	0.1523	0.0427	0.7915	0.1527	0.0428	0.7906	0.1533	0.0429
Threonine	404	0.4657	0.3154	0.1535	0.4619	0.3167	0.1551	0.4577	0.3174	0.1571
	376	0.5608	0.2836	0.1206	0.5559	0.2869	0.1216	0.5509	0.2903	0.1225
Aspartate	418	0.4597	0.3126	0.1588	0.4589	0.3163	0.1567	0.4544	0.3176	0.1587
	390	0.5566	0.2856	0.1219	0.5532	0.2879	0.1225	0.5482	0.2913	0.1234
	316	0.6112	0.2681	0.0938	0.6063	0.2718	0.0946	0.6010	0.2754	0.0965
Glutamate	432	0.5321	0.2902	0.1270	0.5267	0.2939	0.1280	0.5202	0.2971	0.1298
	330	0.6848	0.2155	0.0804	0.6835	0.2163	0.0807	0.6824	0.2173	0.0808
Serine	390	0.6384	0.2305	0.1056	0.6386	0.2303	0.1056	0.6375	0.2311	0.1059
	362	0.6694	0.2263		0.6700	0.2263		0.6698	0.2264	
	288	0.7327	0.1938		0.7324	0.1941		0.7324	0.1940	
Glycine	246	0.7504	0.1774		0.7504	0.1775		0.7494	0.1782	
	218	0.8253	0.1747		0.8254	0.1746		0.8251	0.1749	
Tyrosine	466	0.5701	0.2625	0.1185	0.5714	0.2644	0.1182	0.5725	0.2641	0.1178
	302	0.7281	0.1978		0.7307	0.1960		0.7279	0.1983	
Lysine	431	0.3555	0.3657	0.1840	0.3552	0.3656	0.1845	0.3519	0.3658	0.1864
	329	0.5843	0.2804	0.1010	0.5844	0.2817	0.1002	0.5790	0.2855	0.1012

Table A.4.: Experimental determined and simulated mass isotopomer fractions for *D. shibae* grown on SWM with glucose

Amino acid	Fragment	Simulated data			Experimental data		
		M+0	M+1	M+2	M+0	M+1	M+2
Alanine	260	0.4030	0.4446	0.1144	0.3823	0.4545	0.1221
	232	0.7656	0.1660		0.7536	0.1759	
Valine	288	0.3917	0.4408	0.1208	0.3615	0.4511	0.1336
	260	0.7406	0.1769	0.0698	0.7155	0.1929	0.0756
	186	0.8229	0.1361	0.0373	0.7915	0.1527	0.0428
Threonine	404	0.4531	0.3117	0.1649	0.4619	0.3167	0.1551
	376	0.5689	0.2792	0.1183	0.5559	0.2869	0.1216
Aspartate	418	0.4522	0.3111	0.1655	0.4589	0.3163	0.1567
	390	0.5677	0.2788	0.1193	0.5532	0.2879	0.1225
	316	0.6277	0.2620	0.0895	0.6063	0.2718	0.0946
Glutamate	432	0.5492	0.2818	0.1226	0.5267	0.2939	0.1280
	330	0.7073	0.2003	0.0761	0.6835	0.2163	0.0807
Serine	390	0.6386	0.2300	0.1062	0.6386	0.2303	0.1056
	362	0.6711	0.2244		0.6700	0.2263	
	288	0.7350	0.1918		0.7324	0.1941	
Glycine	246	0.7542	0.1746		0.7504	0.1775	
	218	0.8294	0.1706		0.8254	0.1746	
Tyrosine	466	0.5775	0.2626	0.1178	0.5714	0.2644	0.1182
	302	0.7240	0.1706		0.7307	0.1960	
Lysine	431	0.3661	0.3616	0.1825	0.3552	0.3656	0.1845
	329	0.6120	0.2710	0.0914	0.5844	0.2817	0.1002

A.4. Precursor demand for succinic acid

Table A.5.: Building blocks for anabolic precursor demand for biomass synthesis in *D. shibae* in µmol g_{BTM}^{-1} for growth on SWM supplemented with 10 mM succinic acid as carbon source.

		µmol g_{BTM}^{-1}	G6P	F6P	R5P	E4P	GAP	PGA	PEP	PYR	AcCoA	OAA	AKG	NADPH
Amino acid		3199	0	0	88	190	0	506	347	1524	238	807	827	6149
Alanine	11.8	376								1				1
Arginine	4.6	148											1	4
Aspartate	8.9	286										1		1
Cysteine	1.7	55						1						1
Glutamate	18.5	593											1	1
Glycine	9.7	310						1						1
Histidine	1.7	54			1									1
Isoleucine	4.1	132								1		1		6
Leucine	7.4	238								2	1			2
Lysine	4.3	138								1		1		4
Methionine	2.9	92										1		4
Phenylalanine	3.2	102				1			2					2
Proline	2.7	86											1	3
Serine	4.4	141						1						1
Threonine	5.0	159										1		3
Tryptophane	1.1	34			1	1			1					3
Tyrosine	1.7	54				1			2					2
Valine	6.3	201								2				2
RNA		197	0	0	197	0	0	110	0	0	0	87	0	136
ATP	25	49			1			1						1
UTP	20	39			1							1		1
GTP	31	61			1			1						
CTP	24	47			1							1		1
DNA		143	0	0	143	0	0	71	0	0	0	71	0	263
dATP	17	24			1			1						2
dTTP	17	24			1							1		3
dGTP	33	47			1			1						1
dCTP	33	47			1							1		2
Lipids		195	0	0	0	0	49	49	0	0	852	0	0	1502
Glycerine-P	25.0	49					1							1
Serine	25.0	49						1						1
3-OH 10:0	1.2	2									5			7
12:1	2.0	4									6			9
3-OH 14:1	2.4	5									7			10
18:1ω7c	39.9	78									9			15
18:0	2.7	5									9			16
Cyclo 19:0	1.9	4									10			15
	Average	*98*									*8.7*			*14.4*
LPS		71	27	10	3	0	0	4	0	0	93	0	0	137
Ribose	3.0	2			1									
Arabinose	1.4	1			1									
Mannose	9.9	7		1										
Glucose	9.7	7	1											
Glucosamine	28.7	20	1											
Glucosamine-6P	4.1	3		1										
Glycine	5.5	4						1						1
Alanine	0.2	0								1				1
KDO	0.0	0			1				1					
3-HD	9.6	7									5			7
3-oxo-TD	11.9	8									7			10
Peptidoglycan monomers		83	0	28	0	0	0	0	14	42	28	14	14	11
UDP-GlcNAc		14		1							1			
UDP-MurNAc		14		1					1		1			1
Alanine		28								1				1
DAP		14								1		1		4
Glutamate		14											1	1

	$\mu mol\ g_{BTM}^{-1}$	G6P	F6P	R5P	E4P	GAP	PGA	PEP	PYR	AcCoA	OAA	AKG	NADPH
PHB	4823	0	0	0	0	0	0	0	0	9647	0	0	4823
3-HB	4823									2			1
Bacterio-chlorophyll	3	0	0	0	0	0	23	0	0	0	0	23	29
Bchl a	3						8					8	10
1-Carbon requirement	49	0	0	0	0	0	49	0	0	0	0	0	0
Serine	49						1						
Polyamines	59	0	0	0	0	0	0	0	0	0	0	59	176
ornithine eq.	59											1	3
Sum	8823	27	38	430	190	49	812	361	1566	10858	979	922	13325

A.5. Reactions for metabolic pathway analysis on succinic acid

Table A.6.: Metabolic model for analysis of intracellular free fluxes of *D. shibae* with OpenFlux

rxnID	rxnEQ	cTrans	rates	type	basis	deviation
R01	SUC_EX = SUC	abcd = abcd		F	100	0
R02	SUC = SUC_EX	abcd = abcd		F	X	
R03	SUC = MAL	abcd = abcd		F		
R04	MAL = OAA	abcd = abcd		F		
R05	ACCOA + OAA = ICI	ab + cdef = fedbac		F		
R06	ICI = CIT	abcdef = abcdef		F		
R07	CIT = AKG + CO2	abcdef = abcde + f		F		
R08	AKG = 0.5 SUC + 0.5 SUC + CO2	abcde = 0.5 bcde + 0.5 edcb + a		F		
R09	PYR + CO2 = OAA	abc + d = abcd		F	X	
R10	MAL = PYR + CO2	abcd = abc + d		F	5.26	0.48
R11	OAA = PEP + CO2	abcd = abc + d		F	X	
R12	PYR = ACCOA + CO2	abc = bc + a		F		
R13	PEP = PYR	abc = abc		F		
R14	PEP = 3PG	abc = abc		FR		
R15	3PG = PEP	abc = abc		R	X	
R16	3PG = G3P	abc = abc		FR		
R17	G3P = 3PG	abc = abc		R	X	
R18	G3P = DHAP	abc = abc		FR		
R19	DHAP = G3P	abc = abc		R	X	
R20	DHAP + G3P = F16P	cba + def = abcdef		FR		
R21	F16P = DHAP + G3P	abcdef = cba + def		R	X	
R22	F16P = F6P	abcdef = abcdef		F		
R23	F6P = GLC6P	abcdef = abcdef		F		
R24	GLC6P = 6PG	abcdef = abcdef		F	X	
R25	6PG = KDPG	abcdef = abcdef		F		
R26	KDPG = PYR + G3P	abcdef = abc + def		F		
R27	6PG = P5P + CO2	abcdef = bcdef + a		F	0	0
R28	P5P + P5P = S7P + G3P	abcde + fghij = fgabcde + hij		FR		
R29	S7P + G3P = P5P + P5P	fgabcde + hij = abcde + fghij		R	X	
R30	S7P + G3P = E4P + F6P	abcdefg + hij = defg + abchij		FR		
R31	E4P + F6P = S7P + G3P	defg + abchij = abcdefg + hij		R	X	
R32	E4P + P5P = F6P + G3P	abcd + efghi = efabcd + ghi		FR		
R33	F6P + G3P = E4P + P5P	efabcd + ghi = abcd + efghi		R	X	
R34	GLC6P = GLC6P_B			B	0.116	0.001
R35	F6P = F6P_B			B	0.159	0.002
R36	P5P = P5P_B			B	1.816	0.018
R37	E4P = E4P_B	abcd = abcd		F	0.803	0.008
R38	G3P = G3P_B			B	0.206	0.002
R39	3PG = 3PG_B	abc = abc		F	3.428	0.034
R40	PEP = PEP_B	abc = abc		F	1.522	0.015
R41	PYR = PYR_B	abc = abc		F	6.609	0.066
R42	OAA = OAA_B	abcd = abcd		F	4.132	0.041
R43	ACCOA = ACCOA_B			B	45.820	0.458
R44	AKG = AKG_B			B	3.892	0.039
R45	E4P_B = E4P_BT			B		
R46	3PG_B = 3PG_BT			B		
R47	PEP_B = PEP_BT			B		
R48	PYR_B = PYR_BT			B		
R49	OAA_B = OAA_BT			B		
R50	3PG_B = SER	abc = abc		F		
R51	SER = GLYX + MTHF	abc = ab + c		F		
R51	OAA_B + PYR_B = 0.5 LYSX + 0.5 LYSX + 0.5 CO2 + 0.5 CO2	abcd + efg = 0.5 abcdfg + 0.5 efgdcb + 0.5 e + 0.5 a		F		
R52	PYR_B + PYR_B = VALX + CO2	abc + def = abefc + d		F		
R53	E4P_B + PEP_B = SHKM	abcd + efg = efgabcd		F		
R54	SHKM + PEP_B = CHRM	abcdefg + hij = abcdefghij		F		
R55	CHRM = TYRX + CO2	abcdefghij = hijbcdefg + a		F		
R56	CO2 = CO2_EX	a = a		FR		
R57	CO2_EX = CO2	a = a		R	X	
R58	0.279 GLYX + 0.049 TYRX + 0.181 VALX + 0.125 LYSX = BIOMASS			B	4.22	0.0422
R59	PYR = ALAX	abc = abc		S		
R60	OAA = ASPX	abcd = abcd		S		
R61	AKG = GLUX	abcde = abcde		S		
R62	OAA = THR	abcd = abcd		S		

A.6. Metabolic flux analysis data for succinic acid

Table A.7.: Labelling data for *D. shibae* grown on SWM with succinic acid

Amino acid	Fragment	Measurement 1			Measurement 2			Measurement 3		
		M+0	M+1	M+2	M+0	M+1	M+2	M+0	M+1	M+2
Alanine	260	0.1070	0.6805	0.1513	0.1036	0.6828	0.1519	0.1042	0.6824	0.1517
	232	0.7634	0.1678		0.7631	0.1678		0.7630	0.1679	
Valine	288	0.0945	0.6677	0.1630	0.0918	0.6694	0.1632	0.0922	0.6693	0.1631
	260	0.7350	0.1775	0.0734	0.7341	0.1780	0.0738	0.7342	0.1778	0.0737
	186	0.8104	0.1364	0.0409	0.8114	0.1366	0.0399	0.8118	0.1363	0.0398
Threonine	404	0.0440	0.0645	0.5993	0.0443	0.0628	0.6000	0.0432	0.0628	0.6003
	376	0.0823	0.6124	0.2108	0.0802	0.6139	0.2112	0.0793	0.6148	0.2112
Aspartate	418	0.0447	0.0700	0.5931	0.0462	0.0687	0.5936	0.0441	0.0684	0.5951
	390	0.0847	0.6124	0.2080	0.0832	0.6133	0.2081	0.0821	0.6143	0.2082
	316	0.0949	0.6614	0.1756	0.0930	0.6626	0.1760	0.0924	0.6629	0.1762
Glutamate	432	0.0846	0.5814	0.2104	0.0844	0.5822	0.2103	0.0826	0.5828	0.2108
	330	0.7059	0.2012	0.0759	0.7051	0.2014	0.0764	0.7055	0.2013	0.0761
Serine	390	0.0796	0.6174	0.2082	0.0781	0.6184	0.2083	0.0770	0.6189	0.2086
	362	0.6695	0.2267		0.6695	0.2267		0.6701	0.2264	
	288	0.7358	0.1917		0.7355	0.1915		0.7357	0.1913	
Glycine	246	0.1266	0.7197		0.1231	0.7228		0.1232	0.7225	
	218	0.8272	0.1728		0.8270	0.1730		0.8270	0.1730	
Tyrosine	466	0.0069	0.0383	0.2231	0.0067	0.0372	0.2220	0.0056	0.0368	0.2223
	302	0.0937	0.7289		0.0925	0.7298		0.0909	0.7324	
Lysine	431	0.0324	0.0957	0.5561	0.0318	0.0946	0.5560	0.0306	0.0940	0.05565
	329	0.0850	0.6394	0.1848	0.0826	0.6373	0.1851	0.0816	0.6388	0.1853

Table A.8.: Experimental determined and simulated mass isotopomer fractions for *D. shibae* grown on SWM with succinic acid

Amino acid	Fragment	Experimental data			Simulated data		
		M+0	M+1	M+2	M+0	M+1	M+2
Alanine	260	0.1036	0.6828	0.1519	0.0919	0.6892	0.1550
	232	0.7631	0.1678	0.0691	0.7522	0.1761	0.0716
Valine	288	0.0918	0.6694	0.1632	0.0872	0.6576	0.1732
	260	0.7341	0.1780	0.0738	0.7127	0.1950	0.0763
	186	0.8114	0.1366	0.0399	0.7919	0.1584	0.0440
Threonine	404	0.0443	0.0628	0.6000	0.0525	0.0729	0.5857
	376	0.0802	0.6139	0.2112	0.0802	0.6128	0.2116
Aspartate	418	0.0462	0.0687	0.5936	0.0524	0.0727	0.5849
	390	0.0832	0.6133	0.2081	0.0801	0.6117	0.2116
	316	0.0930	0.6626	0.1760	0.0878	0.6643	0.1799
Glutamate	432	0.0844	0.5822	0.2103	0.0747	0.5735	0.2202
	330	0.7051	0.2014	0.0764	0.6890	0.2116	0.0808
Serine	390	0.0781	0.6184	0.2083	0.0793	0.6149	0.2097
	362	0.6695	0.2267	0.1038	0.6669	0.2274	0.1057
	288	0.7355	0.1915	0.0730	0.7302	0.1953	0.0745
Glycine	246	0.1231	0.7228	0.1541	0.1018	0.7402	0.1580
	218	0.8270	0.1730		0.8280	0.1720	
Tyrosine	466	0.0067	0.0372	0.2220	0.0024	0.0428	0.2421
	302	0.0925	0.7298	0.1777	0.0982	0.7179	0.1839
Lysine	431	0.0318	0.0946	0.5560	0.0291	0.1036	0.5442
	329	0.0826	0.6373	0.1851	0.0832	0.6328	0.1972

A.7. Metabolome data for glucose and succinic acid grown cells.

Table A.9.: LC/MS data of metabolites from the central carbon metabolism of *D. shibae* grown on SWM with glucose or succinic acid as sole carbon source. The values were given in nmol g_{BTM}^{-1}. The LC-MS/MS results were determined in cooperation with Dipl. Biotechnol. Georg Richter (TU Braunschweig).

Pathway	Metabolite	Glucose [nmol g_{BTM}^{-1}]	Succinic acid [nmol g_{BTM}^{-1}]
EMPP	Glucose-6-phosphate	682.1	1667.9
	Fructose 6-phosphate	248.6	903.7
	Fructose 1,6-bisphosphate	377.0	-
	Dihydroxyacetonphosphate	449.5	-
	Glyceraldehyde 3-phosphate	-	-
	3-Phosphoglycerate	1115.8	-
	2-Phosphoglycerate	61.1	-
	Phosphoenolpyruvate	161.0	1240.7
	Pyruvate	645.0	-
EDP	6-Phosphogluconate	200.9	-
	KDPG	+	+
PPP	Ribose-5-phosphate	-	-
	Xylose 5-phosphate	-	-
	Ribulose 5-phosphate	-	-
	Seduheptulose 7-phosphate	-	-
TCA cycle	Acetyl-CoA	2696.7	521.9
	Citrate	+	+
	Isocitrate	+	+
	Oxoglutarate	1478.6	1277.2
	SuccinylCoA	-	-
	Succinate	+	+
	Fumarate	+	+
	Malate	+	+
EMCP	Glyoxylate	-	-
Energy metabolism	AMP	117.7	689.5
	ADP	1267.8	2544.8
	ATP	3997.1	4438.2
	NAD	2650.2	1820.2
	NADH	-	74.6
	NADP	661.0	623.9
	NADPH	400.7	359.8
	FAD	161.8	148.5

A.8. Growth profiles, isotopic and metabolic steady state for Δ*lux* mutants.

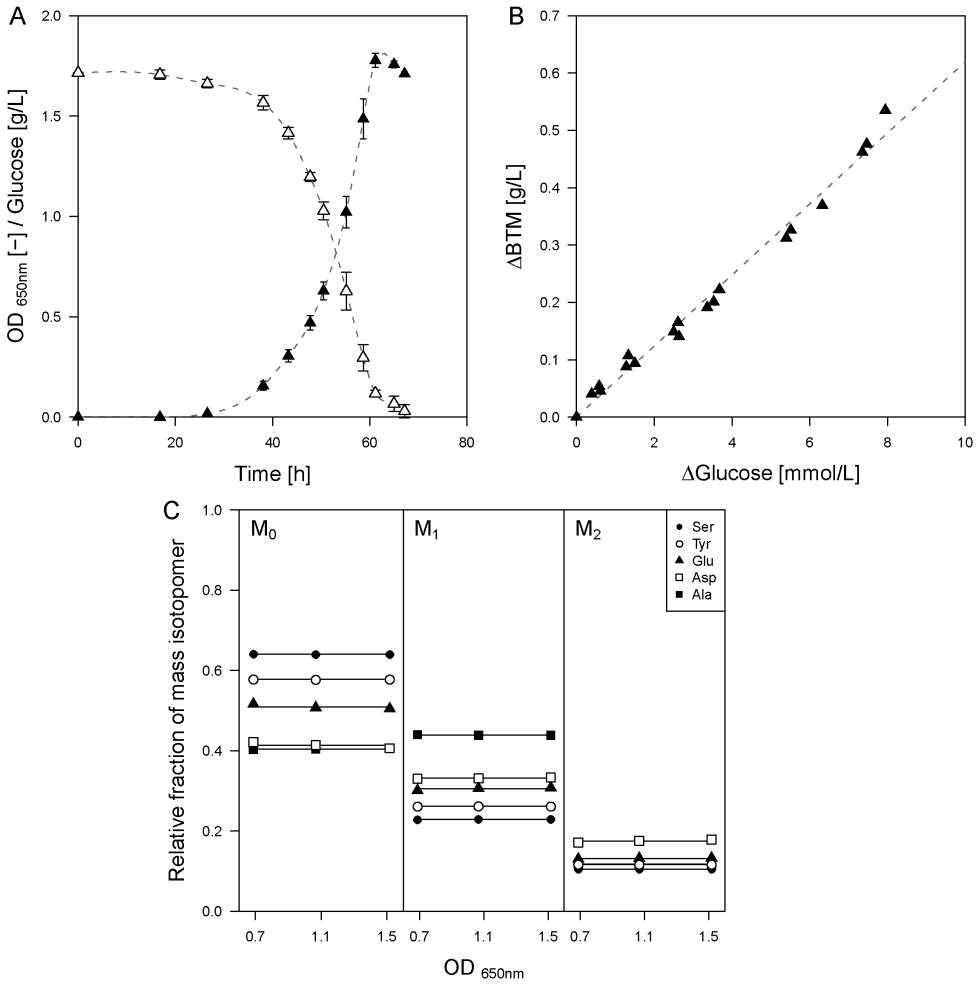

Figure A.1.: Cultivation profile of *Dinoroseobacter shibae* Δ*luxI* grown in permanent dark (A), metabolic steady state (B) and isotopic steady state (C). Experiments were conducted using a mineral salt medium with glucose as carbon source, and the data represent mean values with corresponding standard deviations (n = 3). Biomass was the only product formed.

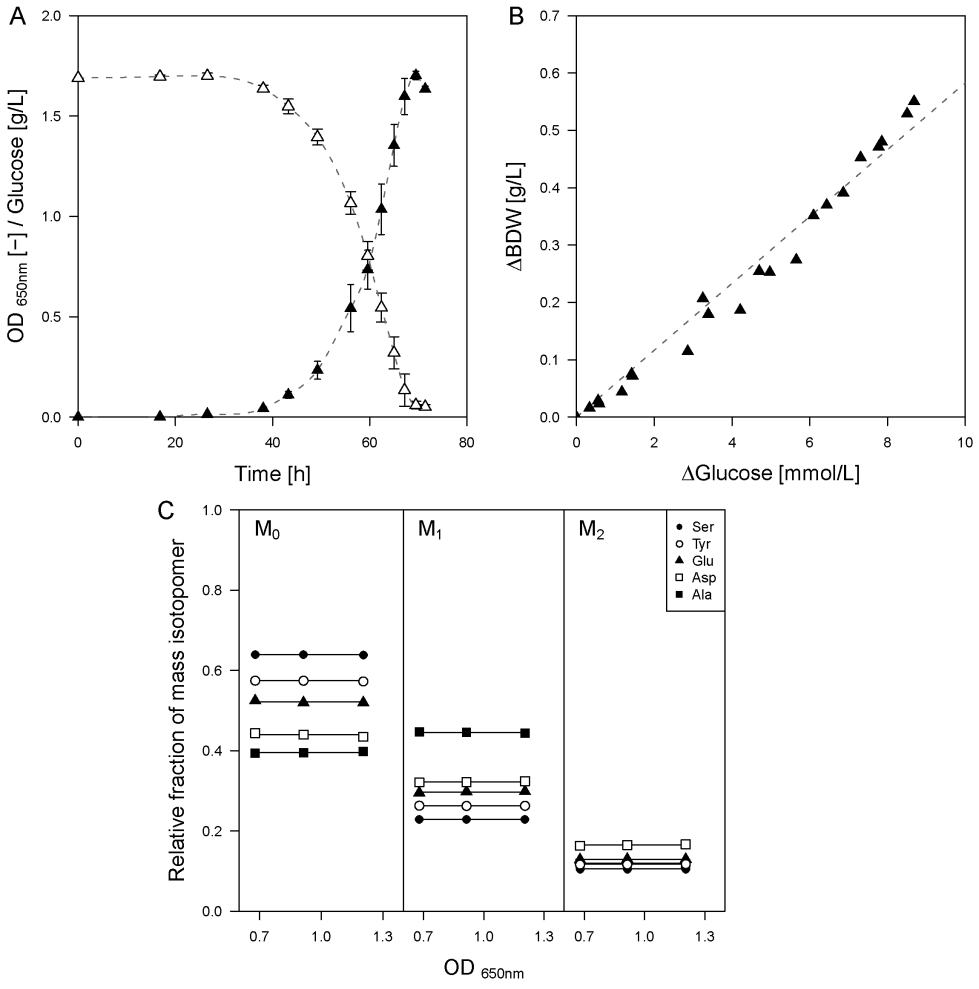

Figure A.2.: Cultivation profile of *Dinoroseobacter shibae* Δ*luxI* grown in permanent dark (A), metabolic steady state (B) and isotopic steady state (C). Experiments were conducted using a mineral salt medium with glucose as carbon source, and the data represent mean values with corresponding standard deviations (n = 3). Biomass was the only product formed.

Table A.10.: Experimental determined and simulated mass isotopomer fractions for *D. shibae* Δ*luxI* grown on SWM with glucose

Amino acid	Fragment	Simulated data			Experimental data		
		M+0	M+1	M+2	M+0	M+1	M+2
Alanine	260	0.4310	0.4224	0.1108	0.4046	0.4387	0.1176
	232	0.7656	0.1660		0.7562	0.1737	
Valine	288	0.4190	0.4200	0.1169	0.3778	0.4422	0.1287
	260	0.7406	0.1769	0.0698	0.7205	0.1893	0.0747
	186	0.8229	0.1361	0.0373	0.7966	0.1483	0.0422
Threonine	404	0.4069	0.3349	0.1785	0.4153	0.3312	0.1746
	376	0.5447	0.2959	0.1228	0.5323	0.3032	0.1258
Aspartate	418	0.4061	0.3343	0.1790	0.4137	0.3309	0.1754
	390	0.5436	0.2955	0.1238	0.5293	0.3040	0.1272
	316	0.6007	0.2822	0.0939	0.5814	0.2912	0.0983
Glutamate	432	0.5254	0.2971	0.1271	0.5071	0.3061	0.1319
	330	0.7073	0.2003	0.0761	0.6906	0.2115	0.0792
Serine	390	0.6393	0.2295	0.1061	0.6404	0.2292	0.1051
	362	0.6711	0.2244		0.6703	0.2257	
	288	0.7350	0.1918		0.7327	0.1935	
Glycine	246	0.7550	0.1739		0.7519	0.1761	
	218	0.8294	0.1706		0.8254	0.1746	
Tyrosine	466	0.5832	0.2593	0.1164	0.5769	0.2616	0.1163
	302	0.7248	0.1990		0.7268	0.1985	
Lysine	431	0.3469	0.3665	0.1910	0.3372	0.3673	0.1966
	329	0.5855	0.2899	0.0962	0.5579	0.2997	0.1053

Table A.11.: Experimental determined and simulated mass isotopomer fractions for *D. shibae* Δ*luxR* grown on SWM with glucose

Amino acid	Fragment	Simulated data			Experimental data		
		M+0	M+1	M+2	M+0	M+1	M+2
Alanine	260	0.4172	0.4334	0.1126	0.3951	0.4455	0.1194
	232	0.7656	0.1660		0.7552	0.1745	
Valine	288	0.4056	0.4302	0.1188	0.3708	0.4461	0.1307
	260	0.7406	0.1769	0.0698	0.7187	0.1906	0.0750
	186	0.8229	0.1361	0.0373	0.7948	0.1498	0.0423
Threonine	404	0.4331	0.3220	0.1706	0.4407	0.3223	0.1645
	376	0.5588	0.2862	0.1202	0.5458	0.2936	0.1234
Aspartate	418	0.4322	0.3214	0.1712	0.4399	0.3218	0.1650
	390	0.5576	0.2858	0.1212	0.5974	0.2791	0.1243
	316	0.6163	0.2705	0.0913	0.5974	0.2791	0.0956
Glutamate	432	0.5392	0.2883	0.1245	0.5196	0.2979	0.1297
	330	0.7073	0.2003	0.0761	0.6880	0.2130	0.0799
Serine	390	0.6388	0.2299	0.1062	0.6403	0.2291	0.1053
	362	0.6711	0.2244		0.6701	0.2258	
	288	0.7350	0.1918		0.7322	0.1940	
Glycine	246	0.7544	0.1745		0.7515	0.1765	
	218	0.8294	0.1706		0.8253	0.1747	
Tyrosine	466	0.5803	0.2610	0.1171	0.5749	0.2628	0.1170
	302	0.7233	0.2003		0.7250	0.2000	
Lysine	431	0.3587	0.3633	0.1859	0.3460	0.3661	0.1893
	329	0.6009	0.2789	0.0934	0.5742	0.2887	0.1020